FUNDAMENTAL UNDERSTANDING OF PHYSICOCHEMICAL PROPERTIES OF ULTRA-THIN POLYMER FILMS

A Dissertation
Presented to
The Academic Faculty

by

Annapoorani Sundaramoorthi

In Partial Fulfillment
of the Requirements for the Degree
Doctor of Philosophy in the
School of Chemical and Biomolecular Engineering

Georgia Institute of Technology
May 2011

FUNDAMENTAL UNDERSTANDING OF PHYSICOCHEMICAL PROPERTIES OF ULTRA-THIN POLYMER FILMS

Approved by:

Dr. Clifford L. Henderson, Advisor
School of Chemical and Biomolecular Engineering
Georgia Institute of Technology

Dr.Dennis W. Hess
School of Chemical and Biomolecular Engineering
Georgia Institute of Technology

Dr. Peter J. Ludovice, Co-Advisor
School of Chemical and Biomolecular Engineering
Georgia Institute of Technology

Dr. David G. Bucknall
School of Polymer, Textile and Fiber Engineering
Georgia Institute of Technology

Dr. Thomas F. Fuller
School of Chemical and Biomolecular Engineering
Georgia Institute of Technology

Dr. Todd R. Younkin
Components Research
Intel Corporation

Date Approved: December 15, 2010

My Thesis is dedicated to

God Almighty, my parents, *Mr. P. Sundaramoorthi & Mrs. Tamilarasi Sundaramoorthi,* my husband, *Mr. Hanmantha Reddy Mothe, my well-wisher, Dr.T.Renganathan,* and my brother, *Mr. Thyagarajan Sundaramoorthi*

ACKNOWLEDGEMENTS

I would like to thank God Almighty, my parents, Mr. P. Sundaramoorthi and Mrs. Tamilarasi Sundaramoorthi, my husband, Mr. Hanmantha Reddy Mothe, my undergraduate professor Dr. Renganathan, my brother Mr. Thyagarajan Sundaramoorthi, my in-laws, Mr. Malla Reddy Mothe, Mrs. Chandrakala Mothe, and Ms. Anjani Mothe for their untiring support throughout the journey of my Doctorate studies. I would like to thank my advisors Prof. Clifford L. Henderson and Prof. Pete J. Ludovice for their advice in research and their invaluable support and guidance during the years of my research study. I would also like to thank my committee members, Prof. Tom Fuller, Prof. Dennis Hess, Prof. David Bucknall, and Dr. Todd Younkin, for their valuable inputs. I would like to thank my research group members, Richard Lawson, Hua-Wei Chu, Wei-Ming Yeh, Jose Baltazar, Jing Chen, and Jassem Abdullah for their cooperation in the lab and help as group members. I would like to thank Prof. Jerry Jean and Dr. Hongmin Chen at University of Missouri, Kansas City for their help with SPALS experiments and Ron Synowicki and Jeremy VanDerslice at J.A. Woollam Inc., for help with UV-VIS and IR ellipsometry measurements. I would also like to express my gratitude to other research groups at Georgia Tech with whom I collaborated, including the research groups of Prof. Dennis Hess, Prof. Laren Tolbert, and the entire Georgia Tech Microelectronics Research Center. I would like to also thank the Components Research group at Intel Corporation for allowing me to pursue a summer internship with them while in graduate school that has helped shape my decision for a future path for my career. Last but not least, I would like to thank my friends, Gokulakrishna Iyer, Manoj Agrawal, Dhaval Bhandari, Ashish Pande, Prashant Kumar and Divya Paruchuri.

Table of Contents

LIST OF TABLES

LIST OF FIGURES

LIST OF ABBREVIATIONS

CAR	Chemically Amplified Resist
DMAP	Dimethylaminopyradine
Ea	Activation Energy
FTIR	Fourier Transform Infrared Spectroscopy
FV	Free Volume
GIR	Grazing angle reflectance
MC	Monte-Carlo
MD	Molecular Dynamics
PAG	Photoacid generators
PALs	Positron Annihilation Lifetime Spectroscopy
PCND	Protracted Colored Noise Dynamics
PEB	Postexposure bake
PEMFC	Polymer Exchange Membrane Fuel Cell
PGMEA	Propylene glycol monomethyl ether
PHOST	Polyhydroxystyrene
PMMA	Polymethyl methacrylate
PTBOCST	Polyhydroxystyrene protected with tert-butoxy carbonyl
TPS.PFBS	Triphenylsulfonium perfluorobutane sulfonate
TPS.TFMS	Triphenylsulfonium trifluoromethane sulfonate
QCM	Quartz Crystal Microbalance

SUMMARY

A variety of physical properties have recently been reported to depend on the sample dimensions for polymers in cases where the dimensions approach the 100 nm length scale. In this work, the diffusion behavior of spin cast polymer thin films was studied in detail as a function of film thickness. Diffusion coefficients of water molecules in poly(methyl methacrylate) (PMMA) films were studied via sorption-desorption experiments using a quartz crystal microbalance (QCM) system. The diffusion coefficients were found to decrease from 10^{-8} cm^2/s in thick films to 10^{-13} cm^2/s in ultra-thin films. In order to probe if there is a characteristic length scale set by the polymer chain size, the effect of PMMA molecular weights on this behavior was tested and no significant differences were observed. Diffusion coefficients in these films were also investigated as a function of aging time at 25°C and were not found to significantly change over the span of times up to approximately four months. In contrast to the diffusion coefficients, the total mass uptake of water molecules in these thin spin cast polymer films was found to decrease in a linear fashion with film thickness, implying constant water solubility regardless of thickness. The films were subjected to rigorous annealing to probe if potentially different residual casting solvent levels in the thick and thin films contribute to the observed diffusion coefficient changes. No substantial change was observed in the diffusion behavior with respect to different annealing conditions. Positron Annihilation Lifetime Spectroscopy (PALs) was used to probe the free volume (FV) pocket size, its distribution within the film, and its total amount as a function of film thickness in PMMA. The results from PALs show that thicker films have a broader distribution of FV pocket sizes than thinner films and that the average free volume pore

radius is smaller in thin films than in thick films. This change in FV size and FV distribution certainly contribute to the significant drop in diffusion coefficient in thinner PMMA films, and this behavior is likely to be one of the general underlying causes for such thickness dependent diffusion behavior observed in a variety of other polymers as well.

Protracted Colored Noise Dynamics (PCND) enables efficient sampling of phase space and faster relaxation of the systems compared to Molecular Dynamics (MD). Its extensibility to three dimensional systems has been investigated and reported to be sensitive to initial conformation.

CHAPTER 1

INTRODUCTION

While natural polymers in the form of latex from tree saps and tar have been in use since time immemorial, chemically modified natural polymers and synthetic polymers came into existence in the early 1800's. Vulcanized rubber, gun cotton, celluloid, bakelite, and rayon are important products that marked the beginning of the era of synthetic polymers. The growth of the polymer industry has been significant and important discoveries in the field that led to substantial expansion of the use of polymers include the discovery of nylon, acrylics, neoprene, and polyethylene. Each of these polymer discoveries can at least in part be traced to work based directly on the need for a particular property associated with an application. Modifications and enhancements of these polymers, both to their basic chemical structure made possible by their long chain nature and the ability to functionalize them with varied side groups and incorporation of new back bone elements, together with development of the ability to manipulate their physical arrangements both of monomers along the chain in terms of their sequence (e.g. chirality and stereo-chemical orientation (e.g. tacticity)), and the alignment of the chains with one another (i.e. enabling control over the amorphous and crystalline phases of the various materials), has kept researchers busy now for more than a century in finding ways to provide materials with interesting and useful properties. Fundamental understanding of the properties and dynamics of such polymers has been and continues to be an important issue in enhancing and exploiting their applicability in a wide range of fields.

In particular, the use of polymers in various thin film forms has grown dramatically over the last several decades. Such polymer thin films are finding wide spread use in applications ranging from membrane separations to microelectronics manufacturing. Recently, it has been demonstrated that the preparation and use of polymers in these thin film forms can give rise to unusual non-bulk properties in such materials. This has led to a general need to better characterize and understand the origin of such phenomena, and it is this quest that motivates much of the work in this thesis.

1.1 Applications of Polymers

Polymers find application in virtually every aspect of modern life, and as such a general discussion of this wide range of applications is beyond the scope of this thesis. A number of excellent books on the subject have been written and can be consulted for the properties needed in various applications, the types of polymers used in those applications, and the methods used in producing and processing them [1-10]. More specifically, in terms of the use of polymers in thin film form, the range of applications is still sufficiently broad to be beyond the scope of a short and simple discussion. Therefore, in the context of this thesis, several particular applications for polymer thin films will be highlighted to help motivate the work discussed throughout the remainder of the thesis. In particular, two application areas where the diffusion behavior of small molecules in polymer thin films is critical to the performance of the polymer materials in those applications will be the focus of this discussion. First, the use of polymer thin films in fuel cell (thickness in the order of micrometers) applications will be discussed. Second, the use of polymer thin films in microelectronics manufacturing and lithography

processes (thickness in the order of nanometers) will be discussed. As will be seen in these cases, control and manipulation of the diffusion coefficient of small molecules in polymer thin films is critical in these fields.

Diffusion and transport of moisture and water molecules forms an integral part of industrial chemical processes and is vital in the fields of biological applications. For example, diffusion of moisture and dyes forms an important step in the process of extraction, washing and drying of chemical fibers [11]. Other applications include water diffusion controlled growth of polymer gradient thin films used in biological separations and protein adsorption [12, 13] and in diffusion controlled phenomena like drug release, in polymer coatings and thermal printing applications [14], toxin barriers in clothing and equipments [15]. These and other similar applications necessitate understanding of diffusion through various forms of polymers, to enable their optimum use.

1.1.1 Polymers in Fuel Cell Applications

At present, energy is foremost in the list of contemporary issues critical to mankind and alternative methods for producing energy in ways that are cleaner, more efficient, and use non-petroleum based fuels are of significant interest. Fuel cell is a promising alternative towards renewable energy resources. A fuel cell is an electrochemical device generating electricity by a chemical reaction and there are different types of fuel cells, using different chemistry. A fuel cell has two electrodes, anode and cathode. The chemical reactions occur at the electrodes and are accelerated by the presence of catalysts. An electrolyte enables transport of charged particles between the electrodes. Hydrogen

source at the anode are split into hydrogen ions and electrons. Electrons flow through the external circuit conducting electricity. Positively charged hydrogen ions travel through the electrolyte and combine with oxygen at the cathode, along with electrons from external circuit and form the by-product water, making fuel cell a clean energy device. A schematic representation of the fuel cell is shown in Figure 1.1. Alkali fuel cell uses potassium hydroxide in water as the electrolyte. The liquid electrolyte poses the disadvantage of possible leakage in this type of fuel cell. This type of fuel cell is easily poisoned by carbon-di-oxide and hence high purity hydrogen and oxygen need to be used. Phosphoric acid fuel cell uses phosphoric acid as electrolyte contained in Teflon-bonded silicon carbide matrix. It is generally used for stationary power generation and operates at high temperature. Molten carbonate fuel cell also operates at high temperature (about 650^0C) and uses molten carbonate salt mixture as electrolyte. Solid oxide fuel cell employ hard, non-porous ceramic compound as electrolyte and operates at a temperature of about 1000^0 C. Unlike other fuel cell, solid oxide fuel cell is not poisoned by carbon-monoxide impurities and is capable of tolerating sulfur impurities. Proton exchange membrane or polymer exchange membrane fuel cell uses a polymer membrane as electrolyte for proton or H^+ conduction from anode to cathode. It has high power density and operates at low temperature. This makes proton exchange membrane fuel cell to be used for transport applications, as the low temperature ensures durability of fuel cell components and low warm-up time. However, hydrogen used as a fuel source poses storage problems. Direct methanol fuel cell is comparable to proton exchange membrane fuel cell except that hydrogen is generated within the fuel cell system by reforming hydrogen rich hydrocarbon fuels.

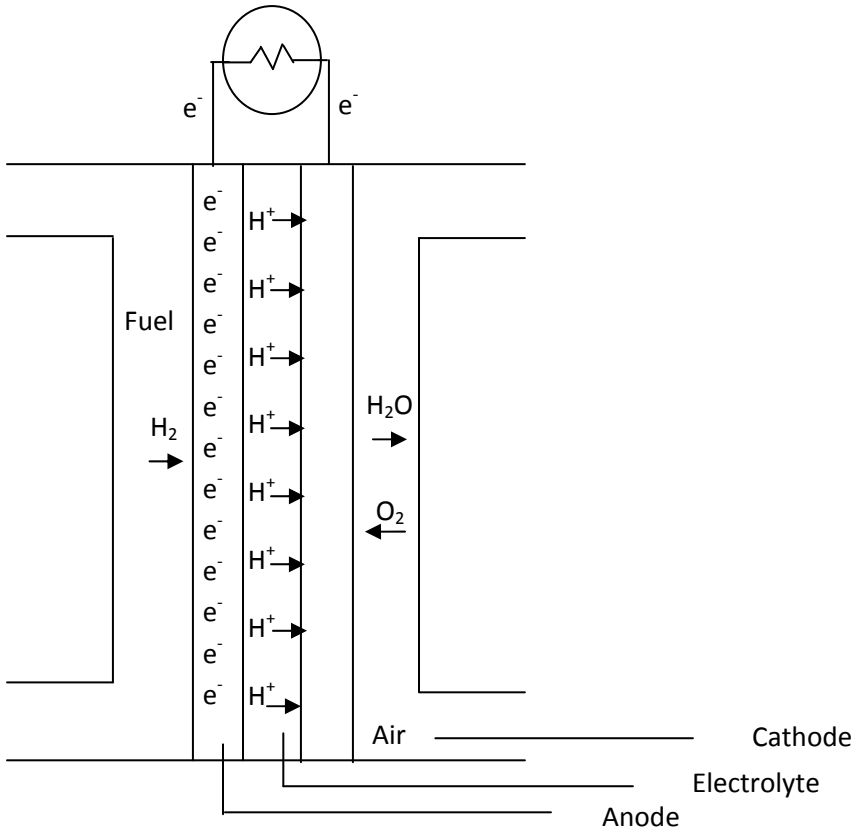

Figure 1.1 Schematic representation of a Fuel Cell

Typically, methanol is used as a fuel source for hydrogen in direct methanol fuel cell. Methanol is easy to transport with the existing infrastructure for gasoline and has high energy density compared to hydrogen used in proton exchange membrane fuel cell. However, permeation of methanol through the polymer electrolyte membrane is a major limitation in fuel cells, as loss of fuel source is economically undesirable. Hence, it is important to understand diffusion of molecules through these polymer membranes to enable control of permeation of fuel source, while enhancing proton transfer through these membranes [1].

1.1.2 Polymers in Photoresist Applications

In semiconductor industry, as feature sizes continue to shrink, thickness of resist films used in advanced lithography applications is also decreasing. As mentioned earlier, it has been reported that the physicochemical properties of polymer ultra-thin films, such as glass transition temperature and Young's modulus, can deviate from bulk behavior when the polymer film thickness is smaller than a critical thickness. This critical thickness has been reported to range from approximately 100 nm to as much as 1 micron depending on the physicochemical property involved. Since polymeric photoresist film thicknesses are already in the order of 100 nm and smaller, it is expected that the physicochemical behavior of these films may deviate from their bulk behavior and show a strong dependence on film thickness. While significant work has been published on the behavior of pure polymer thin films, very little has been reported about the behavior of ultra-thin films of formulated photoresists like chemically amplified resists (CAR) and dependence of the relevant behaviors of these materials on film thickness.

Ultra-thin photoresist films are becoming increasingly important in microelectronics as (1) the International Technology Roadmap for Semiconductors (ITRS) prepares for the transition to wavelength of 13.5 nm and less, (2) the absorption issues at such low wavelengths leads to the use of ultra-thin films <100 nm. The high surface to volume ratio in ultra-thin films makes the interfacial forces dominate. And the contributions from them influence the lithographic performance and hence the device efficiency in the semiconductor industry [16].

The phenomenal progress of the semiconductor industry, driven and described by Moore's Law which states that the number of transistors in an Integrated Circuit (IC) will

double approximately every 18 months [17], has been made possible in large part by the development advanced photolithography materials and technique which are used to print the intricate circuit patterns needed to produce such complex devices. Photolithography involves spin coating a layer of polymer onto a silicon substrate. CAR, usually, is composed of a polymer resin and a photo-acid generator (PAG). CAR used in photolithography, on exposure to radiation, generates acid due to decomposition of photo-acid generator or PAG. Researchers at IBM first introduced the concept of CAR to enable fabrication of fine features and was successfully implemented in the manufacture of dynamic random access memory (DRAM) devices [18]. The polymer used was poly(4-hydroxystyrene) (PHOST) protected by *tert*-butoxycarbonyl (t-BOC) functional group.

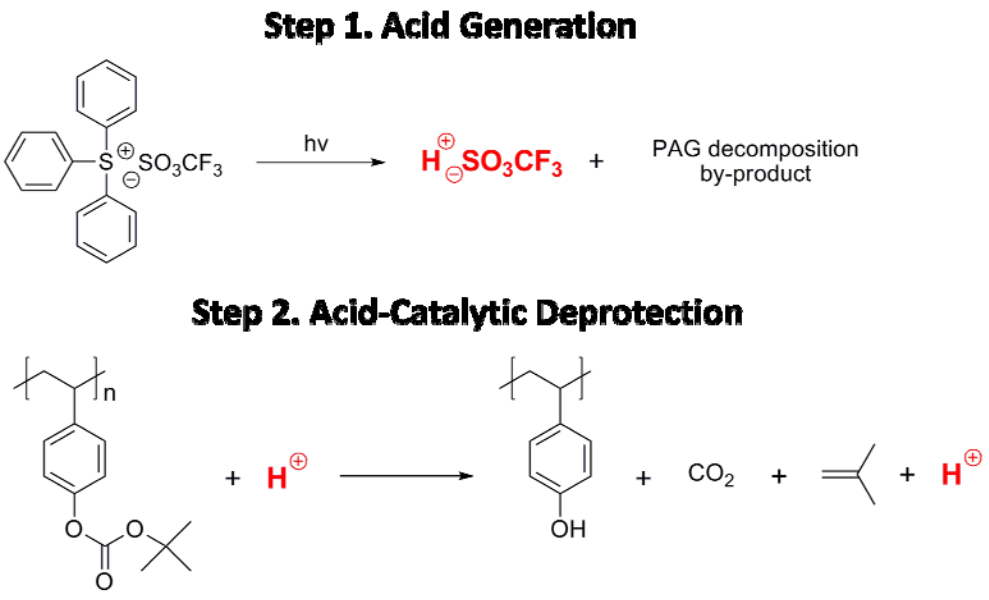

Figure 1.2 Reaction steps involved in photolithography

The growing trend in the semiconductor industry with new challenges, in turn necessitates enhancement of the polymeric materials used in processing and fabrication

of devices. It is essential that the polymer used in photolithography process meets critical imaging properties like high resolution, sensitivity and line edge roughness (LER). Properties of polymer-PAG mixture under the processing condition like glass-transition temperature of the polymer, plasticization of the polymer by the additives and diffusion length of acid in the polymer matrix are some of the key factors that largely impact the performance of a photoresist. Understanding diffusion in thin polymer films used as photoresists would help handle such challenges in semiconductor industry. The overarching goal of the work reported here is to provide such a detailed investigation of thin film confinement effects on photoresist behavior, including both quantifying the magnitude of such effects and the film thickness ranges over which such phenomena occur. The ultimate goal of the work is to understand the fundamental causes for such behavior.

1.2 Diffusion in Polymers

Extensive research literature is available regarding diffusion in polymers. An important step in understanding the process of diffusion in polymers began in the early 1900's with the description of the Brownian motion of particles by Robert Brown, who reported the random movement of particles suspended in a fluid medium [19]. Brownian motion is described as a stochastic process and commonly referred as random walk theory. Later, a law and mathematical representation describing mass transport, analogous to heat transport and charge transport was proposed by Adolf Fick, known as Fick's law of diffusion [20]. The law states that the rate of mass transport through a unit area of material is proportional to the concentration gradient normal to the area. The

mathematical expression below assumes a constant proportionality constant or diffusion coefficient (D).

$$J_z^* = -D\frac{\partial c}{\partial z} \tag{1}$$

This relatively simple model has been shown to well describe mass transport in a variety of applications, and is particularly effective in describing non-convective transport in gases and liquids.

Diffusion of small molecules through polymers can be a more complicated issue and is in many cases not completely described by Fick's law. The diffusion coefficient of a penetrant molecule in a polymer is determined by a variety of factors including the ability of the polymer to rearrange its chains to accommodate the molecules and subsequently allow them to move within the solid. Since the presence of such molecules in a polymer can affect the local chain mobility in some cases (e.g. some penetrants such as solvents can swell the polymer and enhance local chain segmental mobility), description of the transport mechanisms through polymers are more complicated and difficult to explain through simple mathematical models [21]. Mass transport through polymer films involves absorption of molecules into the surface of the polymer, followed by diffusion through the polymer membrane and finally possible desorption from the surface of the polymer on the other side if it is an open or permeable interface. The physical state of a polymer plays a major role in diffusion of small molecules. The rubbery state of a polymer, typified by high chain mobility, enables enhanced accessibility of free volume for a diffusing molecule and enhanced diffusion, as opposed to the glassy state of the polymer, typified by restricted motion of the polymer chain and

its backbone [21]. In all cases of diffusion, Fick's law is applicable only when the surface of a polymer system attains instantaneous equilibrium with the sorption environment and remains constant through the process of sorption. However, swelling characteristics of the polymer, where an internal interface exists between the swollen and unswollen polymer, does not follow this criterion of Fick's law, and this was characterized by Alfrey [22] as Non-Fickian diffusion. A number of mathematical models were developed to explain Non-Fickian transport in polymers, specifically as a time dependent phenomenon. These models explained the time dependent phenomena associated with change in concentration, the structural changes in polymers to accommodate sorption equilibrium at the interface and all the models were finally unified as a time dependent relaxation mechanism associated with molecular rearrangement of the polymer chains [23-25]. Long-Richman model of dual mode sorption and many others were based on the two stage process of diffusion, where the first step is based on surface concentration, followed by relaxation of the polymer accompanying diffusion of molecules through the polymer matrix [26-28]. However, until this time, diffusion was not explained as an activated process or the change in diffusion as a function of physical characteristics of the membrane has not been studied yet. Further, the focus of study has so far been on rubbery membranes only. R.M.Barrer in 1930's pointed that the phenomena of diffusion was an activated process in rubber-like membranes and can be expressed as:

$$D = D_o e^{-E/RT} \qquad (2)$$

This activation energy is required to separate the polymer chains to transport gas molecules through the polymer. The study of gas transport in polymers began in 1954 when Patrick Meares observed the change in diffusion as a function of polymer chain

dynamics reported as a function of temperature, in particular the second order transition. In 1959, Cohen and Turnbull [29] first explained that the unoccupied volume within a polymer matrix, called free volume that regulates molecular transport in polymers. This concept is explained in detail in section 1.4.

Considerable research was performed to study and understand polymer chain dynamics in rubbery polymers and its dependence on temperature, specifically the second-order transition called glass-transition temperature. When amorphous rubbers are cooled, the cooling rate is faster than the time scale for the volumetric relaxation of polymer chains. This leads to a constrained motion of polymer chains during cooling and finally results in a non-equilibrium glassy state where the polymer chains are trapped and have negligible segment mobility to attain equilibrium conformation. Thus the transition from rubbery to glassy state is referred as glass-transition. The study of glass-transition temperature (T_g) in thin polymer films and the influence of thickness on them are discussed in detail in section 1.3.

1.3 Glass-transition temperature

Joseph Keddie and Richard Jones in 1994 measured the thickness dependence of glass-transition temperature (T_g) of poly (methyl methacrylate) (PMMA) by using spectroscopic ellipsometry. The experimentation was done on both strongly and weakly interacting substrates. The high surface to volume ratio in ultra-thin films gains importance over the material behavior in ultra-thin films. Hence, the air/film interface and substrate/film interface become significant in ultra-thin films. PMMA was spin

coated on gold surface and oxide surface of silicon substrate. It was found that the sample when cooled from the equilibrium state exhibited more consistent T_g during different heating cycles. PMMA coated on the native oxide of silicon increases the glass transition temperature than the bulk films while PMMA on gold decreases the glass transition temperature than the bulk films. The hydrogen bonding of the polymer film to the substrate in the case of PMMA on native oxide, facilitated by the acrylate group of PMMA and the hydroxyl group of the oxide favors interaction between PMMA and native oxide, sufficient enough to hinder mobility of the polymer at the film/substrate interface. This force dominates free mobility of the film on the air/film interface thus causing an increase in T_g. Absence of the polymer film/substrate interaction in the case of PMMA on gold thus has a depression of T_g under the influence of increased mobility at the film surface [30]. The bulk value of T_g reported for PMMA film thickness of 232 nm on gold surface in this case is higher than the values reported in literature. This may be attributed to the tacticity difference in PMMA, where an increase in the % of syndio-tacticity of the polymer increases the T_g [31]. In an earlier work by the same authors, on the dependence of glass transition temperature on film thickness, in the case of polystyrene spin coated on hydrogen passivated silicon surfaces, they observed a depression of T_g. The explanation offered for not observing the expected elevation of T_g but rather the suppression of T_g (for the same reason of hydrogen bonding, mentioned above) is that the strength of the hydrogen bond involving a hydroxyl group (PMMA on SiO_2) is much stronger than the hydrogen bond involving polystyrene on silicon (as polystyrene contains only carbon and hydrogen and no oxygen, in contrast to PMMA where there is a carbonyl group with a pair of lone electrons from oxygen for bonding), if

there existed any [32]. The study of T_g has been discussed as a bulk value in this case and is not discussed as a local phenomenon. The study of diffusion and glass transition temperature as a local phenomena began when studies were conducted using fluorescent probes attached to polymers as polymer labels. In 2001, J.M. Torkelson investigated the effect of decreasing film thickness on the glass transition temperature using fluorescence intensity of chromospheres doped or labeled polymers. The study was conducted on polystyrene, poly(isobutyl methacrylate) and poly(2-vinylpyridine) [33]. The error in this measurement was, however, too big to ignore. He used two optically based small molecular probes to measure diffusion as a function of film depth in ultra-thin polymer films. Pyrene was used as the non-radiative energy transfer donor species and lophine was one of the NRET acceptors. Diffusion of the acceptor species through the layer of polymer film until quenched by the donor species was measured. The study was conducted on poly(isobutyl methacrylate) that was as thin as 90 nm [34]. Lovejeet Singh et al., in 2003 studied the dependence of T_g of PMMA on film thickness, molecular weight and substrate used. In the study, it was also found that the coefficient of thermal expansion (TCE) also exhibited dependence on film thickness, molecular weight and substrate. Deviation of T_g from bulk value was reported to scale with the radius of gyration [35]. As mentioned earlier [30], T_g of PMMA on non-interacting substrate such as Hexamethyldisilazane (HMDS) decreased as compared to the bulk value [36].

1.4 Diffusion in Thin Polymer Films

As the study of deviation in glass-transition temperature revealed differences in polymer thin film dynamics from bulk, other properties like coefficient of thermal expansion [37-

39], elastic modulus [40-42] and diffusion coefficient [39, 43-46] also began to be investigated. Diffusion coefficients of water in thin spin cast films of polymers like poly (vinyl pyrrolidone) [47] polyhydroxystyrene, polycarbonate, polyvinylchloride, poly(methyl methacrylate) films [43] studied using X-ray reflectivity, neutron reflectivity, quartz crystal microbalance etc., showed several orders of magnitude drop in diffusion coefficient from bulk. It is to be noted that unlike glass transition temperature deviations (where depression and elevation of glass-transition temperature was observed based on, if the polymer and substrate were weakly interacting or strongly interacting), almost all polymer films so far studied (using different techniques) showed a drop in diffusion coefficient with decrease in film thickness [39, 43-46]. This was largely suggested to be due to the same confinement effects that caused changed in glass-transition temperature due to substrate film interactions. For example, let us consider the orders of magnitude drop in diffusion coefficient reported in polymer films supported on substrates (PMMA on gold) with glass-transition temperature lower than bulk [30]. Decrease in glass-transition temperature due to confinement effects is generally observed in polymers supported on weakly interacting substrate. The weak interaction of the polymer at the film substrate interface in turn leads to increased mobility and hence the observed decrease in glass-transitions. Such increased mobility of polymer films at the film substrate interface, should in turn enhance diffusion of molecules through them, leading to an increase in diffusion coefficient. However, diffusion coefficient dropped with decrease in film thickness. Thus, increased chain mobility does not explain the decrease in diffusion coefficient. Further, in all the properties studied and reported like glass-transition temperature [30, 33-36], coefficient of thermal expansion [37-39], elastic

modulus [40-42], the deviation from bulk was observed only for film thickness less than 150 to 200 nm at the most. Hence, the diffusion studies so far reported in literature have also investigated polymer films up to 200 nm, as confinement effect was largely believed to cause the deviation. However, unlike other properties, diffusion coefficient reported for polymer films of about 200 nm thickness is still a few orders of magnitude lower than bulk. This implies that the deviation in diffusion coefficient extends beyond 200 nm and confinement effects used to explain other reported property deviations (observed below 200 nm) is not sufficient to explain deviation in diffusion coefficient. Also, this deviation in diffusion coefficient is reported for a number of polymer films. However, all the reported polymer films are simple pure polymer films. In order to investigate if the observed deviation is primarily due to sample dimensions viz., film thickness, it is essential to look in to diffusion in composite polymer mixtures like photoresists used in photolithography in semiconductor industry, in addition to pure polymer films. Such a study of diffusion coefficient in composite polymer mixtures would help understand if the observed deviation in diffusion coefficient is applicable to all thin polymer (pure and composite mixture) films and would also prove to be useful in determining the performance of photoresist materials based on their diffusion characteristics.

1.5 Free Volume

The concept of free volume introduced by Cohen and Turnbull [29] in polymer films, was attributed to the space between polymer chains that is unoccupied. According to Cohen and Turnbull, a single step of the diffusion transport was completed when an unoccupied volume is occupied by the diffusing molecule and did not require a molecule

to attain energy level sufficient to overcome activation energy barrier. According to Cohen and Turnbull, dispersion of free volume elements within a polymer of a specific size sufficient to accommodate a diffusing molecule influence the mass transport. Hence, they developed a distribution function that is based on the probability of finding a free volume of a specific size and hence the diffusion coefficient dependence on such probability can be described as,

$$D = A \exp(-\gamma V/V_f) \quad (3)$$

Where, D is the diffusion coefficient, V is the size of diffusing species and V_f is the average free volume within the polymer, γ is a correction factor to account for any overlap of free volume elements and A is proportionality constant. Numerous investigations of free volume both theoretically and experimentally have been attempted since then. Below is a summary of some of the studies in different polymer systems and their interpretation.

Most popular technique used in measuring free volume is by Positron Annihilation Lifetime Spectroscopy (PALs). In this technique, a positron emitted from a Na^{22} isotope is injected into a polymer, it forms positronium, which prefers to stay in free volume space. Monitoring the lifetime of positronium inside a polymer matrix can then be analytically related to the radius of free volume space, as the positronium annihilated when it comes in contact with the electron from the surrounding polymer chains. This technique has been widely used to study the properties of polymers including crystallinity, electro-negativities and polymerization [48]. Paul et al., in 1987, related the observed antiplasticization in polysulfones and poly (phenylene oxide) to mixture-free

volume reduction in these polymers, when diluents were added. The approach was very simple in that the free volume was calculated from the specific volume and the volume occupied, which was individually calculated from the group contribution. The conclusion thus was that the best antiplasticizer was the one with the lowest free volume and miscible with the polymer. It was also observed that there was a change in solubility of the gases, but their contribution was less significant when compared to the contribution from the free volume change [49-51]. This is, however, a theoretical explanation and is not completely acceptable because the method of group contribution is complementary but is not a sufficient explanation for the observed phenomenon. McCaig and Paul, in 1999, developed a mathematical model that explained two simultaneous mechanisms of free volume loss, such as (1) free volume diffusion to the film surface, which is thickness dependent and (2) lattice contraction, which is thickness independent [52]. Simha–Boyer proposed the concept of iso-free volume in 1962, according to which, glass transition occurs in a polymer when the ratio of free volume and specific volume in polymers approaches a value of 0.025 ± 0.003 [53, 54]. Alentiev and Yampolskii in 2002, observed good relation between the size and concentration of free volume elements to diffusion length using Meares equation [55]. Thus, as it is seen in the above literature, estimation of free volume pocket size within polymer matrix is an essential parameter that describes mass transport through polymer membranes.

1.6 Conclusions

The lack of fundamental understanding of the physicochemical properties and their dependence on film dimensions in the above mentioned applications like mass

transport in polymer membranes, photoresists used in semiconductor industry and proton exchange membrane in fuel cells, pose a significant roadblock to the rational design of improved materials and processes for these applications. Thus, the work reported here aims at a clear understanding of the mechanism involved in the discontinuity of the physicochemical behavior in such ultra thin films in the hopes that, useful phenomena can be exploited while undesirable effects can be mitigated through proper choice of resist design, formulation, and processing. The overall hypothesis of the research is that, both changes in chain mobility as well as free volume contributions can lead to a rich diversity of polymer thin film behavior, observed thus far.

1.7 References

1. Rebai, M., Prat, M., *Scale effect and two-phase flow in a thin hydrophobic porous layer. Application to water transport in gas diffusion layers of proton exchange membrane fuel cells.* Journal of Power Sources, 2009. **192**(2): p. 534-543.
2. Pearce, E.M., ed. *Polymers*. 1995, National Academy Press: Washington D.C.,.
3. Seymour, R.B., Battista, O.A., et al., ed. *Applications of polymers*. 1988, Plenum Press.
4. Jones, D., ed. *Pharmaceutical Applications of Polymers for Drug Delivery*. 2004, Rapra Technology: Shropshire, UK.
5. Goosey, M.T., ed. *Electronics Applications of Polymers II*. 2000, Rapra Technology Ltd: Shropshire, UK.
6. Smith, R., ed. *Biodegradable polymers for industrial applications*. 2005, Woodhead Publishing Limited and CRC Presss LLC: Boca Raton.
7. Lee, K.-S., ed. *Polymers for photonics applications: Volume 2*. 2003, Springer-Verlag Berlin Heidelberg New York: Berlin.
8. Mahapatro, A., et al., ed. *Polymers for biomedical applications*. 2008, American Chemical Society.
9. Blythe, A. R., et al., ed. *Electrical properties of polymers*. 2005, Cambridge University Press: New York.
10. Chandrasekhar, P., ed. *Conducting polymers, fundamentals and applications: a practical approach*. 1999, Springer.

11. Kosheleva, M., et al., *Investigation and calculation of diffusion processes in thin fibre materials and fibre-forming polymers.* Fibre Chemistry, 2007. **39**(3): p. 178-179.

12. Jiang, D., et al., *Synthesis of Polymer Thin Film Gradient with Nanometer Thickness through Water Diffusion Controlled Surface Polymerization.* Macromolecules, 2009. **43**(1): p. 71-76.

13. Van Dover, R.B., Schneemeyer, L.F., Fleming, R.M., *Discovery of a useful thin-film dielectric using a composition-spread approach.* Nature, 1998. **392**(6672): p. 162-164.

14. Deppe, D.D., Dhinojwala, A., Torkelson, J.M., *Small Molecule Probe Diffusion in Thin Polymer Films Near the Glass Transition: A Novel Approach Using Fluorescence Nonradiative Energy Transfer1.* Macromolecules, 1996. **29**(11): p. 3898-3908.

15. Edwards, D.A., *Non-fickian diffusion in thin polymer films.* Journal of Polymer Science Part B: Polymer Physics, 1996. **34**(5): p. 981-997.

16. Uzodinma, O., *Thin film instabilities and implications for ultrathin resist processes.* Journal of Vacuum Science and Technology B, 2000. **18**(6): p. 3381.

17. Moore, G.E., *Cramming more components onto integrated circuits.* Electronics, 1965. **38**.

18. Ito, H., Willson, C. G., *Chemical amplification in the design of dry developing resist materials.* Polymer Eng. and Sci, 1983. **23**: p. 1012-1018.

19. Brown .R., *Brownian motion.* Reports on Progress in Physics, 1939. **5**.

20. Fick, A., *On Liquid Diffusion.* Philosophical Magazine and Journal of Science, 1855. **10**: p. 5.

21. Kee, D.D., Liu, Q., Hinestroza, J., *Viscoelastic (Non-Fickian) Diffusion.* The Canadian Journal of Chemical Engineering, 2005. **83**(6): p. 913-929.

22. Alfrey, T., Gurnee, E.F., Lioyd, W.G., *Diffusion in Glassy Polymers.* Journal of Polymer Science Part.C, 1966. **12**: p. 249-261.

23. Frisch, H.L., Dennelly, R. J., Herman, R., Prigogine, I., ed. *Irreversible Thermodynamics of Internally Relaxing Systems in the Vicinity of the Glass Transition, in Non-Equilibrium Thermodynamics, Variational Techniques and Stability*. 1966, University of Chicago Press: Chicago.

24. Crank, J., Park, G.S., ed. *Diffusion in Polymers*. 1968, Academic Press: London and Newyork.

25. Frisch, H.L., *Isothermal Diffusion in Systems with Glasas like Transitions.* Journal of Chemical Physics, 1964. **41**: p. 3679-3683.

26. Long, F.A., Richman, D., *Concentration Gradients for Diffusion of Vapors in Glassy Polymers and their Relations of Time-Dependent Diffusion Phenomena.* Journal of American Chemical Society, 1960. **82**: p. 513-519.

27. Long, F.A., Richman, D., *Measurement of Concentration Gradients for Diffusion of Vapors in Polymers.* Journal of American Chemical Society, 1960. **82**: p. 509-513.

28. Thomas, N.L., Windle, A.H., *A Deformation Model for Case II Diffusion.* Polymer, 1980. **21**: p. 613-619.

29. Cohen, M.H., Turnbull, D., *Molecular transport in liquids and glasses.* Journal of Chemical Physics, 1959. **31**: p. 1164.

30. Keddie, J.L., Jones, R.A.L., Cory, R.A., *Interface and surface effects on the glass-transition temperature in thin polymer films.* Faraday Discussions, 1994. **98**: p. 219-230.

31. Wittmann, J.C., Kovacs., A.J., Journal of Polymer Science C 1969. **16**: p. 4443.

32. Gutowski, W., ed. *Fundamentals of Adhesion*. ed. L.-H. Lee. 1991, Plenum: London.

33. Ellison, C.J., *Confinement and processing effects on polymer thin films.* Journal of European Physics E, 2002. **8**: p. 155-166.

34. Torkelson, J.M., *Molecular Probe Techniques for studying diffusion and relaxation in thin and ultrathin polymer films.* Journal of Polymer Science B. Polymer Physics, 1997. **35**: p. 2795.

35. Singh, L., Ludovice, P., Henderson, C.L., *The influence of film thickness and molecular weight on the thermal properties of ultrathin polymer films*, in *Chemical and Biomolecular Engineering*. 2003, Georgia Institute Of Technology: Atlanta.

36. Singh, L., Ludovice, P., Henderson, C.L., *Influence of film thickness, molecular weight and substrate on the physical properties of photoresist polymer thin films.* Proceedings of SPIE, 2003. **5039**.

37. Pochan, D.J., Lin, E. K., Satija, S., Cheng, Z. D., Wu, W-L., *Thermal Expansion and Glass Transition Behavior of Thin Polymer Films With and Without a Free*

Surface Via Neutron Reflectometry. Materials Research Society Symposium Proceedings, 1998. **543**.

38. Kahle, O., Wielsch, U., Metzner, H., Bauer, J., Uhlig, C., Zawatzki, C., *Glass transition temperature and thermal expansion behaviour of polymer films investigated by variable temperature spectroscopic ellipsometry.* Thin Solid Films, 1998. **313-314**: p. 803-807.
39. Singh, L., Ludovice, P.J., Thin Solid Films, 2004. **449**(1-2): p. 231.
40. Soles, C.L., Jones, R.L., et al., Proceedings of SPIE, 2003. **5039**: p. 366.
41. Tweedie, C.A., Constantinides, G., Lehman, K.E., Brill, D.J, Blackman, G.S, Van Vliet, K.J., *Enhanced Stiffness of Amorphous Polymer Surfaces under Confinement of Localized Contact Loads.* Advanced Materials, 2007. **19**(18): p. 2540-2546.
42. Miyake, K., Satomi,N., Sasaki, S., *Elastic modulus of polystyrene film from near surface to bulk measured by nanoindentation using atomic force microscopy.* Applied Physics Letters, 2006. **89**(3): p. 031925.
43. Soles, C.L., Douglas, J.F., et al., Journal of Polymer Science Part B-Polymer Physics 2004. **42**(17): p. 3218.
44. Vogt, B.D., Soles, C.L., Langmuir 2004. **20**(4): p. 1453.
45. Soles, C.L., Douglas, J.F., Wu, W.L., et al., Macromolecules, 2003. **36**(2): p. 373.
46. Soles, C.L., Lin, E.K., Lenhart, J.L., Jones, R.L., Wu, W-L., Goldfarb, D.L., Angelopoulos, M. *Thin film confinement effects on the thermal properties of model photoresist polymers*. 2001: AVS.

47. Vogt, B.D., Soles, C.L., Lee, H-J., Lin, E.K., Wu, W-L., *Moisture absorption into ultrathin hydrophilic polymer films on different substrate surfaces.* Polymer, 2005. **46**(5): p. 1635-1642.

48. Chen, Z.Q., *Positron Annihilation Study of Free Volume Holes in Polymers.* Journal of Radioanalytical and Nuclear Chemistry, 2003. **255**(2): p. 291.

49. Maeda, Y., Paul, D.R., *Effect of Antiplasticization on Gas Sorption and Transport III: Free Volume Interpretation.* Journal of Polymer Science B. Polymer Physics, 1987. **24**: p. 1005.

50. Maeda, Y., Paul, D.R., Journal Polymer Science Polymer Physics, 1987. **25**: p. 957.

51. Maeda, Y., Paul, D.R., Journal of Polymer Science Polymer Physics, 1957. **25**: p. 981.

52. McCaig, M.S., Paul, D.R., Barlow, J.W., *Effect of film thickness on the changes in gas permeability of a glassy polyarylate due to physical aging II. Mathematical Model.* Polymer, 2000. **41**: p. 639.

53. Fox, T.G., Flory, P.J., *Second order transition temperature and related properties of polystyrene - Part 1. Influence of molecular weight.* Journal of Applied Physics, 1950. **21**: p. 581.

54. Simha, R., Boyer, R.F., *On a general relation involving glass temperature and coefficient of expansion of polymers.* Journal of Chemical Physics, 1962. **37**: p. 1003.

55. Yu, A., Alentiev, A., Yampolskii, Y.P., Journal of Membrane Science, 2002. **206**: p. 291.

CHAPTER 2

DIFFUSION IN PURE POLYMER FILMS

Thin and ultra-thin polymer films are very critical today in a variety of applications including semiconductor manufacturing, biomedical and tissue engineering, and industrial gas separations [1-4], as discussed in section 1.1. In particular, mass transport within and through polymer films and membranes is an important issue in a range of applications including membrane-based industrial gas separations [3], controlled drug release in drug delivery [5], encapsulation materials used to prevent oxygen and moisture penetration into electronic devices [6], photoresist materials used in microelectronics fabrication [7], and polymer proton exchange membranes used in fuel cells [1]. A wide range of polymer properties, including glass-transition temperature [8-15], coefficient of thermal expansion [13, 16-18], diffusion coefficient [11, 19-24] and elastic modulus [25-28], have been reported to deviate from their bulk values as polymer samples are prepared in thin film form. Recent studies of diffusion coefficients of penetrants (e.g. water, acid etc.,) in thin spin cast films of various polymers (e.g. polymethyl methacrylate, polystyrene, polycarbonate etc.,) using different techniques (e.g. neutron scattering, X-ray reflectivity, quartz crystal microbalance etc.,) have shown that the diffusion coefficients exhibit several orders of magnitude deviation from expected bulk values [11, 19-24, 29] for thin films. Such strong dependence of the physical property behavior of thin polymer films on sample dimensions could potentially be either detrimental or beneficial depending on the particular application. More importantly, the simple lack of a fundamental understanding of the underlying causes for

such deviations in the physicochemical properties of polymer thin films, the ability to predict the magnitude of the expected property changes in a given situation, the relationship between the polymer behavior and factors such as sample dimensions and preparation methods poses a significant roadblock to the rational design of materials and processes, for a particular application involving the use of such thin polymer films. Therefore, the objectives of this research work are to: (1) investigate the possibility to develop a set of rules to better predict the diffusion behavior in thin polymer films, (2) to provide a more fundamental explanation as to the root causes of the observed dependence of diffusion coefficient on polymer thin film dimensions, and (3) to probe the degree to which such anomalous diffusion behavior impacts the performance of polymer thin films systems in which transport processes other than simple concentration gradient-based diffusion of neutral molecules occurs (e.g. proton, water, and fuel transport in polymer proton exchange membranes and photoacid diffusion in photoresist ultra-thin films). In this chapter, the diffusivity and solubility of water molecules in films of poly (methyl methacrylate) (PMMA) has been studied as a function of film thickness for film thicknesses ranging from 25 nm to 2000 nm and this behavior has been correlated with changes in the free volume distribution in such thin films as determined by Positron Annihilation Lifetime Spectroscopy (PALS).

2.1 Introduction

Recent studies have shown that a wide variety of polymer film properties deviate from bulk behavior as the film thickness decreases below a critical value include glass-transition temperature [8-15], coefficient of thermal expansion [13, 16-18], diffusion

coefficient [11, 19-24] and elastic modulus [25-28]. Scaling of this critical film thickness has been found to vary over a wide range of length scales. For example, it has been observed that the apparent T_g of supported polymer thin films can decrease when the film is coated on a weakly interacting substrate (e.g. a weakly interacting substrate-polymer combination is represented by PMMA on a gold surface as used in the experiments reported in this chapter) [30]. Current explanations for this behavior are based on increased polymer chain mobility near the film substrate interface due to the weak interaction. On the other hand, recent experiments have shown that the diffusion coefficient of small molecules (e.g. water, solvents, and gases) in such supported thin films decreases dramatically as the film thickness decreases [4, 19, 20]. If the entire set of phenomena are due to variations in polymer chain mobility and dynamics as others have suggested, the T_g results suggest higher chain mobility in thinner films (or perhaps more accurately that a larger portion of the film is made up of chains exhibiting higher mobility) while the diffusion results would seem to indicate decreased chain mobility and slower segmental dynamics. If the explanations describing the effects of thickness on local and apparent global T_g are correct, then the reduced diffusion coefficient reported [4, 19, 20] and this current polymer ultra-thin film study must be due to some other phenomenon.

While many of these diffusion studies have investigated the effect of thickness, they have only investigated films with a thickness of 200 nm and less. While T_g over this thickness range of up to 200 nm has been shown to approach the value of bulk samples, the reported diffusion coefficients are often still at least one order of magnitude lower than bulk values. To date, there has been little explanation for why they do not approach

bulk values and likewise, little investigation has been done on the effect of thickness on diffusion for films of intermediate thickness (greater than 200 nm). In order to better understand why these ultra-thin films do not approach bulk values, this study looks at the diffusion coefficient in both ultra-thin (< 100 nm thick) and thin films over a large enough thickness range to approach bulk values of diffusion coefficient. Also, since previous studies of supported polymer films have reported concentration gradients near the substrate film interface, two different substrates are used here in the diffusion study of ultra-thin polymer films [31-33] to understand the influence of the substrate on the interpretation of such results. In addition, Positron Annihilation Lifetime Spectroscopy, widely used in the quantitative evaluation of free volume size and distribution [34] in polymers, has been used here to study the free volume in thin spin-cast polymer films since the size and distribution of free volume in a polymer is expected to directly affect the diffusion of small molecules through the polymer matrix.

2.2 Experiment

Diffusion measurements were made using PMMA, Mw = 298,000, Mn = 292,000, PDI = 1.02 (Scientific Polymer Products Inc.,). The polymer was dissolved in toluene and spin-coated onto gold coated quartz crystal microbalance (QCM) crystals (CEE Model 100 CB spin coat and bake system) and soft-baked at 90ºC for 4 minutes in contact on a hot-plate, to create polymer films. Films of different thicknesses were made by varying polymer content in the solution (0.5 wt% to 8 wt% solids) and spin speed of the spin coater (1000 rpm to 4000 rpm for 60 seconds). An M-2000 ellipsometer (J.A. Woollam, Inc.) was used to measure film thicknesses using a Cauchy layer to model the

stack of polymer film on gold. This procedure was used for making all the films used in the study of diffusion, free volume and for the substrate influence. The substrates were different depending on the study. A gold coated quartz crystal was used in diffusion study (Section 2.3), silicon wafer pieces with native oxide were used in free volume study (Section 2.5) and silicon dioxide deposited gold quartz crystals were used in substrate influence study (Section 2.7).

A Maxtek Inc., quartz crystal microbalance (QCM) with 5MHz gold plated quartz crystals (model SC-501-1) was used to measure mass uptake and mass loss in polymer films during sorption/desorption cycles. QCM is a sensitive mass sensing device that accurately relates mass deposited on the surface of the crystal to frequency shift of its oscillation. This is explained in detail in Section 2.3. A custom built flow-cell system shown in Figure 2.1 was used to introduce low and high humidity nitrogen streams into the QCM sample holder. Pressurized nitrogen was obtained from the head space of a liquid nitrogen container. The stream was split, one branch (dry) was introduced directly into the QCM sample holder chamber; the other branch (wet) was passed through three bubblers of de-ionized water. The flow rate of both streams was balanced and controlled by passing them each through individual mass flow controllers set at 0.350 cubic feet per minute. All sorption and desorption experiments were performed almost within few minutes to an hour of film preparation.

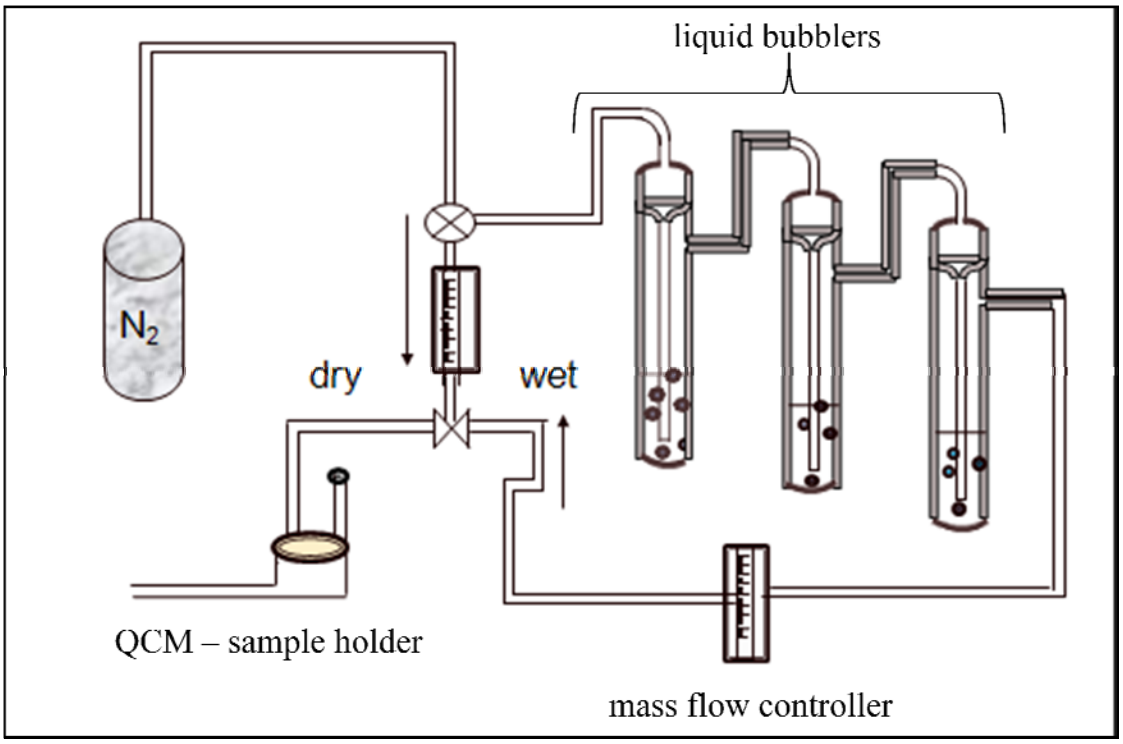

Figure 2.1 Schematic representation of the flow cell used with Quartz Crystal Microbalance

2.3 Results and Discussion

QCM is a useful tool to measure mass uptake in thin and ultra-thin films because it has very high sensitivity to mass changes. This is required because the total amount of penetrant sorbed into the film during sorption is relatively low in thin and ultra-thin films. Raw QCM data is collected as oscillation frequency of the crystal and can be converted to mass using Equation (1), the Sauerbrey equation [35]. In the Sauerbrey equation, Δf is the frequency change (before and after sorption for mass uptake or before and after desorption for mass loss), Δm is the mass change, f_0 is the resonant frequency of the crystal, A is the electrode surface area, ρ_q is the density of quartz, μ_q is the shear modulus

of the quartz crystal, and C_f is a constant that describes the sensitivity of the QCM based on the crystal parameters.

$$\Delta f = -\frac{2 f_0^2}{A\sqrt{\rho_q \mu_q}} \Delta m = -C_f \Delta m \tag{1}$$

When penetrant is sorbed into the polymer film on quartz crystal, the frequency of the crystal decreases due to increase in mass of the polymer film. Likewise, during desorption, the frequency increases due to mass loss of sorbed penetrant from polymer film on the crystal. Figure 2.2 shows a typical QCM frequency response for sorption and desorption of water vapor into and out of a film of PMMA. Using Equation (1) the frequency change can be converted to a mass change to obtain mass uptake curves that can be fit to models to obtain diffusion coefficient for different samples.

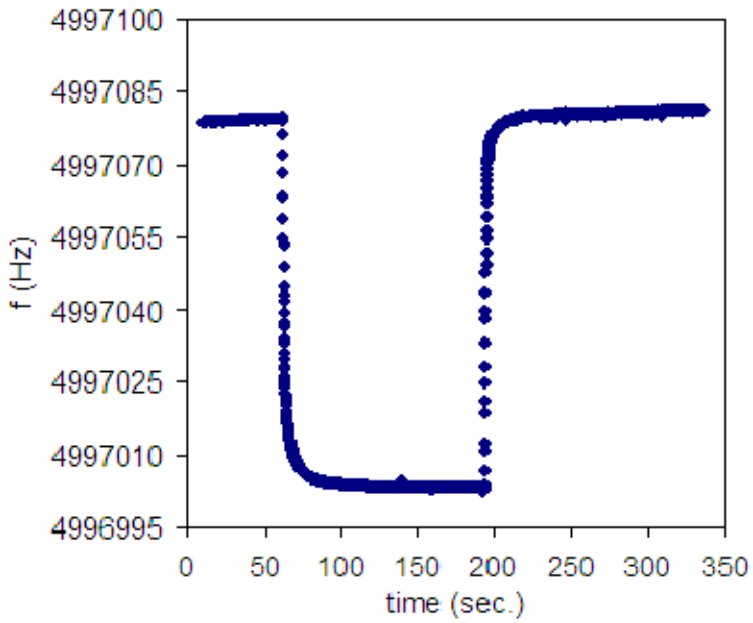

Figure 2.2 Typical QCM frequency change data for sorption and desorption of water vapor in PMMA films on quartz crystals for a film thickness of 905 nm

Since thickness of the films is much less than their width, one can model the system as a semi-infinite slab with one-dimensional diffusion through film thickness. For one-dimensional diffusion on an impermeable substrate with a constant diffusion coefficient, Fick's second law, given in Equation (2), can be solved to give Equation (3) or Equation (4) [5, 36].

$$\frac{\partial c}{\partial t} = D\nabla^2 c \tag{2}$$

$$\frac{M_t}{M_\infty} = 1 - \frac{8}{\pi^2}\sum_{n=0}^{\infty}\frac{1}{(2n+1)^2}\exp\left[-\frac{(2n+1)^2\pi^2 Dt}{h^2}\right] \tag{3}$$

$$\frac{M_t}{M_\infty} = 2\left(\frac{Dt}{h^2}\right)^{1/2}\left(\frac{1}{\pi^{1/2}} + 2\sum_{n=1}^{\infty}(-1)^n \, ierfc\frac{nh}{\sqrt{Dt}}\right) \tag{4}$$

M_t is the mass of penetrant sorbed into or desorbed from the film at any time t, M_∞ is the final equilibrium mass of penetrant in the film, D is the diffusion coefficient of penetrant in the film, and h is the film thickness. While the complete mass uptake curve can, in principle, be fit using Equation (3) or Equation (4) to obtain D, they are both non-linear equations. So, it is easier if one can directly obtain D from the mass uptake curve. The initial mass change in Fickian diffusion processes shows a linear dependence between M_t/M_∞ and $t^{1/2}$. This linear region provides a way to obtain D directly from the initial slope of a plot of M_t/M_∞ vs. $t^{1/2}$ by using Equation (5), obtained from Equation (4) in the limit of short times.

$$\frac{M_t}{M_\infty} = \frac{2}{h}\left(\frac{Dt}{\pi}\right)^{1/2} \tag{5}$$

Figure 2.3 shows a comparison between typical experimental mass uptake curves, the full Fickian diffusion model (Equation (3)), and the short time Fickian model (Equation (5)). The short time model, the full model, and the experimental data all overlap at low fractional mass uptakes ($M_t/M_\infty < 0.6$), while they all deviate at higher fractional mass uptakes. Thus, it is clear that the simple constant diffusion coefficient Fickian model does not appear to adequately describe the complete sorption behavior of the polymer. This is not unexpected since polymers are well known to exhibit non-Fickian behavior. However, at short times, the behavior can be, and conventionally is,

described by Fickian diffusion; this is shown to be valid later in this section. Since the Fickian behavior is valid at short times, and the short time Fickian model is valid over this time range, diffusion coefficients reported are obtained using the slope of M_t/M_∞ vs. $t^{1/2}$ curves for periods where $M_t/M_\infty < 0.6$.

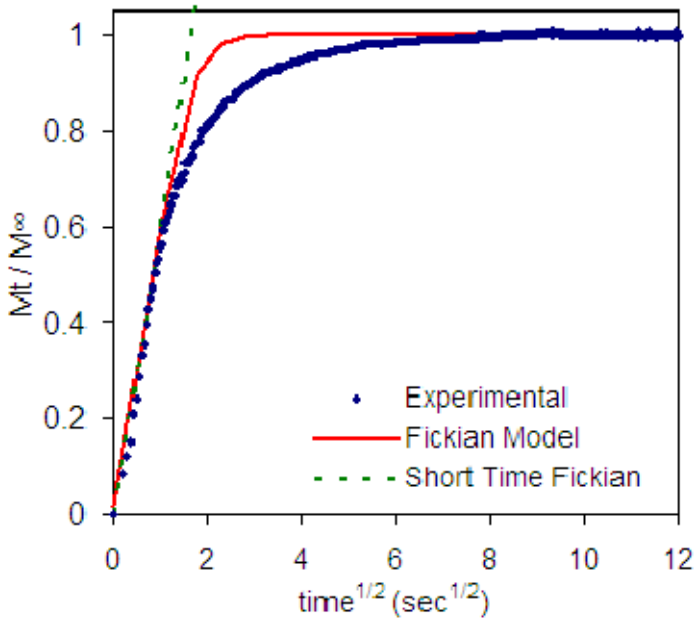

Figure 2.3 Mass uptake plot of M_t/M_∞ vs. $t^{1/2}$ showing water vapor sorption in 545 nm PMMA film. Experimental data is compared with full Fickian model (Equation (3)) and short time Fickian model (Equation (5))

As mentioned earlier, diffusion in polymers is often found to not be purely Fickian. Diffusion in polymers has often been characterized by different uptake behaviors like Case II diffusion [5] and two-stage mass uptake [36] processes. One common model that is used for polymers is the Long-Richman model, which is a two-stage mass uptake model and is shown in Equation (6) [37]. The Long-Richman model describes what is referred to as dual mode sorption, that is, there are two modes of

sorption, one a standard Fickian mass uptake controlled by chain mobility and free volume, and the other a polymer relaxation controlled mass uptake wherein the polymer changes conformation or swells to allow additional penetrant to be sorbed into the polymer matrix. The Long-Richman equation can be thought of as a linear superposition of diffusion and relaxation controlled uptake.

$$\frac{M_t}{M_\infty} = \varphi\left(1 - \frac{8}{\pi^2}\sum_{n=0}^{\infty}\frac{\exp\left(-\frac{(2n+1)^2\pi^2\theta}{4}\right)}{(2n+1)^2}\right) + (1-\varphi)\left(1 - \frac{\tan\sqrt{\psi}\exp(-\psi\theta)}{\sqrt{\psi}} - \frac{8}{\pi^2}\sum_{n=0}^{\infty}\frac{\exp\left(-\frac{(2n+1)^2\pi^2\theta}{4}\right)}{(2n+1)^2\left(1-\frac{(2n+1)^2\pi^2}{4\psi}\right)}\right) \quad (6)$$

In the Long-Richman model given in Equation (6), Φ relates fraction of mass uptake that is diffusion controlled to the fraction that is relaxation controlled, ψ relates rate of polymer relaxation to rate of diffusion (i.e. the inverse of the diffusion Deborah number) and dimensionless time θ is Dt/h^2, D is the diffusion coefficient, t is time and h is film thickness. Figure 2.4 shows a comparison of the fit of Fickian diffusion model with the fit of dual mode Long-Richman model of mass-uptake in PMMA. This figure shows that the Long-Richman model adequately fits the experimental data for the diffusion of penetrant and any macromolecular relaxation of the polymer film and it is typical for all film thicknesses. Furthermore, the value of diffusion coefficient obtained from the fit of dual mode model is, within error, the same as the value obtained from the

short time Fickian model fit. This implies that the short time Fickian model can be used to obtain diffusion coefficients for this system.

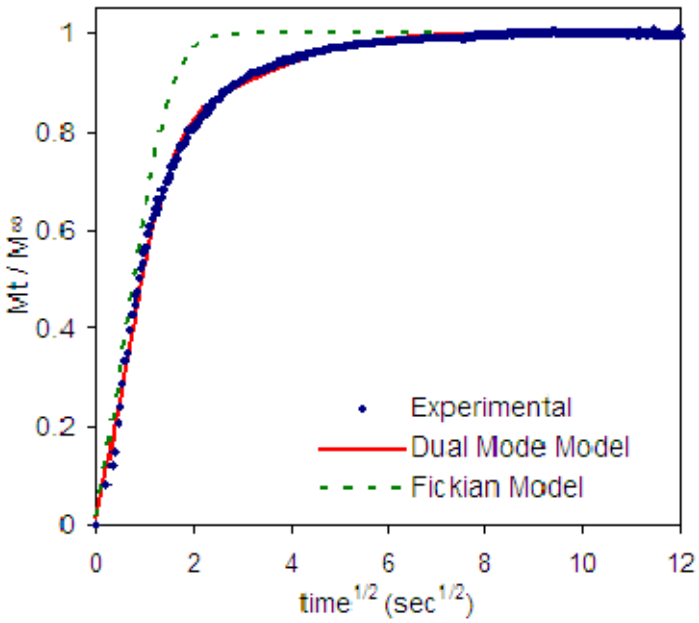

Figure 2.4 Mass uptake plot of M_t/M_∞ vs. $t^{1/2}$ showing water vapor sorption in 545 nm PMMA film compared with the dual mode (Long-Richman) model (Equation (6)) and the Fickian model (Equation (5))

Using the methods described above from Equation (3) to Equation (6), one can generate a plot of diffusion coefficient as a function of film thickness as shown in Figure 2.5. The bulk value obtained for an 8 μm film from literature [16] is shown as red line in the figure. For comparison, diffusion coefficients from both Fickian and dual-mode models are presented in Figure 2.6 (a) over the entire thickness range. In this case, the observed differences in diffusion coefficients are within the confidence intervals. The diffusion coefficients plotted in Figure 2.5 and 2.6(a) is from absorption cycles. The

diffusion coefficients calculated from absorption and desorption did not vary much and are listed in Table 2.1(a) for comparison.

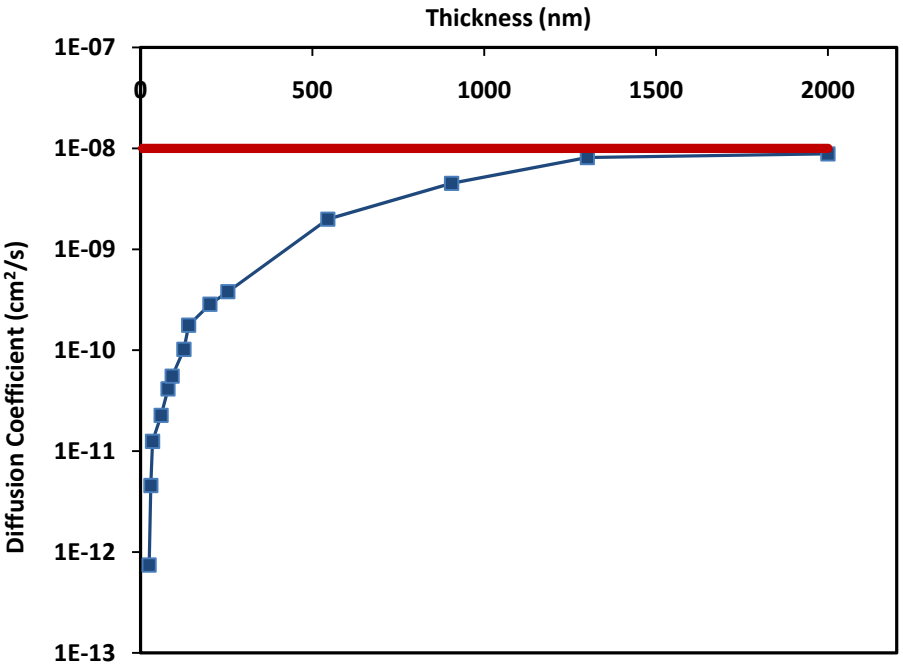

Figure 2.5 Diffusion coefficient of water in PMMA as a function of film thickness determined using short time Fickian model given in Equation (6). Red line represents bulk value reported in literature [16]

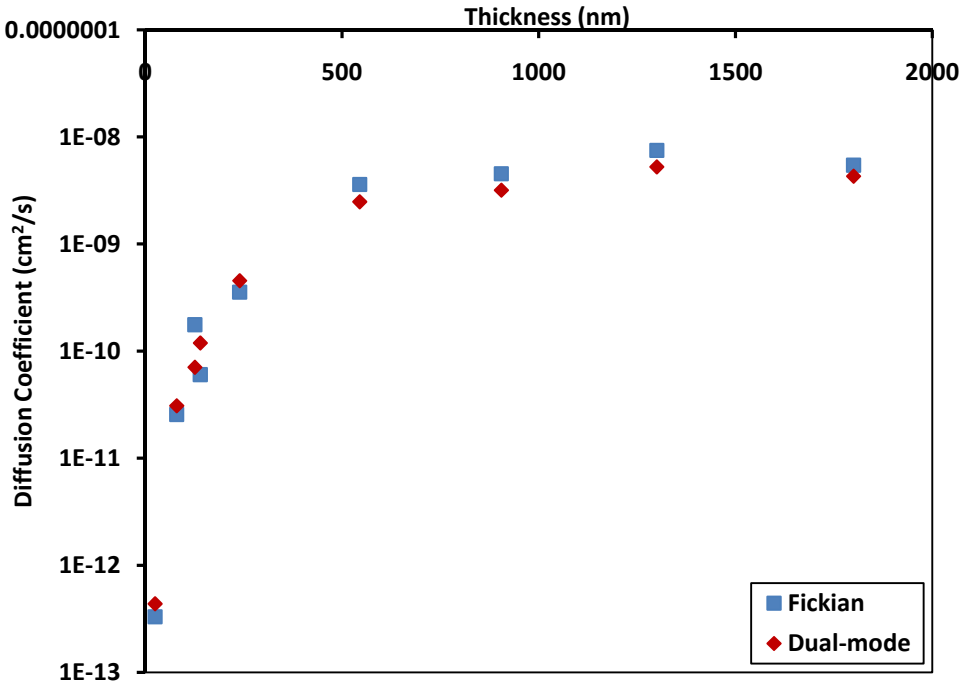

Figure 2.6 (a) Diffusion coefficient of water in PMMA as a function of film thickness determined using short time Fickian model and dual-mode model

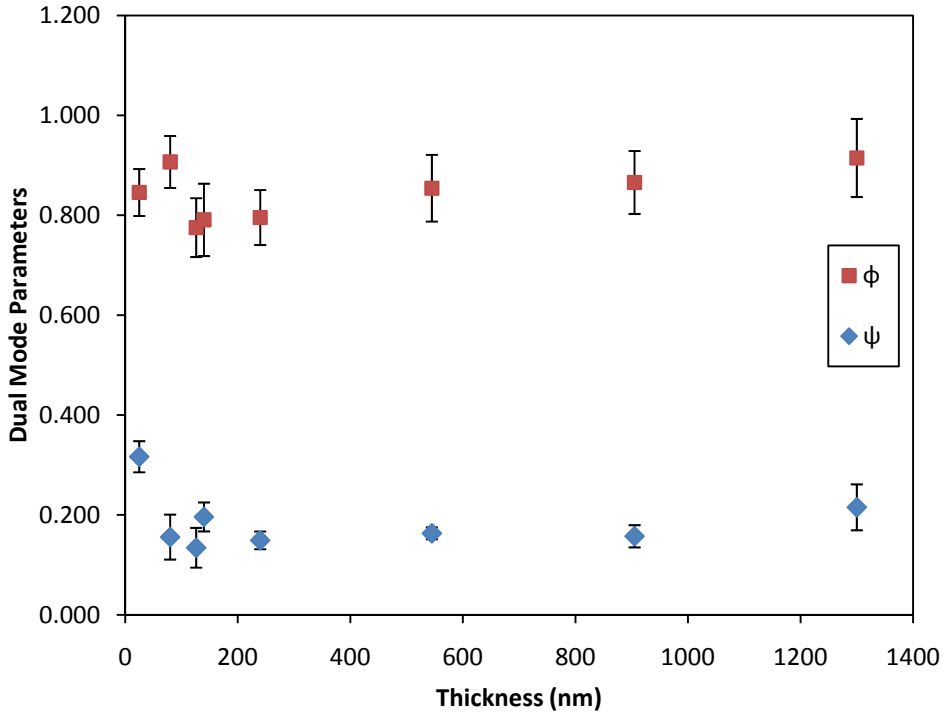

Figure 2.6 (b) Fit parameters for the dual-mode Long-Richman absorption model for different film thicknesses: dimensional quantities, ψ is Deborah number inverse and φ is C_0/C_∞, ratio of mass uptake due to diffusion to mass uptake due to relaxation

Table 2.1(a) Diffusion Coefficients calculated by Fickian model for absorption and desorption cycles

Thickness	Dsorption	Ddesorption
nm	cm^2/s	cm^2/s
25	7.43E-13	9.74446E-13
80	4.14E-11	4.43378E-11
126.2	1.02E-10	1.39044E-10
140	1.77E-10	1.3421E-10
545	1.99E-09	2.54688E-09
254	3.8E-10	5.10345E-10
905	4.51E-09	6.33473E-09

Table 2.1(b) Diffusion Coefficients by Fickian and dual mode models and fit parameters for the dual mode Long-Richman model

Thickness	D - Fickian	D - Dual	ϕ	ψ
nm	cm^2/s	cm^2/s	C_0/C_∞	kh^2/D
25	3.31E-13	4.37E-13	0.846 ± 0.047	0.317 ± 0.0312
80	2.56E-11	3.08E-11	0.907 ± 0.052	0.156 ± 0.045
126.2	1.76E-10	7.06E-11	0.775 ± 0.059	0.134 ± 0.04
140	6.03E-11	1.19E-10	0.791 ± 0.072	0.196 ± 0.029
240	3.55E-10	4.53E-10	0.795 ± 0.055	0.149 ± 0.018
545	3.59E-09	2.47E-09	0.854 ± 0.067	0.163 ± 0.012
905	4.53E-09	3.17E-09	0.865 ± 0.063	0.157 ± 0.022
1300	7.48E-09	5.24E-09	0.915 ± 0.063	0.215 ± 0.046

Also, analysis of the data with dual mode sorption model yields fit parameters shown in Figure 2.6 (b) comparable to those reported in literature [25]. As it can be seen from Figure 2.6 (a), diffusion coefficient deviation with film thickness is observed in case of both Fickian and dual mode sorption models, the values of diffusion coefficient show small differences because diffusion coefficient in calculated from the initial absorption where the two models are similar. When diffusion of water molecules is controlled by confinement effects, relaxation controlled absorption should be influencing the amount absorbed. From Figure 2.6 (b) it can be seen that, based on the trend of the dual mode parameter φ the ratio of the amount of diffusion controlled to relaxation controlled absorption are almost a constant for the entire thickness range. Also, the ratio of diffusion time constant to relaxation time constant is also observed to not change significantly with change in film thickness except in case of films less than 50 nm as this could be due to influence of substrate film interface, but no firm conclusion can be drawn given the small number of data points in this thickness range.

In addition to the investigation of the two models, the rate limiting step in mass transport of water molecules through PMMA was also analyzed. For short time mass uptake, the rate of absorption was observed to be identical to the rate of desorption, which confirms that the mass transport in PMMA is diffusion controlled and not interface mass transport limited. Further, the normalized fractional mass uptake curve (M_t/M_∞) was found to be a function of time normalized by thickness squared (t/h^2). This shows that, for the system under consideration, Fickian diffusion with constant diffusivity is the rate limiting step. Also, in case of interface mass transfer limited absorption and desorption in polymer films, mass uptake curves scale with time normalized by membrane thickness

(t/h) [38], which was not observed for the mass uptake curves of water in PMMA. All these observations justify the modeling of mass transport of water in PMMA as Fickian diffusion at short time scales. Further, the time scales for diffusion and mass transfer through cell volume was analyzed and compared to ensure that the rate of mass uptake observed was only due to diffusion resistance within the film. At the flow rate of 0.35 cu.ft/min used for the flow of gases, it takes 44.1 milliseconds to fill the flow cell volume with the penetrant gas. With reference to Figure 2.4, the first 60% of mass uptake (short-time Fickian diffusion), happens in about 4 seconds. So the time taken for mass uptake observed is about 100 times slower than that taken for external mass transfer of penetrant gas through the cell volume. This confirms that the mass uptake reported here is entirely due to mass transfer within the film. Also, the gas phase boundary layer offering any resistance to the transport (interfacial mass transfer coefficient, $k_{interface}$) of water from the gas phase into thin polymer film is also analyzed. Diffusion coefficient of water vapor in nitrogen gas is 0.29 cm^2/s [39]. The gas phase boundary layer thickness (δ), if any, should be less than the diameter of the sample holder, 2.54 cm. This shows that $k_{interface} = D_{gas}/\delta >$ 0.114 cm/s. Biot number ($Bi = (k_{interface}h)/D_{film}$), which is ratio of mass transport across vapor film interface to diffusion rate through film thickness, was calculated and found that $Bi >> 1$ for the entire range of film thickness investigated in this work. This shows that the mass transport is controlled by diffusion transport within the membrane and the time scale for the transport is characterized by h^2/D. This further confirms that the process of diffusion of water vapor within the polymer films is slow and is the rate-limiting step.

Figure 2.5 and Figure 2.6 (a) show that the diffusion coefficient decreases in a highly non-linear fashion with decrease in film thickness. This trend is similar to the trend reported in previous studies of this type [16, 40, 41], but with a few important differences. The major difference is that this study shows diffusion coefficients and film thicknesses that extend from the ultra-thin regime all the way to the bulk regime. Previously, measurements were made only in the ultra-thin regime up to film thicknesses of approximately 200 nm. This failure to carefully investigate diffusion in larger thickness range is most likely due to the fact that other deviations from bulk behavior, like glass-transition temperature, were observed in films of about 200 nm thickness. Thus, in these earlier studies, the values of diffusion coefficient obtained at even the largest film thicknesses reported were still at least a few orders of magnitude lower than values obtained on bulk samples [25] and thicker films were not investigated. Since the deviation from bulk film diffusion behavior extends to films thicker than 1000 nm as seen in Figure 2.5, it cannot simply be argued that interfacial effects, which were invoked in explaining anomalous thin film glass-transition behavior, are also responsible for the observed deviation in diffusion. Instead, it is believed that the observed behavior could be an intrinsic property of the thin films and may be due to the processing conditions used in preparing the films.

2.4 Effect of Casting Solvent

One of the processing effects that could be a cause for the observed differences in the diffusion coefficient of thick and thin films is differences in residual casting solvent content as a function of film thickness; as the standard processing conditions outlined in

section 2.2 is identical for all films, the thick films may contain more residual casting solvent than the thin films after soft bake. To test the effect of residual casting solvent, seven new films of different thicknesses, within the thickness range reported in the previous section, were studied again. Diffusion coefficients of these films were measured using QCM immediately after standard processing (casting followed by soft-bake of 90°C for 4 minutes). These diffusion coefficients are marked as pre-oven in the Figure 2.7. The films were then heated to 125°C (i.e. above the glass transition temperature of the polymer (105°C) and the boiling point of the casting solvent (110.6°C)) for 72 hours in a vacuum oven. This heating, combined with high vacuum, was expected to eliminate any residual casting solvent within practically achievable limits. Shown in Figure 2.7 is a comparison of diffusion coefficient of chosen films before and after oven treatment. As it can be seen from the figure, there is some change in the average diffusion coefficient of the film after the oven treatment, but there is no apparent correlation. Also, none of these deviations are statistically significant. Further, these deviations are not of the same orders of magnitude as that observed due to change in film thickness. These observations imply that residual casting solvent does not cause the observed deviation in diffusion coefficient. This is in agreement with a similar annealing study reported by Vogt et al., in films as thin as 5.6 nm [41]. Looking at the figure as a whole, it is apparent that any changes due to the extended vacuum oven annealing, if they exist, are very small relative to the changes due to film thickness.

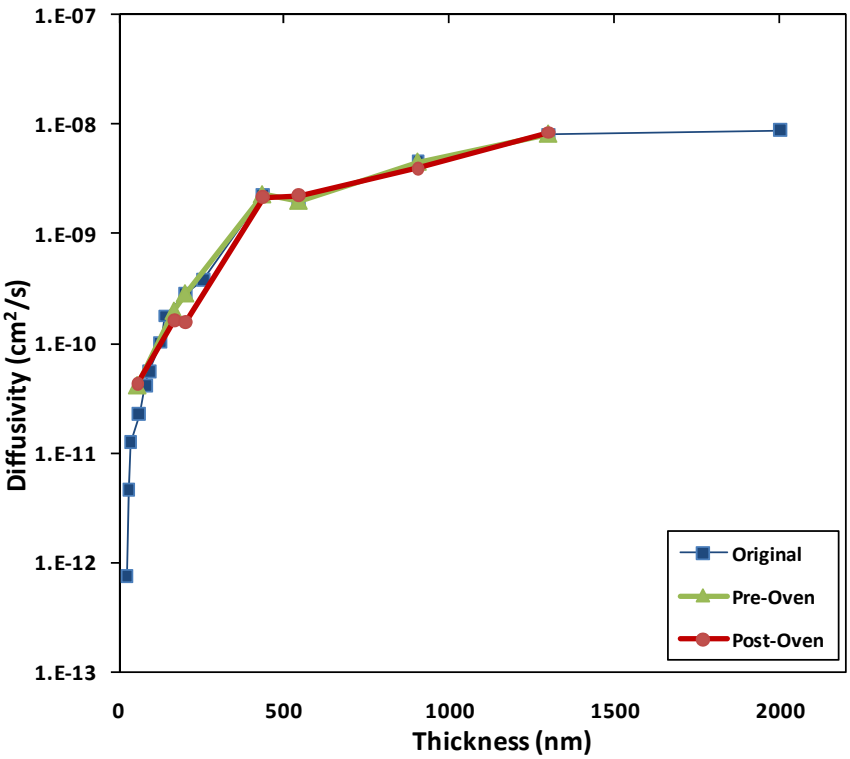
1.E-07
1.E-08
1.E-09
1.E-10
1.E-11
1.E-12
1.E-13
Diffusivity (cm²/s)
0
500
1000
1500
2000
Thickness (nm)
Original
Pre-Oven
Post-Oven

(a)

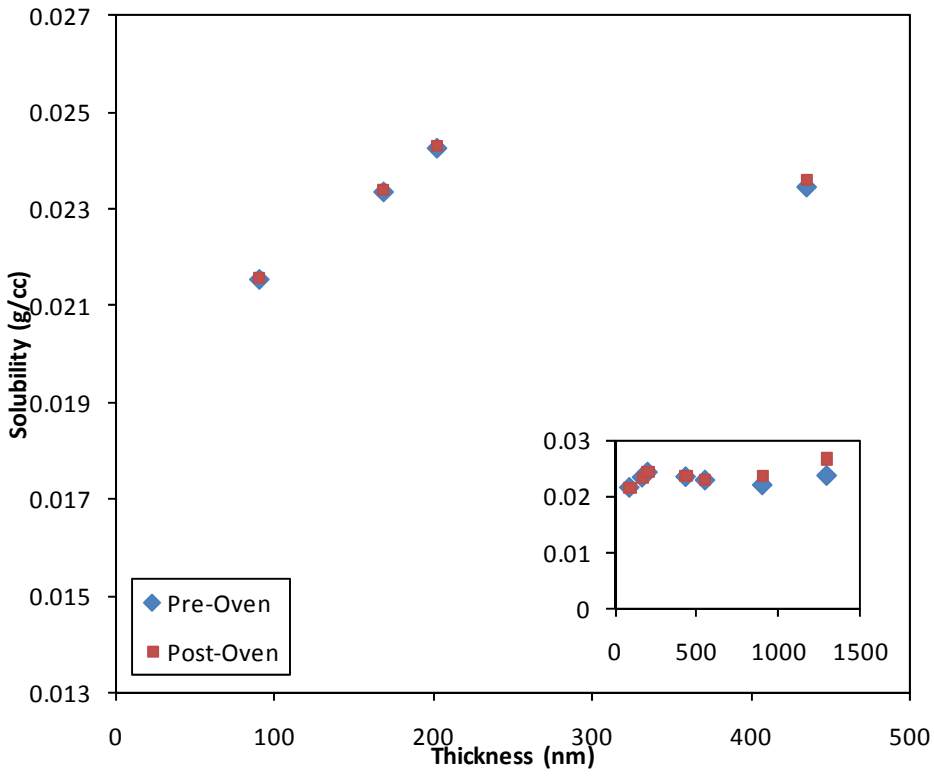
0.027
0.025
0.023
0.021
0.019
0.017
0.015
0.013
Solubility (g/cc)
0
100
200
300
400
500
Thickness (nm)
Pre-Oven
Post-Oven
0.03
0.02
0.01
0
0
500
1000
1500

(b)

Figure 2.7 Comparison of measured (a) diffusion coefficient - Original is the curve shown in Figure 2.5 (b) Solubility – inset shows the entire range. Pre-oven - films immediately after spin casting. Post-oven - after heating the films in a vacuum oven at 125^0C for 72 hours

In addition to measuring diffusion coefficient, mass changes in the films due to loss of residual casting solvent and changes in mass uptake of water before and after the oven treatment were also analyzed. Both thick and thin films lost mass after heating due to loss of residual casting solvent; Figure 2.8 shows mass loss in the films after oven treatment. The amount of mass loss is linearly proportional to the film thickness over this range of film thicknesses, implying that thicker polymer films do, in fact, retain more casting solvent than thinner films after initial casting and post-application baking or soft baking. This relation however, does not continue linearly down to zero residual casting solvent at zero film thickness but at a finite film thickness about 180 nm. This would indicate that there is likely very little extractable solvent left in the ultra-thin films (< 200 nm). This solvent could not be extracted even under rigorous evaporation in vacuum oven above glass-transition temperature of the polymer.

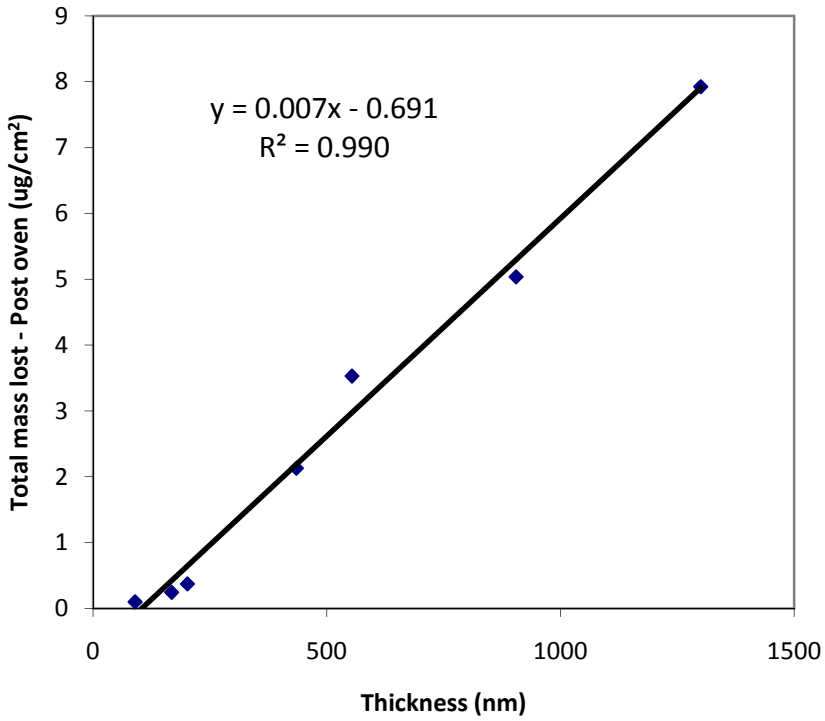

Figure 2.8 Relation between mass loss in film and film thickness after high temperature (125 ^{0}C) vacuum oven treatment for 72 hours

Since there is a loss of mass in the films due to loss of residual casting solvent, it is possible that there is, in turn, more free volume available for mass uptake. Figure 2.9 shows the change in mass uptake in each of the films as a function of film thickness after the vacuum oven treatment. That is, the difference in the amount of penetrant sorbed into the film at equilibrium, before and after oven treatment. It is observed that thicker films that lost more casting solvent uptake more mass after oven treatment.

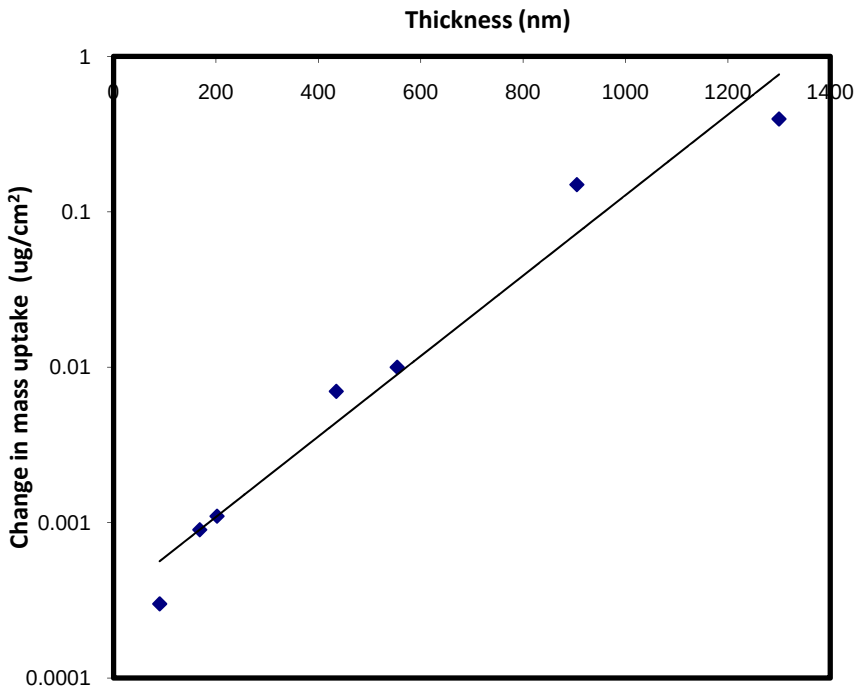

Figure 2.9 Change in total mass uptake for each film after high temperature (125 ^{0}C) vacuum oven treatment for 72 hours as a function of thickness

Although the films uptake more water after oven treatment, a more interesting comparison is the amount of change in mass uptake compared to the amount of mass lost. This is basically Figure 2.9 data divided by Figure 2.8 data. This ratio of change in mass uptake to mass lost, is also observed to increase with increase in film thickness. But the change in mass uptake is small relative to the mass lost; it is less than 5% for the thickest film (1300 nm) reported here and 0.3% for films thinner than 200 nm. This is probably because, when the solvent is leaving the film during the bake, it is also likely that the film has enough mobility to change chain conformation to effectively re-pack and fill many of the new voids left by the solvent. In other words, the total accessible free volume of the

film is likely not significantly different in the film before and after the extended vacuum oven treatment.

In summary, from this collection of experiments to examine the effect of casting solvent, while an increase is observed in the amount of residual casting solvent in thicker films, it is also shown to have little effect on the diffusion behavior in these films. Also, the accessible free volume created in these films due to rigorous evaporation of most of the residual casting solvent is not significantly different from that in as-cast films. So, other possible explanations for deviation in diffusion could be free volume and energy barrier involved in the activated diffusion process, which may be different in thin films.

2.5 Free Volume

The process of diffusion inside a polymer matrix involves two parameters: (i) the probability of finding free volume or unoccupied space in between the polymer chains, and (ii) the energy needed to move through the polymer chains from one free volume site to another, called activation energy for diffusion. It would be interesting to probe these parameters involved in the process of diffusion, as functions of film thickness.

Free volume size in the polymer matrix and its distribution was probed using Slow Positron Annihilation Lifetime Spectroscopy (sPALS) in Dr. Jerry Jean's lab at University of Missouri – Kansas City. sPALS was developed for analysis of microstructure in polymers by measuring the size and content of free volume holes [42]. This is possible because the positronium probe is generally trapped in the free volume holes, with a diffusion length of 10-100 Å and lifetime in the order of a few nanoseconds.

Free volume holes in polymers of the order of a few Angstorms can therefore be easily detected from the length of the existence (lifetime) of positroniums within the polymers. The conventional positron lifetime measurement is possible when a positron is emitted from a ^{22}Na isotope and γ-quantum energy of 1.27 MeV is emitted simultaneously. Other sources of positron are neutron-deficient radioisotopes like ^{58}Co nuclei. The emitted positron loses energy through elastic collision with other molecules within the first few picoseconds. Thus the positron reaches a thermalized stage when it picks up an electron from the environment molecule and forms a positronium, Ps. The time between the formation of this positronium and its annihilation enables the calculation of the size of the free volume. Ps has two states due to different spin, a parallel state called ortho-positronium (o-Ps) and an anti-parallel spin state called para-positronium (p-Ps). However, the annihilation rates of the two states are different, such that the lifetime of o-Ps is in the order of 10^{-9} s while it is in the order of 10^{-10} s for p-Ps. The lifetime and annihilation rate of positrons and p-Ps are smaller than o-Ps. The lifetime of long-lived o-Ps is thus correlated to the free volume pocket size in a polymer. The detailed derivation of the relation between o-Ps lifetime and free volume radius, and approaches for the estimation of free volume size and concentration are discussed in detail in the textbook by Jean Y.C. [42]. A brief description of the model used is discussed here.

For the estimation of the size of free volume hole, a simple model in which positronium particle resides in a spherical well having an infinite potential barrier is considered. The annihilation rate λ, of this positronium which is the reciprocal of the positron lifetime τ_3, is given by the overlap of the positron density $n_+(r) = |\psi_+(r)|^2$ and electron density n.(r) locally in that environment as,

$$\lambda = \frac{1}{\tau_3} = \pi r_0^2 c \int \left|\psi^+(r)\right|^2 n_-(r)\gamma dr \qquad (7)$$

Where r is the position vector, ψ_+ is the positron wave function based on quantum mechanical approach, r_0 is the classical electron radius and c, the speed of light. This simple model for Positronium (Ps) confined in a spherical well and its annihilation inside the electron layer yields a relationship between the annihilation rate and the free volume radius R as

$$\lambda = \frac{1}{\tau_3} = 2\left[1 - \frac{R}{R_0} + \frac{1}{2\pi}\sin\left(\frac{2\pi R}{R_0}\right)\right] \qquad (8)$$

Here, $R_0 = R + \Delta R$ where ΔR is a fitting parameter determined by fitting λ to $1/\tau_3$ for a known free volume hole in molecular substrate and is found to be 1.656 Å.

To evaluate free volume as a function of film thickness, four PMMA films of thicknesses 167 nm, 197 nm, 325 nm, and 5.6 um were investigated using positron spectroscopy. For this, as-cast films that were spin cast and soft-baked at 90^0C for 4 min (standard-processing) on silicon wafer with native oxide, were used. sPALS experiments were performed at 1.5 KeV (which corresponds to 65 nm depth within the film, from the surface) in each sample using slow positron beam (resolution ~ 500 ps). Each sPALS spectrum contains 1 million counts. All sPALS spectra were fitted into three lifetimes using LT-9 and also PATFIT programs: τ_1 ~ 0.125 ns with intensities I_1 ~ 10%, representing p-Ps and annihilation lifetime, τ_2 ~ 0.5 ns with intensities I_2 ~ 60%, representing positron (unbounded) annihilation lifetime, and τ_3 ~ 2.2 ns with intensities

I_3 ~ 30-40%, representing o-Ps annihilation lifetime [34, 42, 43] The free volume pocket size is evaluated from the longest o-Ps lifetime using Equation (8).

Figure 2.10 shows the plot of o-Ps lifetime converted into free volume radius using Equation (8), for different PMMA film thicknesses. This shows that there is a change in the free volume pore radius and it decreases with decrease in film thickness. Free volume, calculated based on the radius and assuming spherical free space, shows a change of approximately 5.6% between film thicknesses 325 nm and 197 nm.

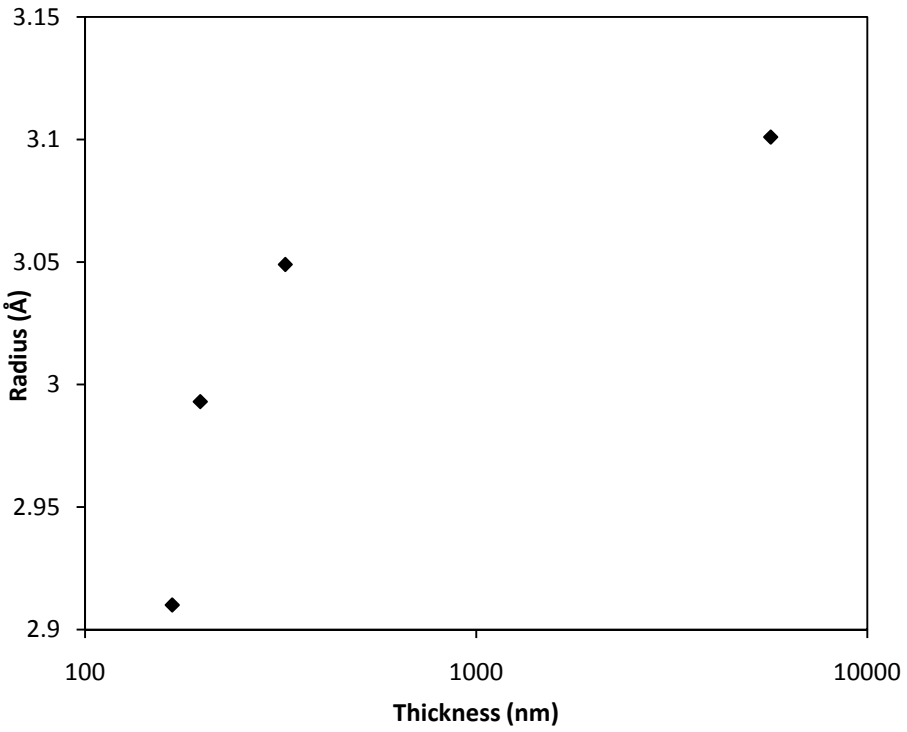

Figure 2.10 Free volume pore radius in thin and thick films calculated from o-Ps lifetime using Equation (8)

To understand if the observed change in free volume size with film thickness explains the observed change in diffusion coefficient, further analysis was based on the theoretical free volume model adopted from literature [44]. The free volume model used in literature to describe mass transport through films of average free volume pocket size V_f was given by Cohen and Turnbull [57]. The model describes redistribution of free volume in a polymer that enables movement of penetrant molecule into a void space larger than critical volume V_c dependent on the size of the penetrant. This definition based on the probability that the polymer segments with free volume pocket volume V_f can form a void space V_c is given as

$$D = A\exp\left(\frac{-B}{V_f}\right) \tag{9}$$

Where D is the diffusion coefficient, A is the pre-exponential factor, $B = \gamma V_c$ and γ ($\sim$ 1 for all polymers) is the overlapping factor for the free volume pockets. Equation (9) that relates diffusion coefficient (D) to free volume pocket size (V_f) is also called activation volume theory because of its similarity to activation energy processes described by Arrhenius relationship, described in detail in Section 2.7. It is interesting to note that, because of the exponential dependence of D on free volume, a small change in free volume could greatly affect the diffusion coefficient in thin films. Hence, attempt was made to relate the measured diffusion coefficient to the observed change in free volume pocket radius from sPALS experiment.

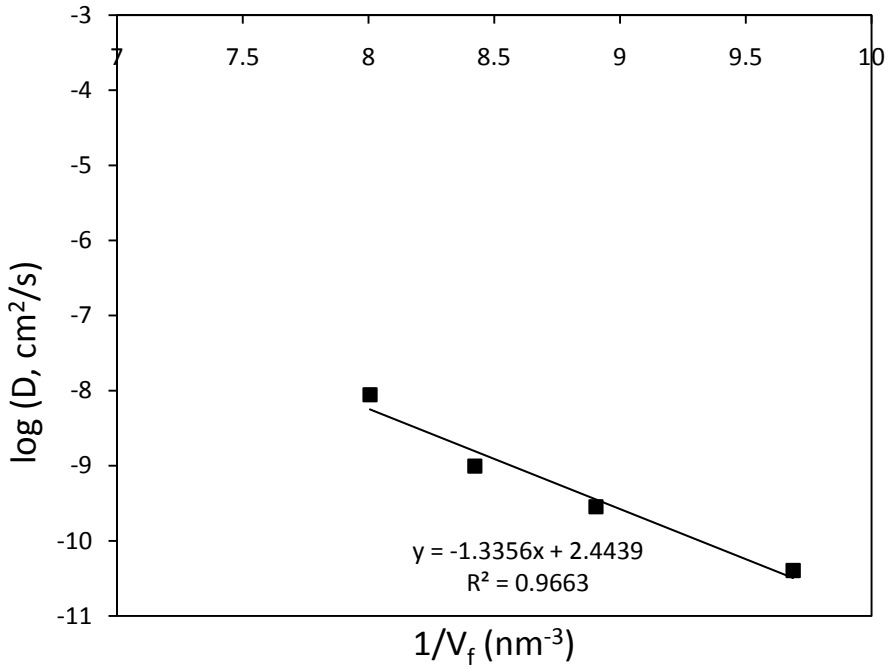

Figure 2.11 Free-volume in polymer films calculated using the pore radius from sPALS experiments, assuming spherical free spaces in polymer films, fitted to measured diffusion coefficient using theoretical model given in Equation (10)

The regression coefficient for the fit is approximately 0.96 in Figure 2.11. This fairly explains that the drop in diffusion coefficient with decrease in film thickness is due to decrease in the free volume pocket size. This is in agreement with similar predictions of drop in free volume size based on increase in selectivity and permeability of gases in the aging studies reported by D.R. Paul et al., [43, 45]. Further investigation of concentration of free volume in thin polymer films by analyzing o-Ps intensity (I_3%) revealed interesting results as shown in Figure 2.12. The intensity of o-Ps gives the number density of free volume holes in polymer films. As it can be seen from Figure 2.12, with decrease in film thickness the number density of free volume pockets is also decreasing, in addition to drop in free volume pocket radius (in Figure 2.10).

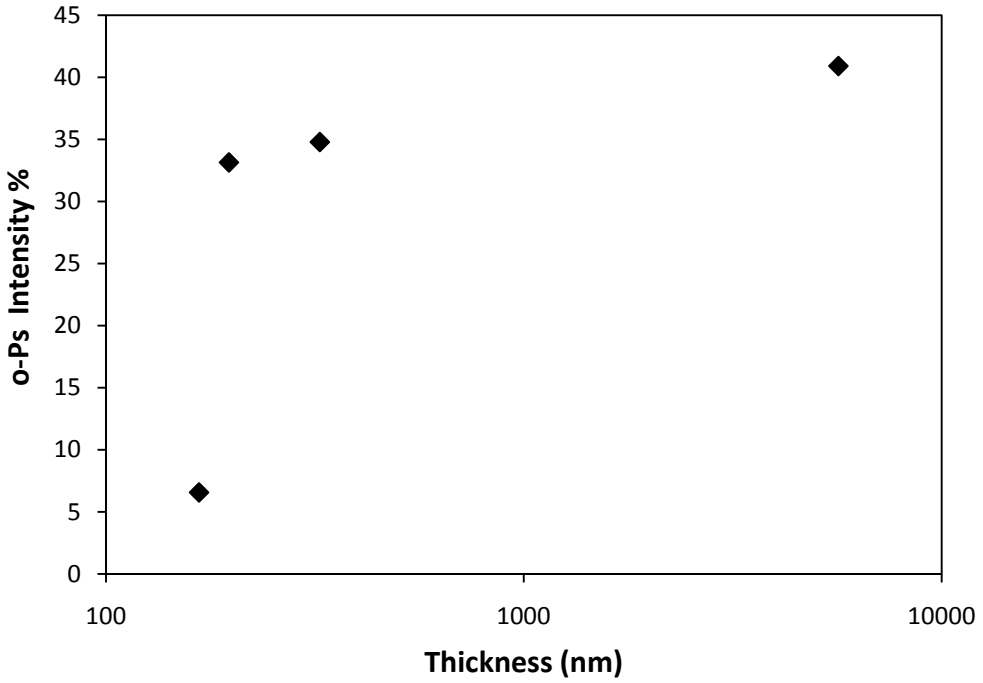

Figure 2.12 o-Positroniums intensity% at a depth of 65 nm in films of different thicknesses measured using sPALS

It is important to note the large difference in the o-Ps intensity for films of thicknesses 167 nm and 197 nm. For a 30 nm difference in film thickness, the observed change in I_3% appears to be very large. It is important to point out here that, the source of positron was changed during the measurement of the last data point 167 nm. Therefore, the large decrease in intensity seen at this thickness may not be accurate. While the entire trend observed in Figure 2.12 is reliable, the quantitative value of intensity may not be far different for 167 nm from that of 197 nm, and hence this may be an experimental artifact. Further, o-Ps intensity (I_3%) does not equal the fractional free volume (ffv) in a polymer matrix [42]. I_3 is usually a small factor of fractional free volume [42]. Fractional free volume is given by,

$$ffv\ (\%) = C\ V_f\ I_3 \quad (10)$$

where V_f is the free volume and C is material constant. The value of C for amorphous PMMA was reported by Jean et al., [42] to be 0.0018 based on WLF (Williams-Landel-Ferry) free volume theory. The plot of fractional free volume as a function of film thickness is shown below.

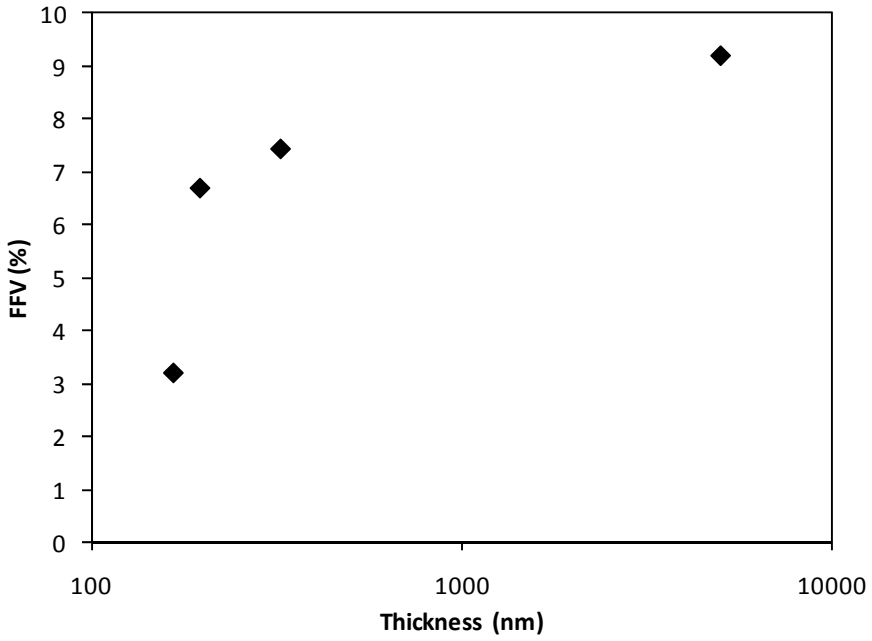

Figure 2.12 Fractional free volume (FFV %) at a depth of 65 nm in films of different thicknesses calculated using Equation (10) from sPALS measurement

The value of free volume lifetime, pocket size, intensity and fractional free volume from literature are compared to point out the impact of experimental conditions on the measured o-Ps intensity. For PMMA of molecular weight (Mw = 280000) reported in literature (comparable to the molecular weight of PMMA used in our sPALS study (Mw = 298000)), the free volume pocket radius is 2.9 Å, o-Ps intensity (I_3%) is 11.8 and

ffv % is 2.18 [42]. These values reported in literature, reiterates that the contribution of intensity to fractional free volume is far less than free volume pocket radius. Also another important factor to be noted here is the difference in intensity (I_3%) reported in literature (11.8) and reported here (~35) for almost comparable molecular weight PMMA while the free volume pocket radius is closely comparable between the value reported in literature (2.9 Å) and reported here (~3.1 Å). This points out the large impact of experiment conditions especially positron source and energy used on o-Ps intensity (I_3%), while lifetime measurements are consistent even under such variations in experimental conditions. This suggests the large difference in intensity I_3% for 167 nm could be an experimental artifact caused by changing sodium (Na^{22}) source. Because of significant contribution of free volume pocket size to fractional free volume relative to I_3%, free volume pocket size change seemed to be sufficient to explain the observed deviation in diffusion coefficient with change in film thickness (Figure 2.11). The impact of change in free volume content though small was investigated by analyzing the dependence of diffusion coefficient on fractional free volume analogous to Figure 2.11.

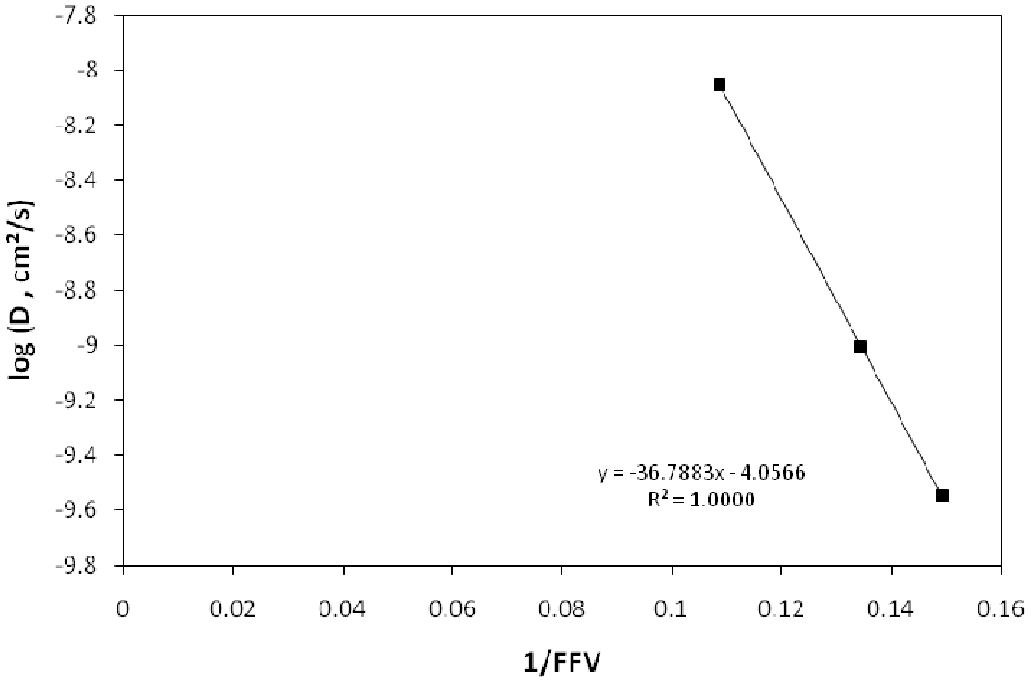

Figure 2.13 Fractional free-volume in polymer films calculated using the pore radius and intensity from sPALS experiments using Equation (10), fitted to measured diffusion coefficient analogous to Figure 2.11

On comparing Figures 2.11 and 2.13, it can be seen that the fractional free volume change fits the data very well compared to free volume pocket size. However, the change in the goodness of the fit (coefficient of regression) is small, about 4% between the two figures (free volume pocket size and fractional free volume). Further, in Figure 2.13, because of the experimental artifact explained previously in case of I_3% for 167 nm thick film, that data point is not included. As mentioned earlier, the impact of sPALS experimental condition on intensity is far pronounced than in case of free volume pocket radius. Further the percentage contribution of free volume pocket size to fractional free volume is much higher than intensity as explained previously and as can be seen from Figures 2.11 and 2.13. For this reason, following theoretical correlations explained with

change in free volume pocket size was observed to be sufficient for understanding purposes. The perfect correlation observed between fractional free volume and diffusion coefficient suggests that the observed decrease in diffusion coefficient is due to decrease in free volume pocket size and decrease in number density of the free volume pockets. Such changes in free volume pocket size and number density should be deducted by change in density of the thin films. Also, the decreased free volume pocket size and decrease in the number of free volume pockets should lead to an impact the energy barrier involved in the process of diffusion. So, activation energy for diffusion in thin and thick films is studied in the Section 2.7.

The change in free volume pocket size should translate as change in density of about the same order in these films. Change in density can be deduced by change in refractive index from optical ellipsometry. However, very small changes in refractive index could get coupled into film thickness measurement, when measured using an ellipsometer. So, in order to be able to precisely calculate change in density, a smaller wavelength optical source like X-ray reflectivity (XRR) was used to measure film thickness and then using this film thickness, the refractive index of the films were then measured using ellipsometer. XRR data was collected on PMMA films made by spin casting and soft baking them at 90 deg C for 4 min on silicon wafers. The XRR experimental data was collected using Cu-K alpha radiation on a sample about 1 inch square in size and 2 Theta scan (from 0 to 3 degrees) was performed using X'Pert Pro MRD (PANalytical Inc.,) in reflection mode. Sample XRR experimental data collected for a film about 17.5 nm in thickness, is shown below. The data was fit using RCRefSimW software (IHC Inc.,) for a Si/SiO_2/PMMA stack. Thickness of films

deduced from XRR data was precise up to 5 Å. This thickness was then used to find the refractive index change for different film thicknesses using optical ellipsometry.

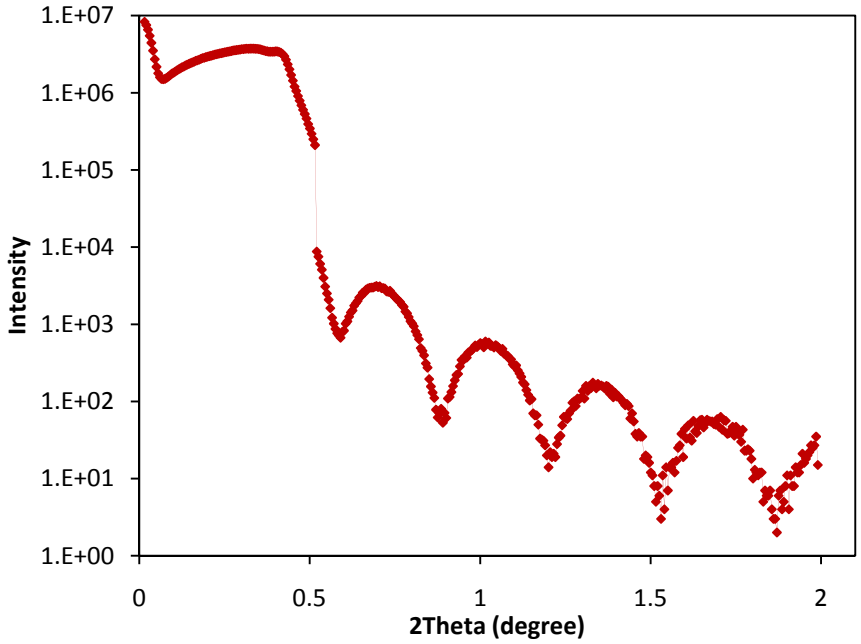

Figure 2.14 A sample X-ray reflectivity data for PMMA film of thickness 17.505 nm supported on silicon with native oxide, made by spin casting the solution and soft baking at 90 ^{0}C for 4 min

The refractive indices of films were measured using an ellipsometer. The observed change in refractive index was used to calculate the change in density using Lorentz-Lorentz relation [6] given in Equation (11). In the equation, n is the refractive index, ρ is the density and C is the constant for the material based on its polarizability. Refractive index of bulk PMMA (1.496) at 500 nm wavelength and its bulk density (1.18 g/cc) was used to calculate the constant C for the material using Equation (11). The measured refractive indices for film thicknesses calculated from XRR data was then used

to calculate their density using Lorentz-Lorentz relation [6] given in Equation (11) and is shown in the table below. Tabulated below are the values of density calculated from this equation. The observed change in density is about 6%, which is in close agreement with the change in free volume pocket size.

$$\frac{n^2 - 1}{n^2 + 2} = \rho C \tag{11}$$

Table 2.2 Refractive index and density of thin films of PMMA

Thickness	**Refractive index**	**Density**
nm	**n at 500 nm**	**g/cc**
17.505	1.5502	1.2861
89.904	1.5122	1.2115
125.36	1.5020	1.1911

A more precise comparison of the free volume data collected by sPALS and density measurements made independently would help understand if the change in free volume pocket size (which significantly contributes to fractional free volume, as explained earlier) and density of the films are comparable. For this let a be the side of a cube of polymer chains only and R_h be the radius of a free volume sphere, such that a^3 is volume of polymer chains only and $4/3\pi R_h^3$ be the volume of free volume spheres. Now

if V and V_0 are volumes of polymer cube and polymer cube with free volume; ρ and ρ_0 are densities of polymer cube and polymer cube with free volume respectively then,

$$\left(\frac{\rho}{\rho_0}\right) = \frac{a^3 - \frac{4}{3}\pi R_h^3}{a^3}$$

$$\rho = \rho_0 - \frac{4\pi R_h^3}{3a^3} \tag{12}$$

From Equation (12) it can be seen that if the measured density scales with free volume radius cube, then the shrinking free volume pockets are the contributors of fractional free volume and hence the change in density. In the figure below, density in Table 2.1 is plotted against free volume radius. For thin films like 89.9 nm free volume radius cannot be measured due to experimental limitation of sPALS technique, as the injected positron would enter the substrate and the data obtained from such low film thicknesses will not contain information about the polymer films only but also of the substrate. Hence for such films, since diffusion coefficients were measured for thin films extensively, the free volume radius was obtained from the relation in Figure 2.11.

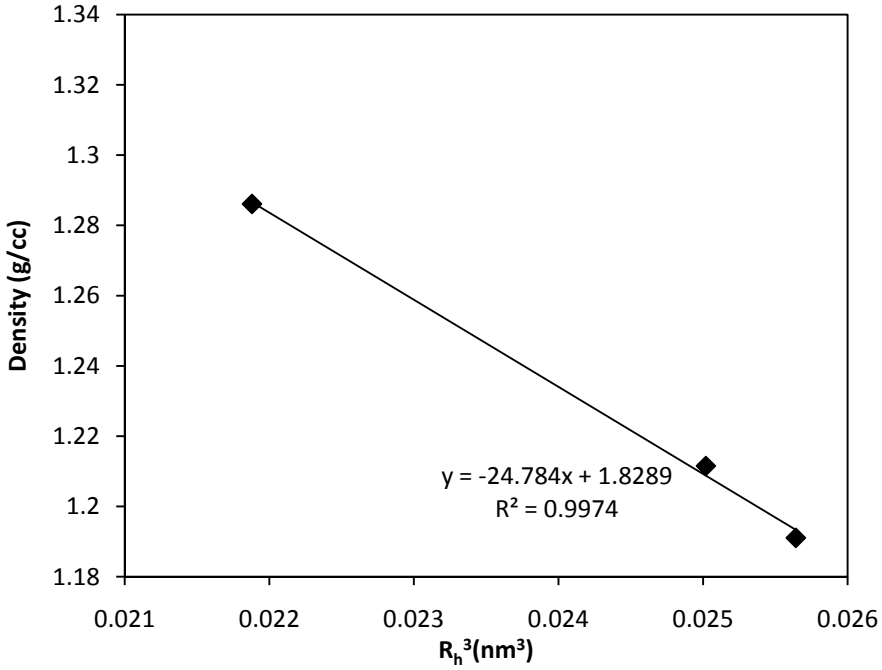

Figure 2.15 Plot of density measurements made using XRR and ellipsometry versus free volume radius from sPALS measurement and relation in Equation (10)

From Figure 2.15, it can be seen that the density change measured independently greatly correlates with the free volume radius measured from sPALS. This suggests that the free volume pocket shrinkage directly contributes majorly for any change in fractional free volume (total free volume decreases because of the decrease in each individual free volume pocket size), such that density of the film changes. Since in the above illustration density was observed to scale with R_h^3 and not as R_h^3/a^3, it also means that the density increase with decrease in film thickness due to shrinkage of free volume, while chain density of polymers between the free volume pockets are not affected. Similar observations of density change, chain stiffening and activation energy increase have been reported in literature from time-to-time. Increase in the density of thin PMMA films from

1.25 in 70 nm thick film to 1.32 in 20 nm film have been reported [46] using a three-layer model similar to the one reported by DeMaggio in [47], to capture the influence of substrate, bulk film and free surface.

2.6 Solubility

As has been observed so far diffusion coefficient was observed to decrease with decrease in film thickness. During the process of sorption and desorption in polymer films studied here, the fractional free volume change reported in the previous section, should have significant impact on the equilibrium mass uptake of water in these films. From the dual mode model investigated in Section 2.3, it can be seen from the average value of φ reported in Figure 2.6(b) and Table 2.1, about 80% of the mass uptake in these films is in free volume in polymers (Henry's absorption regime) and 20% of mass uptake is due to relaxation of polymer (as water is not a good solvent for PMMA). Since, on an average 80% of the mass uptake is in free volume pockets in almost all film thicknesses (φ in Figure 2.6(b)), the equilibrium mass uptake as a function of film thickness was analyzed for any corresponding impact of change in fractional free volume.

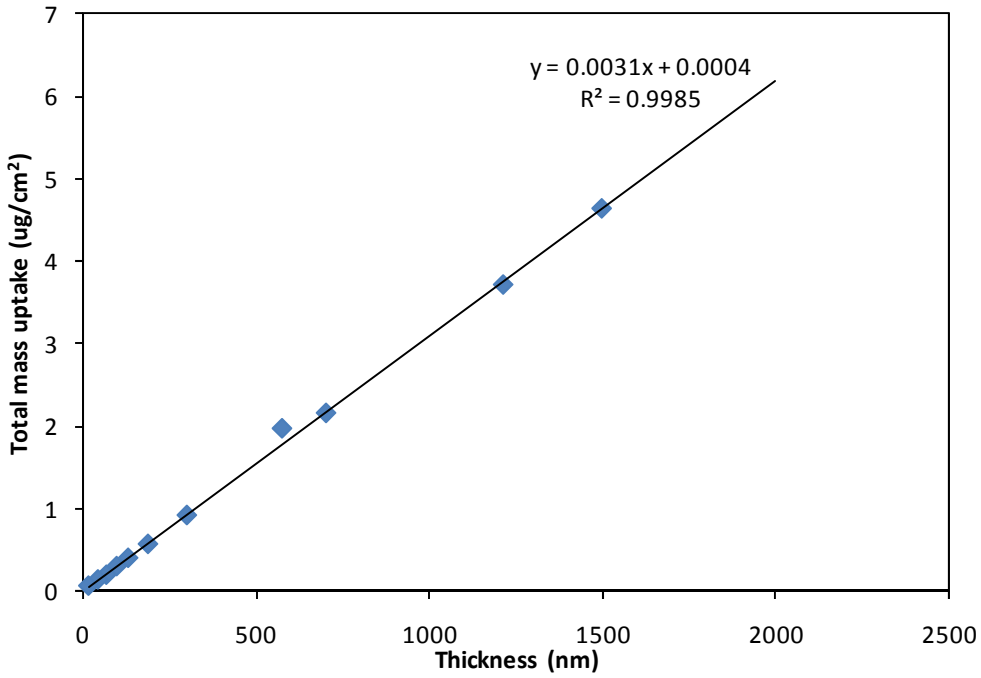

Figure 2.16 Plot of total equilibrium mass uptake of water in spin coated films of PMMA supported on silicon dioxide deposited quartz crystal

In Figure 2.16, the equilibrium mass uptake of PMMA supported on silicon dioxide is reported. This system was chosen due to gold substrate influence on the anomalous mass uptake in PMMA films described in detail in Section 2.8. As it can be seen from Figure 2.16, the total mass uptake increases with increase in film thickness over the entire range of film thickness investigated here. This suggests an equilibrium mass uptake proportional to film thickness. However, careful observation of the data reveals that the mass uptake does not continue down to zero at zero film thickness, but rather a positive intercept. This suggests the possibility of presence of a layer of water on the surface of the films as silicon dioxide substrate does not show any concentration gradient at the substrate film interface in case of water penetrating through PMMA [24]. This contribution due to any surface layer of water to the total mass uptake would be

significant in case of thin films and hence the thinnest films investigated 17 nm to 60 nm were used to estimate the amount of mass uptake affected by such a surface layer, while the contribution from this surface layer becomes increasingly insignificant in thicker films.

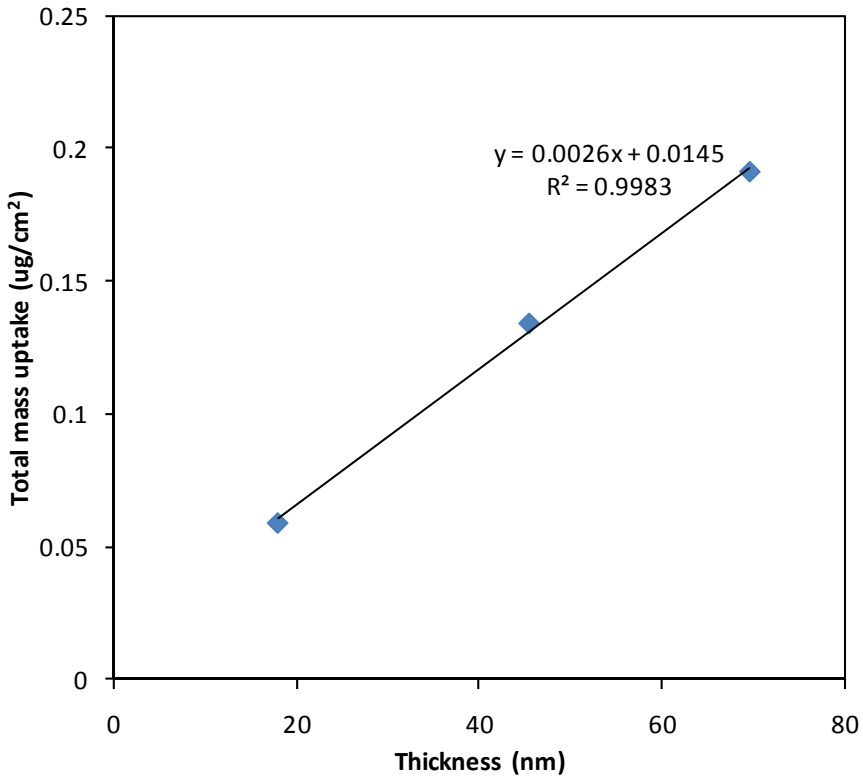

Figure 2.17 Total mass uptake in thin films of PMMA supported on SiO_2. The positive intercept shows the amount of mass uptake due to surface layer of water on thin PMMA films

The amount of mass uptake affected by the surface layer was found to be 0.0145 ± 0.0001 ug/cm^2 from the intercept of the line fitted for total mass uptake in thin films in Figure 2.17. This amount of mass uptake was subtracted from the total mass uptake in all the films to enable the estimation of total mass uptake within the polymer films only. The

solubility thus calculated from the mass uptake within the polymer films is plotted in the figure below.

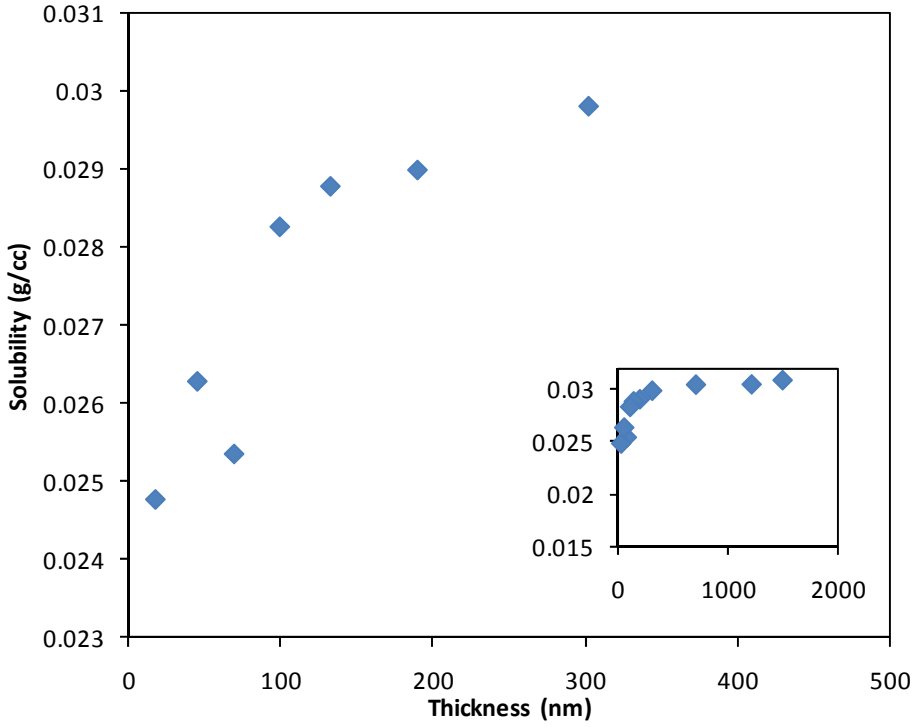

Figure 2.18 Plot of solubility as a function of film thickness for PMMA films supported on silicon dioxide for film thicknesses upto 500 nm. The inset shows solubility over the entire range of film thickness

From Figure 2.18, it can be seen that the solubility is observed to decrease with decrease in film thickness. Failure to include this adsorbed surface layer results in an apparent solubility that looks constant with film thickness. In order to quantitatively compare the change in solubility to change in fractional free volume, the percentage change in solubility for film thicknesses of (302.19 nm and 189.9 nm) was estimated to be 2.73%. The percentage change in fractional free volume in comparable film thicknesses (325 nm and 197 nm) was about 9.94%. Thus it can be seen that the

percentage change in solubility is far less than the percentage change in fractional free volume. This can be explained by free volume distribution in these films.

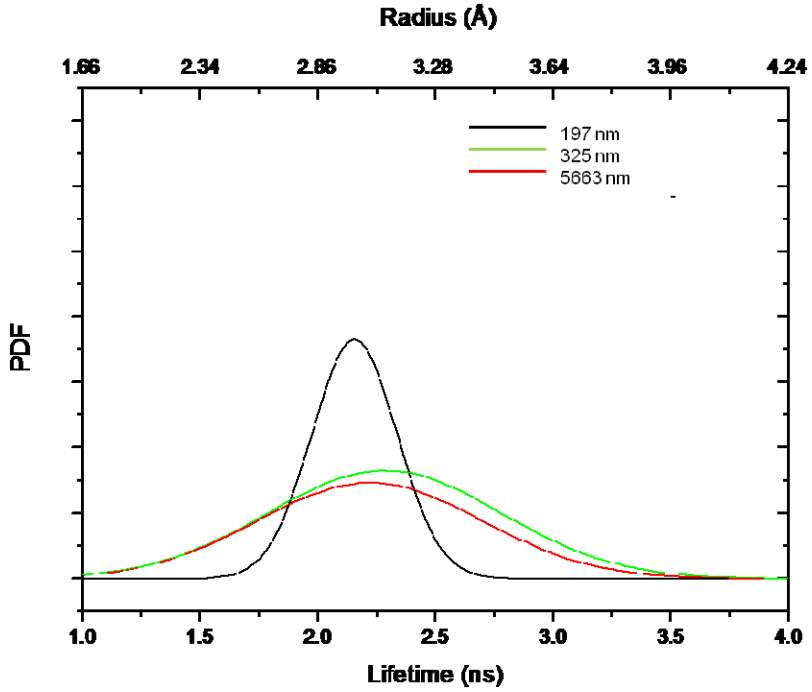

Figure 2.19 Plot of the free volume distribution in thin and thick films measured using PALs

From Figure 2.19, it can be seen that 95% of the free volume pocket radii for thick film (325 nm) ranges from about 2.45 Å to 3.59 Å and in thin films (197 nm) from 2.75 Å to 3.3 Å. Each of these free volume pockets are larger than the penetrant diameter of 2.75 Å. It is possible that the percentage change in solubility (2.73%) is lower than the percentage change in fractional free volume (9.94%) because of loss of some this excess volume (relative to the size of penetrant about 2.75 Å in diameter) from each free volume

pocket, which is reflected in the percentage change in fractional free volume, while solubility is unaffected by such change.

2.7 Activation Energy

Since diffusion is an energy activated process according to the Arrhenius equation, it would be interesting to know the influence or contribution of activation energy to observed trend in diffusion in thin polymer films.

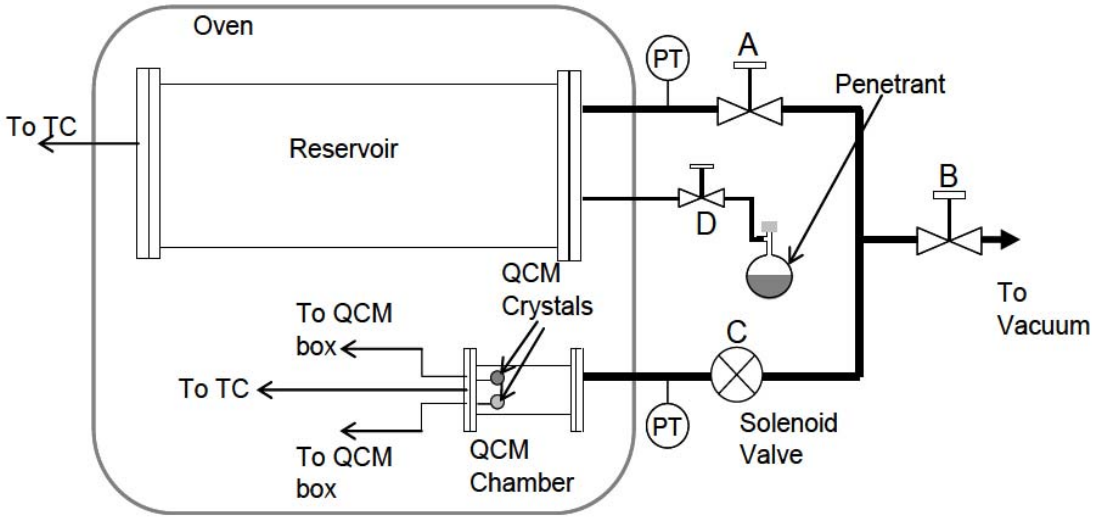

Figure 2.20 Schematic representation of the apparatus used for activation energy measurement in thin polymer films. PT – Pressure Transducer; TC – Thermocouple; QCM – Quartz Crystal Microbalance; A, B, C, D – Valves

The apparatus in its simple version is a quartz crystal microbalance operated under controlled temperatures. The apparatus was designed and constructed by Sinha, A. and the design details are explained in detail in his dissertation document [48]. The

apparatus has two steel chambers - a reservoir and a QCM chamber - inside an oven (Yamato Scientific, DKN 600 series), whose temperature can be controlled. The QCM chamber consists of a QCM crystal with the polymer film coated on it and another blank QCM reference crystal to deduct any frequency change induced because of the pressure change in the chamber. The penetrant water molecules were stored in the reservoir at a pressure of 20 Torr until equilibrated to the desired temperature. The temperature was varied from 23^{o} C to 43^{o} C for each film thickness. The water molecules were then opened into the QCM chamber, where the mass uptake of water in polymer films was observed as a change in frequency of the quartz crystal. The diffusion coefficient at each temperature was calculated using short time Fickian model as explained in Section 2.2. Activation energy for diffusion of water molecule in films of different thicknesses was calculated using Arrhenius equation as,

$$D = D_0 \exp\left(\frac{-E_a}{RT}\right) \tag{13}$$

A sample plot of natural logarithm of diffusion coefficient versus inverse of temperature in Kelvin, whose slope yields the activation energy for diffusion, is presented below (Figure 2.21). The activation energy calculation is repeated for each of the film thicknesses. A plot of activation energy change as a function of film thickness is given in Figure 2.22.

.

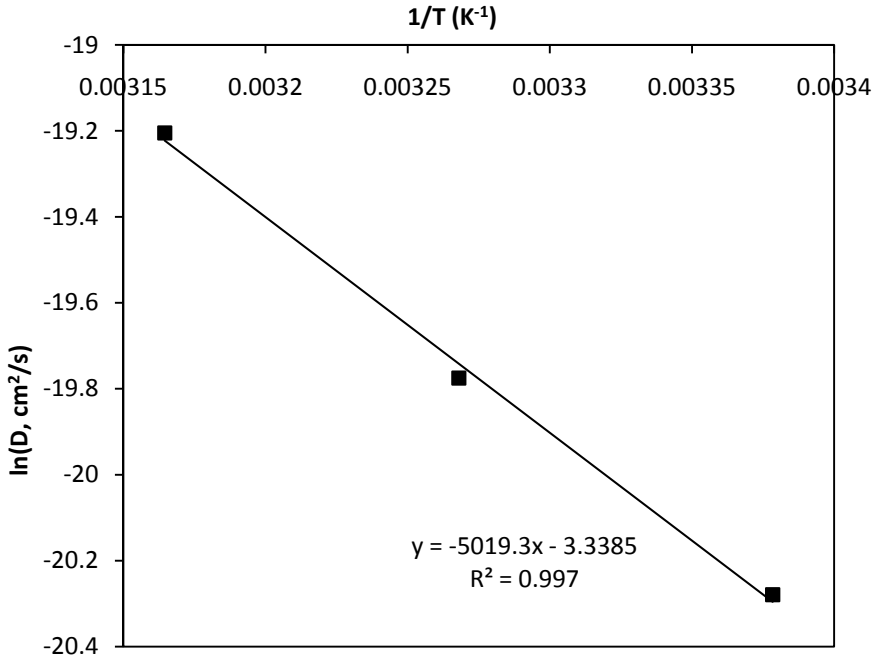

Figure 2.21 Plot of natural logarithm of diffusion coefficient versus inverse of temperature for 275 nm thick film, based on Arrhenius relation given in Equation(13)

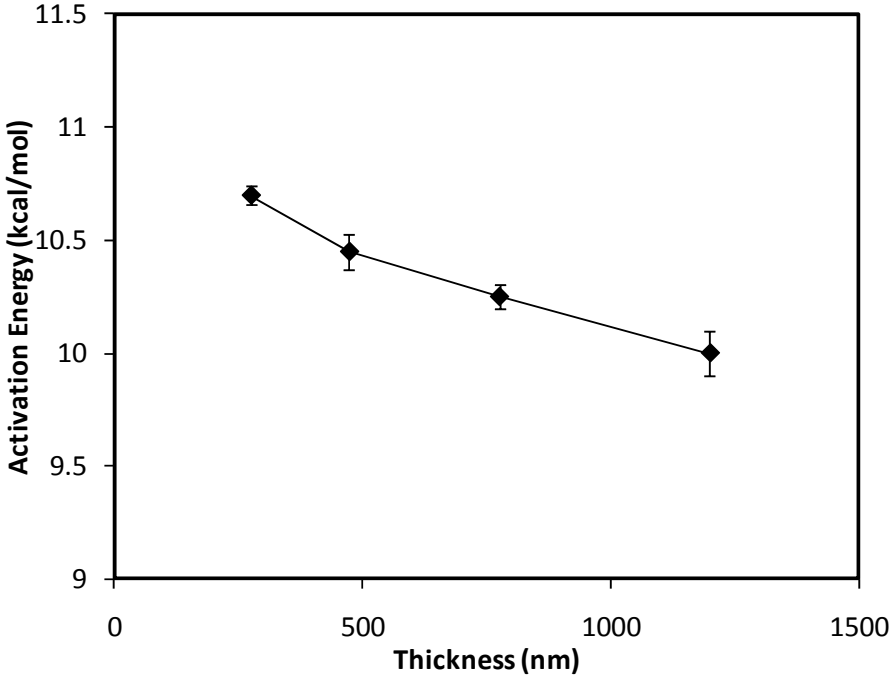

Figure 2.22 Activation energy for diffusion of water in thin polymer films as a function of PMMA film thickness

The observed increase in activation energy with decrease in film thickness is in agreement with the loss of free volume content. With the disappearance of some of the free volume holes in thin films, the distance between the remaining free volume holes increases, causing the need for higher activation energy to enable movement of penetrant molecules through the polymer chains. A modified theory by Vrentas and Duda [49] suggests that diffusion coefficient depends not only on free volume pocket size but also on activation energy. In other words, the theory suggests that the availability of free volume and the probability of finding a free volume (energy associated with such probability is activation energy) together influence diffusion coefficient. This accounts for the effect of free volume pocket size and on the diffusion coefficient. However, the activation energy for diffusion of penetrant molecule is itself a function of free volume pocket size. This explains the correlation between free volume pocket size and diffusion coefficient depicted in Figure 2.11.

In order to verify the dependence of activation energy on free volume pocket size, relation between activation energy and free volume pocket size at a given temperature was derived as shown below:

Arrhenius relationship from Equation (13):

$$D = D_{01} \exp\left(\frac{-E_a}{RT}\right) \tag{14}$$

Free Volume model from Equation (10):

$$D = D_0 \exp\left(\frac{-B}{V_h}\right) \tag{15}$$

From Equation (14) and (15), it can be seen that, at a given temperature,

$$D_0 \exp\left(\frac{-B}{V_h}\right) = D_{01} \exp\left(\frac{-E_a}{RT}\right) \tag{16}$$

Taking natural logarithm on both sides,

$$\ln D_0 + \left(\frac{-B}{V_h}\right) = \ln D_{01} + \left(\frac{-E_a}{RT}\right)$$

$$\left(\frac{E_a}{RT}\right) = \ln \frac{D_{01}}{D_0} + \left(\frac{B}{V_h}\right) \tag{17}$$

Equation (17) shows that activation energy is inversely related to average free volume pocket size. Theoretically, this relationship is meaningful, as any decrease in free volume pocket size would mean higher energy for the diffusion of penetrant and hence higher activation energy.

As activation energies were measured in PMMA films and free volume pocket radius was also measured using sPALS measurements, it is possible to see if the above relationship holds good for these two independently collected experimental data. Since diffusion coefficient is measured at high frequencies for film thicknesses over a large range, for some of the films for which activation energy was reported earlier, free volume radius was interpolated based on the fit shown in Figure 2.11.

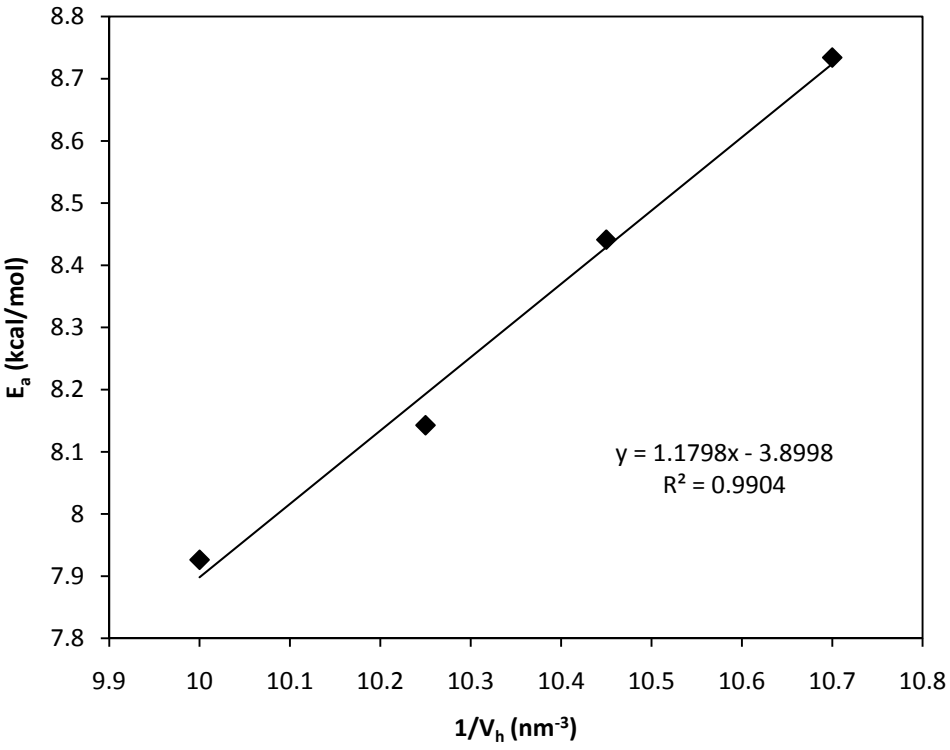

Figure 2.23 Plot of activation energy measured versus inverse of free volume ($4/3\pi r^3$), where r is the free volume radius

Figure 2.23 shows a good fit of measured activation energy and free volume pocket size (volume). The value of B (1.98 nm^{-3}) obtained from the slope in the above figure is comparable to the typical values reported in literature [45].The physical significance of this relationship implies that the change in free volume pocket size is entirely responsible for change in activation energy and hence diffusion coefficient. The linear correlation between activation energy and free volume suggests that the change in free volume pocket size in turn changes the activation energy for the process of diffusion due to the free volume pocket shrinking only. In other words, activation energy which is commonly known as a function of temperature is now observed to change with change in

film thickness. This is primarily because of change in free volume pocket size in these thin spin cast films with changing film thickness.

2.8 Influence of Substrate

The correlation between diffusion coefficient and film thickness was investigated by plotting logarithm of diffusion coefficient versus logarithm of film thickness. The plot is shown in the figure below (Figure 2.23). This plot shows linear behavior between log D and log h with a slope of approximately 2. This fits the data very well for film thicknesses from above 40 nm to around 1300 nm. It implies that over this thickness range, D scales with polymer film thickness squared. This relation deviates for very thick films above 1300 nm, as expected, because diffusion coefficient (D) then becomes a constant property of the material. It also appears to deviate for ultra-thin films, below 40 nm in thickness. The data suggests that there are three main regimes of different observed diffusion behavior: ultra-thin (sub-40 thickness), thin (~40 nm-1300 nm thickness), and bulk (>1300 nm thickness). The bulk behavior is the classical diffusion regime, where D of a particular penetrant is constant for a given material at the given conditions. The thin film behavior is previously a little investigated regime, where D appears to scale with thickness squared. The ultra-thin film behavior is likely a regime that is dominated by interface effects or by a combination of the thin film behavior and interface effects. As a result of this analysis, the deviating trend of diffusion coefficient was identified to have two different regimes, where the correlation for change in diffusion coefficient with film thickness was different in each regime. In regime 1, diffusion coefficient dropped as approximately thickness squared for film thicknesses of about 40 nm to 1300nm. In

regime 2, diffusion coefficient dropped at a much faster rate below 40 nm thickness. While deviation in regime 1 is explained in the previous section, as due to the changes in parameters (such as free volume and activation energy) involved in diffusion process, the abrupt change below 40 nm could be a combination of the above mentioned effects and substrate influence.

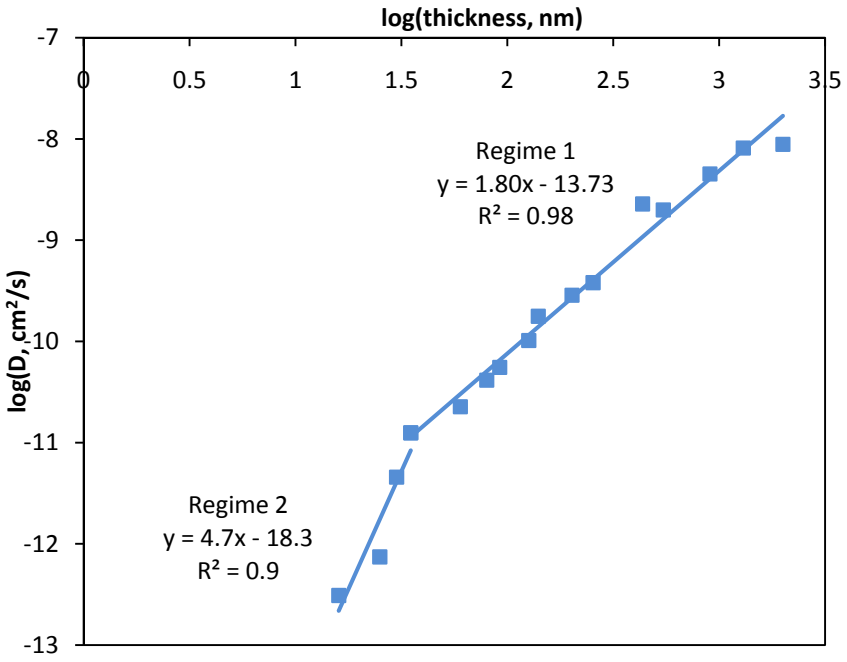

Figure 2.24 Plot of logarithm of diffusion coefficient of water in PMMA supported on gold versus logarithm of film thickness

In order to investigate if deviation observed in the ultra-thin film regime (regime 2), below 40 nm, is due to substrate influence, the experiment was repeated for PMMA supported on SiO_2 using SiO_2 deposited, gold coated quartz crystals (model 149270-1 Ti/Au : Ti/SiO_2). The resulting diffusion coefficient extracted from the short time Fickian model (discussed in Section 2.3), is shown below. The observed trend in the deviation of

diffusion coefficient for PMMA supported on SiO_2 was identical to that supported on gold in terms of the deviation from bulk and orders of magnitude drop in diffusion coefficient.

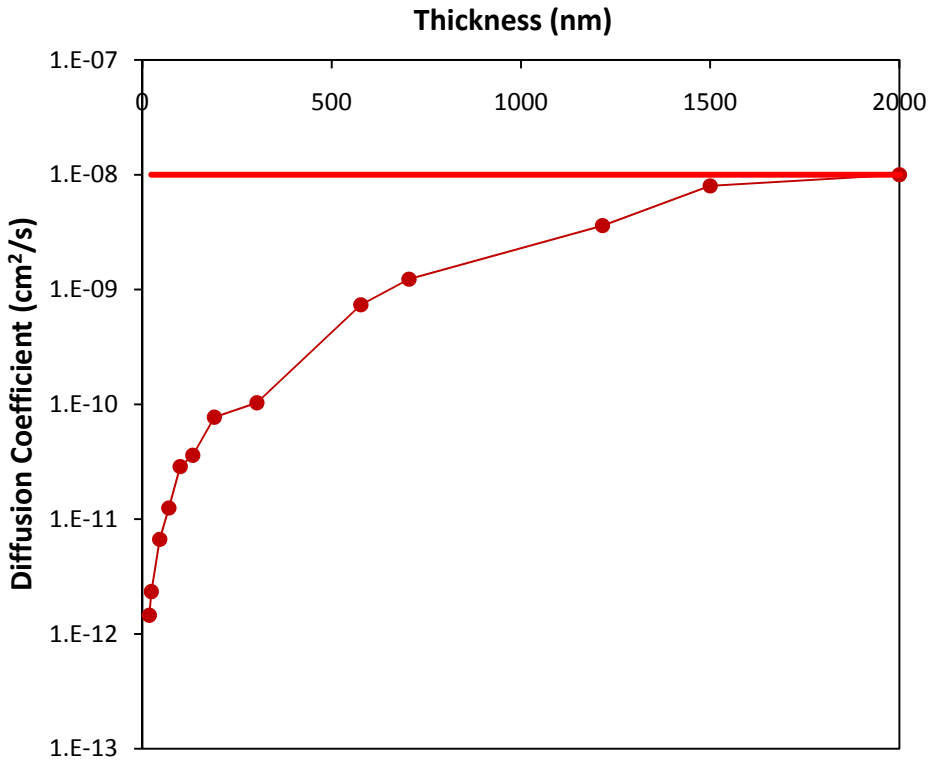

Figure 2.25 Diffusion coefficient of water in PMMA supported on SiO_2 as a function of film thickness, determined using short time Fickian model. Red line shows the bulk diffusion coefficient from literature [16]

However, a more careful analysis of the scaling, and correlation of diffusion coefficient and film thickness was performed for SiO_2 substrate by plotting logarithm of diffusion coefficient versus logarithm of film thickness, as was shown earlier for PMMA on gold. This analysis showed a continuous drop in diffusion coefficient with film

thickness with an approximate slope of 2 for film thicknesses ranging from 1200 nm to 17.5 nm.

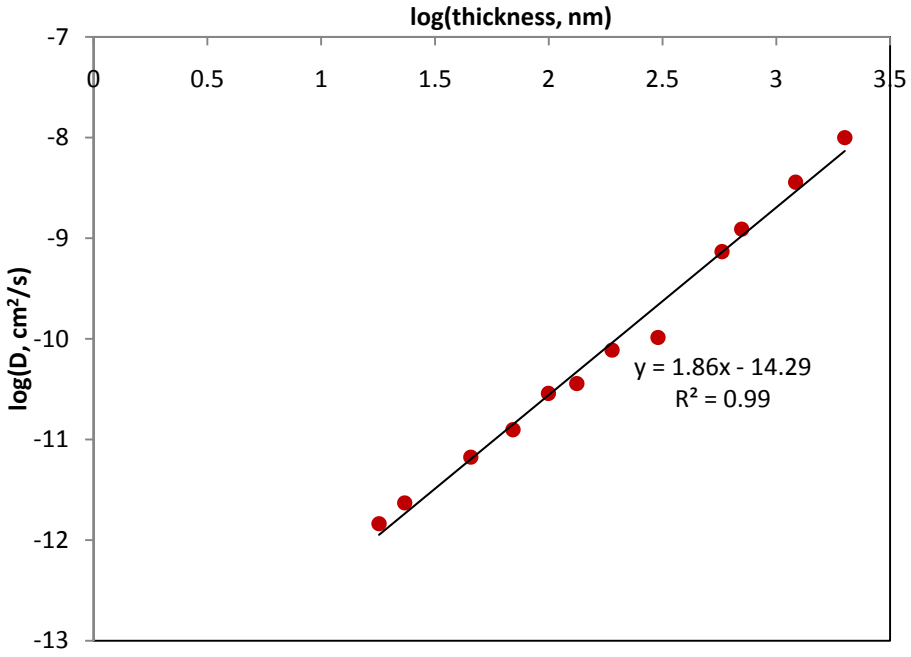

Figure 2.26 Plot of logarithm of diffusion coefficient of water in PMMA supported on SiO_2 as a function of logarithm of film thickness

Unlike the observed deviation in diffusion coefficient for PMMA supported on gold that showed two different regimes from 1300 nm to 40 nm and below 40 nm, the diffusion coefficient of water in PMMA supported on SiO_2 showed a thickness squared dependence in the entire thickness range, from 1200 nm to 17.5 nm. This is in an indication that the observed characteristics of thin films (1300 nm to 40 nm) while consistent on the two different substrates, the observed deviation in ultra-thin films below 40 nm in case of PMMA supported on gold could primarily be due to the influence of the

substrate in addition to intrinsic properties of thin films. This is further illustrated in the plot below.

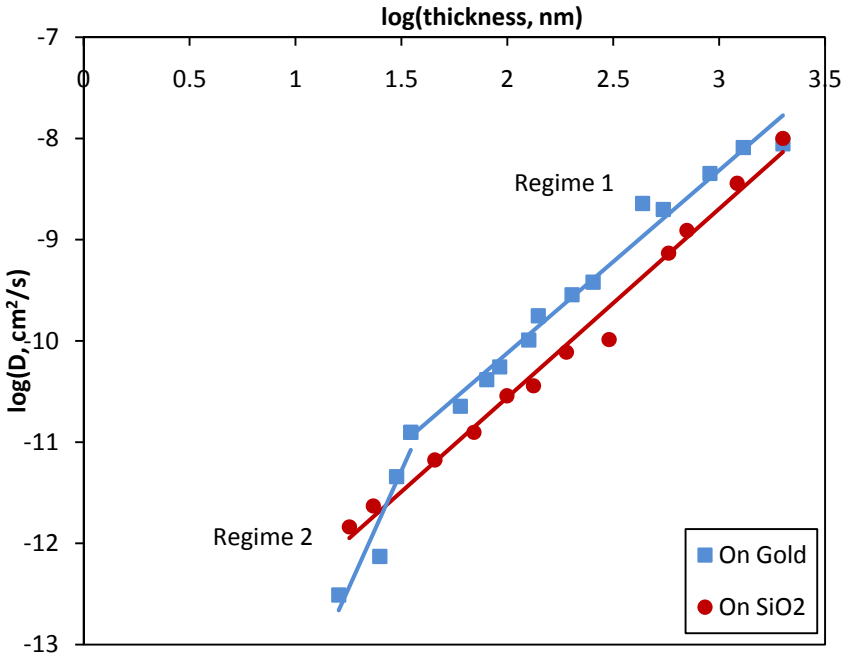

Figure 2.27 Comparison of diffusion coefficients of thin and ultra thin films on gold and SiO_2 substrates

Investigation of the substrate influence on water concentration at the substrate film interface was previously illustrated in literature [32, 33, 50]. For a supported polymer film, the difference in the affinity of the polymer and the substrate to the penetrant molecule is very significant at the substrate-film interface. A study of distribution of deuterium oxide (D_2O) penetrant in photoresist polymer films supported on oxide and hexamethyldisilazane substrate have identified and reported an interfacial depletion layer at the substrate film interface, where the concentration of water deviates

from bulk [24]. The thickness of this depletion layer at the substrate film interface has been reported to be about 40 nm [51] in a glass transition temperature study of ultrathin films on polymer films supported on different substrate. Since it is this thickness range below which regime 2 (< 40 nm) deviations in diffusion coefficient is observed in case of PMMA supported on gold, the influence of substrate in such ultra-thin films is obvious. In case of silicon dioxide supported PMMA films, the chemical affinity of water is comparable between the polymer and the oxide substrate. Whereas, in case of PMMA supported on gold, the hydrophilicity of PMMA is higher than that of gold, resulting in a depletion layer of water at the substrate film interface. This is further confirmed by the surface energy differences between gold and oxide substrates that was used to explain the observed difference in chemical affinity of penetrant between polymer and substrate [24].

2.9 Molecular Weight

As mentioned in Section 2.2 all the studies about diffusion coefficient so far were done using monodispersed PMMA with a molecular weight of 29800. In order to investigate if the observed deviation in diffusion coefficient and it thickness squared dependence has a molecular length scale associated with such deviation, the diffusion study was performed in different molecular weight polymers. Monodispersed PMMA of molecular weights 17900 (17.9K) and 815000 (815K) from Scientific Polymer Products Inc., were used to prepare polymer thin films in a way similar to that described in Section 2.2. Sorption and desorption cycles were run on the polymer films within few minutes to an hour of their preparation. Plotted below is the diffusion coefficient versus film

thickness for these two molecular weights (17.9K and 815K) and 298K molecular weight data from Figure 2.5 has also been included for comparison.

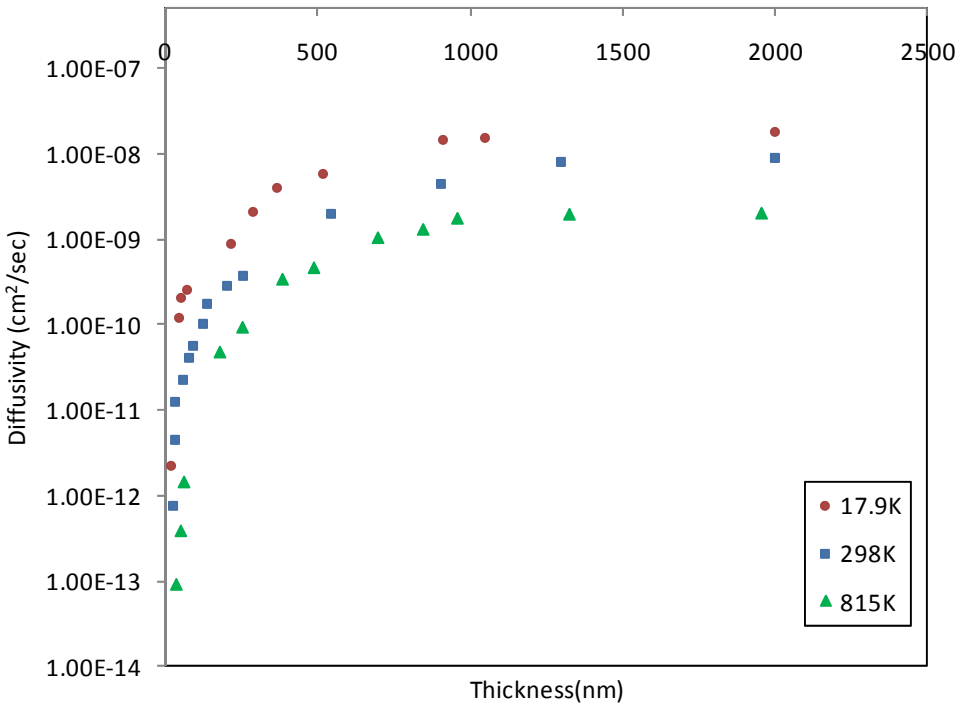

Figure 2.28 Diffusion coefficient versus film thickness for monodispersed PMMA of molecular weights 17900 (17.9K), 298000 (298K) and 815000 (815K)

As it can be seen from Figure 2.28, diffusion coefficients of PMMA for all the three molecular weights studied are observed to deviate from bulk. Further, three to four orders of magnitude drop in diffusion coefficient from bulk is also observed to be identical for all the three molecular weights. Because of larger number of free polymer chain ends in lower molecular weight, it can be observed that the bulk diffusion coefficient of lower molecular weight PMMA is higher than higher molecular weight PMMA (17.9K > 298K > 815K). A plot with diffusion coefficient normalized by bulk diffusion coefficient would enable the comparison of the impact of film thickness. Shown

below in Figure 2.29 is a modified plot of Figure 2.28, where diffusion coefficient of each film thickness is normalized by bulk diffusion coefficient of that molecular weight PMMA.

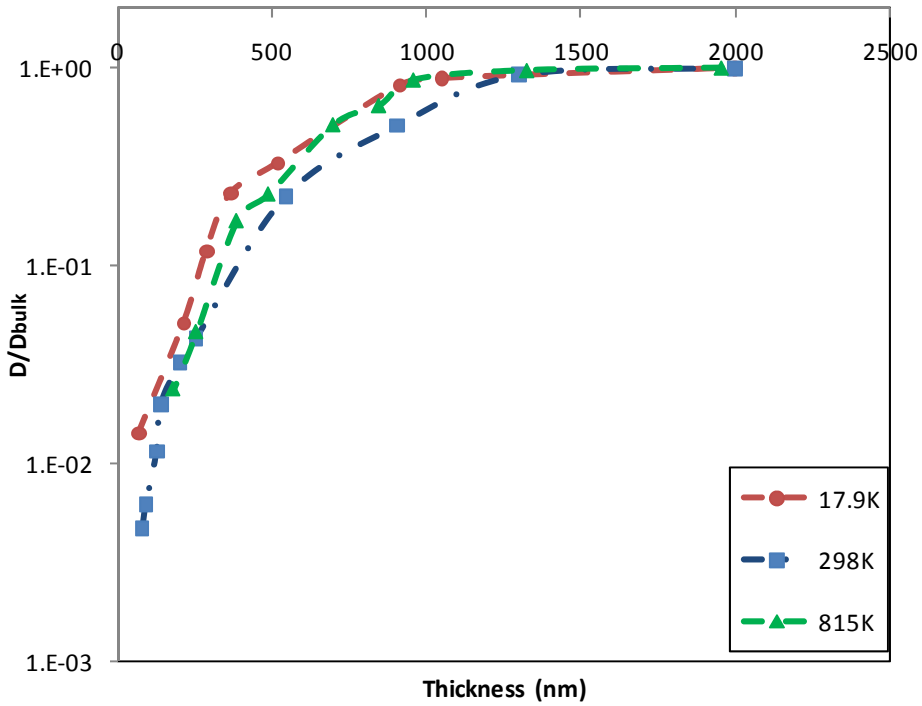

Figure 2.29 Normalized diffusion coefficient (Diffusion coefficient divided by bulk diffusion coefficient) versus film thickness for monodispersed PMMA of molecular weights 17900 (17.9K), 298000 (298K) and 815000 (815K)

From Figure 2.29, it can be observed that the deviation from bulk in all the three different molecular weight PMMA (17.9K, 298K and 815K) is observed at a film thickness of about 1200 – 1300 nm, which is much higher than the thickness at which other deviations like coefficient of thermal expansion and glass-transition temperature was observed [22]. Thus the observed deviation in diffusion coefficient with film thickness occurs at much higher length scales than that for other properties (like T_g) and

this deviation is common for all the molecular weight PMMA investigated. Thus the reported decrease in free volume pocket size with change in film thickness may be extended for the observed deviation, in all the molecular weight studied here. Although, it is recommended that the free volume pocket size for different film thicknesses may be tested in different molecular weight polymers, in future studies. In conclusion, the deviation in diffusion is due to the thickness dependent intrinsic property of the film and hence is observed to exist at all polymer length scales or molecular weights studied.

Also, the fact that deviation in diffusion for all the three molecular weight is observed at 1200-1300 nm is interesting. This thickness at which the deviation is observed when normalized by radius of gyration (R_g) would take into account the polymer chain length associated with the molecular weight. Such an analysis reveals that deviation in diffusion coefficient is observed at about 500 times the radius of gyration for 17.9K, compared to 100 times for 298K and 815K. This large difference in the length scale of deviation for low molecular weight and high molecular weight PMMA needs further investigation. However, based on other deviation studies like glass-transition, it is possible to suggest that this could be due to difference in enthalpy relaxation of the low and high molecular weight glassy polymer films as pointed by Marshall et al., [52]. Also, the effect of this enthalpy relaxation has been reported to reach a limiting value at a molecular weight about 50000 for glassy atactic polystyrene used in their study. Thus, it is possible that in case of PMMA, 298K and 815K are above this critical molecular weight such that the length scale at which deviation in diffusion coefficient is observed is identical ($h/R_g = 100$) for these both 298K and 815K molecular weight PMMA. As mentioned earlier, further investigation of diffusion coefficient deviation in other

molecular weight PMMA would help identify any trend in length scale (h/R_g) where diffusion coefficient deviates from bulk and its association with enthalpy relaxation as suggested in glass transition studies.

2.10 Aging

As pointed out in the beginning of this chapter, mass transport through polymer membranes is widely applicable in industrial gas separations. Hence, the study of deviation in diffusion coefficient with decrease in film thickness is compared to any related observations reported in polymer membranes literature. Studies of gas transport through polymer membranes have reported deterioration of performance of polymer membranes with time and this has been reported to be due to decrease in permeability with time, in other words, due to physical aging of polymer membranes [53]. Such observation has been consistent in different polymer membranes and hence has been investigated in depth using different techniques [43, 44, 53, 54]. Also, investigation of permeability with aging has been reported in films of different thicknesses [54]. Selectivity and permeability of glassy polymers are better suited characterization parameters for mass transport applications of polymer membranes. Permeability is the product of diffusivity and solubility. Based on the observations reported here so far, diffusion coefficient is observed to decrease with decrease in film thickness and solubility is also reported to change with change in film thickness. This implies that permeability which is product of diffusivity and solubility should in turn be decreasing with decrease in film thickness.

Before discussing the results and trend observed for permeability, a brief note about the process involved in preparation of membranes for permeability measurements is pointed. For testing permeability of membranes, it is essential to have free surface on both sides of the film. In order to achieve this, in permeability studies reported in literature [44, 54], films are floated off their supporting surfaces and are sandwiched between supports with small sample area open, for permeability of gases into and out of the film. The permeability data reported for thin films (about 400 nm) prepared by this technique are often higher than bulk permeability of membranes in the first few hours of the measurements [53, 54] and then the trend with time the permeability of thin films are lower than the bulk permeability of polymer membranes. This anomalous trend in permeability was found to be due to the processing technique, of floating off the films from the substrate during which relatively high free volume is introduced in the films and then sandwiching them between supports which introduces stress in these films that eventually fades out over time [56]. Thus, most reliable data for thin films about 400 nm are obtained above this time period (about 10 hours) when the influence of prior history on the state of the film is lost. In case of experiments described in this chapter to determine diffusion coefficients of thin polymer films, spin coated films were used in the same state as they were made, i.e., attached to the substrate. Further, as annealing studies reported in Section 2.4 revealed that diffusion coefficient measured in films immediately after spin casting did not change after rigorous annealing treatment and this was observed in both thin 67 nm and thick films about 1200 nm (Figure 2.7), it is believed that diffusion coefficient of films reported here are not affected by processing conditions.

The extensive study of diffusion characteristics of thin films discussed in this chapter when extended to study the response as a function of time could be useful in gas separations, where loss of permeability due to aging is a concern. In an attempt to investigate the phenomenon of aging in thin polymer films, thin polymer films that were spin-cast and soft-baked at 90^0C for 4 min was used. The diffusion experiment using the QCM set up was carried out as soon as the films were prepared (within a few minutes to an hour as mentioned earlier). The films were then stored in isolated boxes in the lab, to avoid contamination. The diffusion experiment was then repeated at regular time intervals, of a few days since the films were made. The diffusion coefficient in thin polymer films was calculated using the mass uptake data collected at different intervals of time (as described in detail in Section 2.3) and the influence of time on the transport behavior was studied. The graphs are presented below.

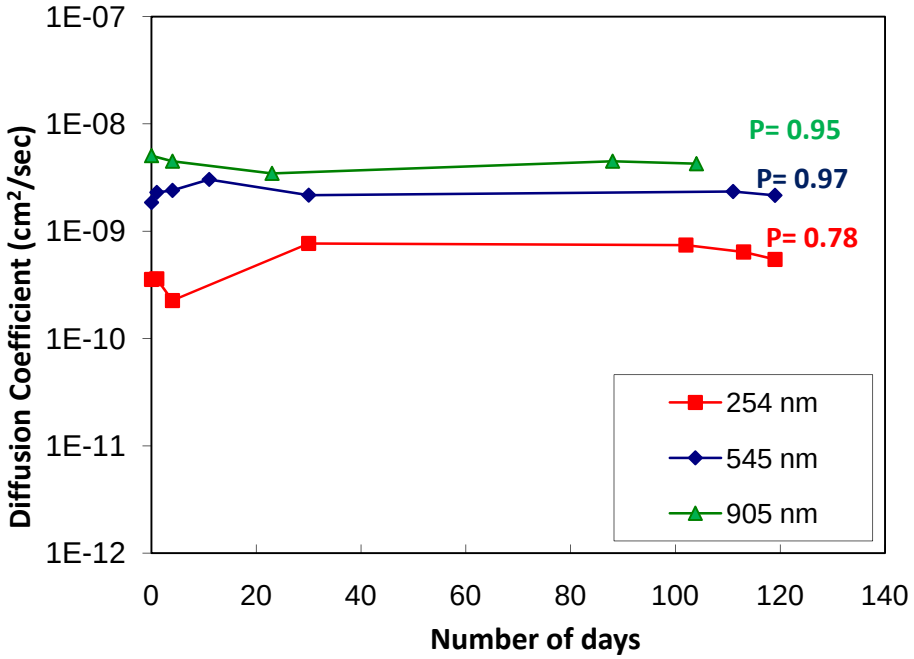

Figure 2.30 Aging studies in PMMA – Diffusion coefficient of thin films of PMMA supported on gold, measured immediately after spin casting (0^{th} day) and at different intervals of few days after the films were prepared

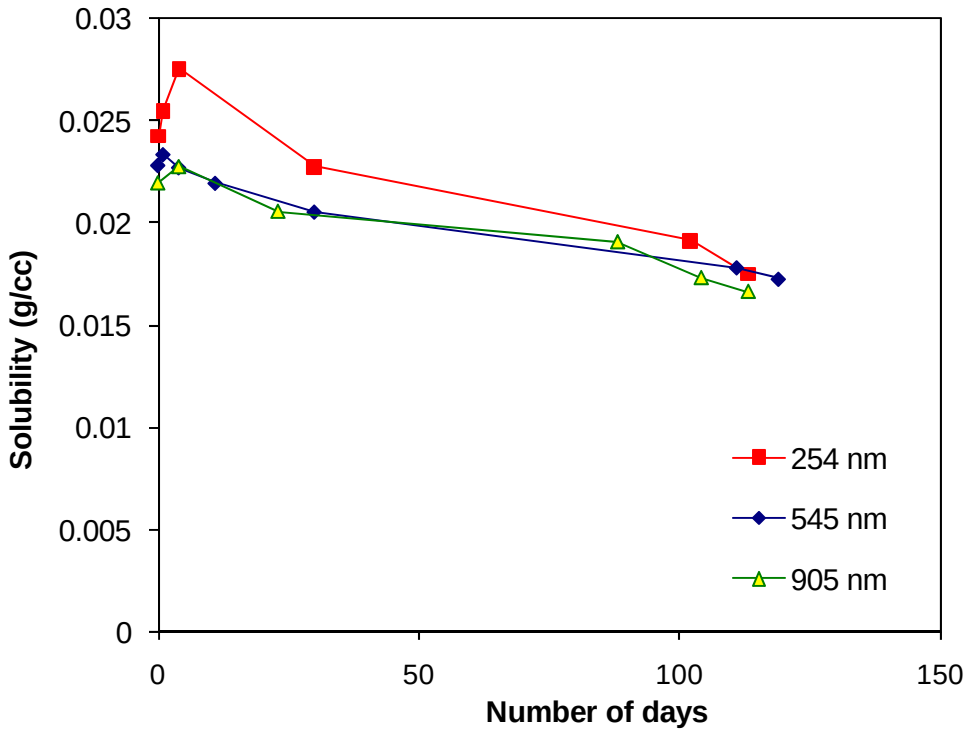

Figure 2.31 Aging studies in PMMA – Solubility coefficient of thin films of PMMA supported on gold, measured immediately after spin casting (0^{th} day) and at different intervals of few days after the films were prepared

From Figure 2.30 and Figure 2.31, it is observed that diffusion coefficient does not change with time while solubility decreases with time. From this observation, it is believed that the impact of physical aging on transport behavior and the decrease in permeability with time or aging, reported in literature [43, 44, 53, 54] should be largely due to decrease in solubility with time. Comparison of the observed trend in diffusivity and solubility to the trend in permeability reported in literature enables further understanding of polymer thin film dynamics. Observed decrease in permeability with aging reported in literature has been investigated for films of different thicknesses, as a function of temperature [55]. Loss of free volume due to diffusion of free volume to the

surface, similar to diffusion of defects to the surface of the film, was proposed to cause the observed drop in permeability with aging of polymer films [54]. However, while permeability decreased with time, selectivity of membranes increased by up to 15% in approximately the same time scale (about 10000 hr) in which permeability was studied. The increased selectivity with aging suggests a decrease in the size of free volume pockets within the polymer films. Since loss of free volume due to decrease in the size of free volume pockets would lead to an increase in density of films, optical property such as refractive index was used to monitor change in density of polymer films with physical aging. This study did not reveal any significant change in density to support the loss of free volume [54]. Recently Rowe et al., [45] reported sPALS measurements in aging polysulfone films and concluded that the degradation of transport property (permeability) in polymer films with time, was due to decrease in free volume pocket size only. The intensity (I_3%) of o-Positroniums that measures the number of free volume pockets was reported to be constant and hence fractional free volume (ffv) was calculated based on free volume pocket size only ($ffv = C' \times \tau_3^3$). But the reported data for I_3% suggests an increase of about 2% and hence the fractional free volume calculated from the reported τ_3, I_3 and tabulated C according to the equation, $FFV = C \times I_3 \times \tau_3^3$ is shown in the figure below.

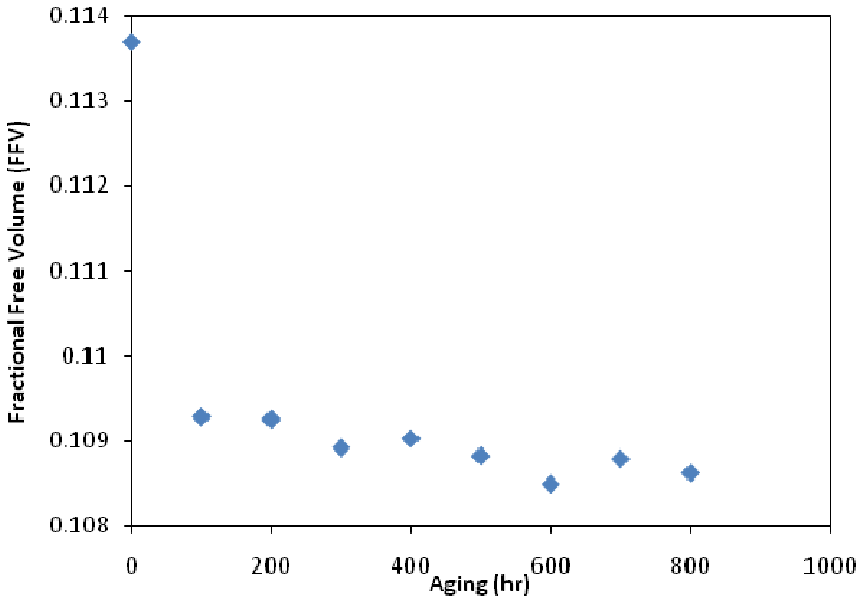

Figure 2.32 Fractional free volume calculated from τ_3 and I_3 reported by Rowe et al., [45] for polysulfone membrane

From Figure 2.32, fractional free volume is observed to almost remain a constant with time except for the 0^{th} hour, which could be due to residual stress in the films, as mentioned earlier. This suggests that the decrease in free volume pocket size is compensated by an increase in intensity or the number of free volume pockets, such that the fractional free volume remains unchanged. This is possible when the larger free volume pockets in polysulfone films during aging reduce to more number of smaller free volume pockets. In other words, decrease in free volume pocket size and increase in number of free volume pockets while fractional free volume remains a constant is possible only when, free volume pockets reduce in size by splitting into one or more free volume pockets, such that the total amount of fractional free volume remains a constant and there is an increase in number of free volume pockets. This is represented schematically in the figure below.

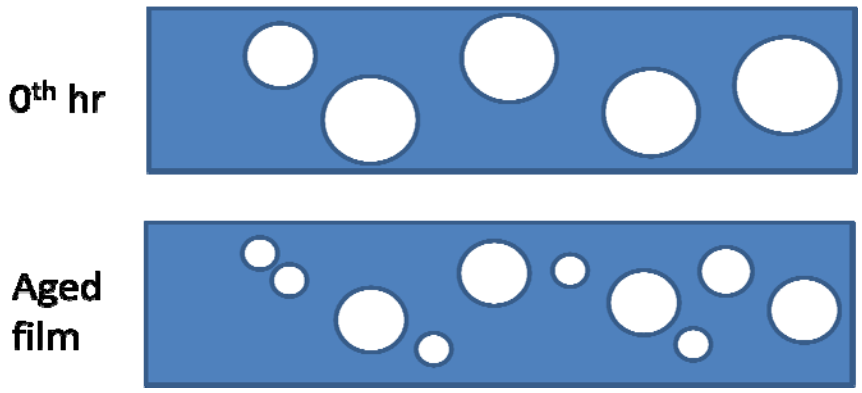

Figure 2.33 Schematic representations of reduced free volume and pocket size and increase in number of free volume pockets to maintain a constant fractional free volume in a film at it 0th hour and after aging

Correlation of the observed trends in fractional free volume, free volume pocket size and number of free volume pockets from the sPALS study by Rowe et al., to the results obtained here for diffusion coefficient and solubility (Figures 2.30 and 2.31) with aging leads to further understanding of polymer thin films dynamics. Based on the constant fractional free volume and observed unchanged diffusion coefficient with aging, it is possible to hypothesize that the penalty on diffusion coefficient due to decrease in free volume pocket size could be compensated by lesser activation energy needed for propagation from one free volume to another, as the distance between them is shorter with increase in number of free volume pockets. It is because of such counter acting effect of lower activation energy, no change in diffusion coefficient is observed in our aging studies. However, this is just a hypothesis based on our measurements of diffusion coefficient with aging and the reported observation of decrease in free volume pocket size by Rowe et al., [45]. This can be studied by measuring the activation energy for

diffusion in thin films with aging. The observed decrease in solubility (Figure 2.31) with aging could however be because some of the smaller free volume pockets in aged films are not capable of accommodating a penetrant molecule. In other words, the smaller free volume pockets that resulted in aged films could lead to increase in number of inaccessible free volume pockets for mass uptake and hence solubility decreases. It is possible to compare the range of free volume pocket radius before and after aging based on the data reported for o-Positroniums lifetime at different depths in 450 nm polysulfone film reported by Rowe et al., [45]. The life time ranges from 1.9 ns to 2 ns with a mean of about 1.99 ns before aging and 1.82 ns to 1.91 ns with a mean of about 1.905 ns after aging. The differences in the range of o-Ps lifetime is an indication of similar differences in free volume pocket radius in films before and after aging, suggesting the possibility of large amount of inaccessible free volume leading to decreased solubility.

2.11 Conclusions

Diffusion coefficient of water molecules in films of poly (methyl methacrylate) (PMMA) has been studied as a function of film thickness. Film thicknesses investigated range from 25 nm to 2000 nm. Over this thickness range, diffusion coefficient of water decreases by over four orders of magnitude as the films get thinner. Above 2000 nm thickness, diffusion coefficient approaches the reported bulk value of diffusion coefficient for water in PMMA ($10^{-8}cm^2/s$). The diffusion coefficient is observed to scale with film thickness squared below 1300 nm. This change in diffusion coefficient occurs over a much larger range of thicknesses than has been previously reported in polymer ultra-thin film confinement effect studies on properties such as glass-transition

temperature, coefficient of thermal expansion [16] and penetrant diffusion behavior [41]. In the study of glass-transition temperature (T_g) and coefficient of thermal expansion (α') [16], the bulk value of Tg and α' are reached at a film thickness of about 200 nm. The deviation in the properties below 200 nm, have been explained to be due to film confinement on the substrate. However, the deviation observed here in diffusion coefficient extends up to 1300 nm and hence film confinement cannot be the explanation for deviations at such length scales. Thus, it is important that thickness be considered for all diffusion studies, even those that were previously thought to behave as bulk films. The thickness dependence does not appear to be due to residual casting solvent. Slow Positron Annihilation Lifetime Spectroscopy (sPALS) was used to probe the free volume pocket size, its distribution within the film, and its total amount as a function of film thickness in PMMA. The results from sPALS showed that thicker films have more free volume pockets than thinner films and that the average free volume pore radius is smaller in thin films than in thick films. This change in free volume size was observed to correlate with the measured activation energy change with film thickness for the process of diffusion. The density measurements also agreed with change in free volume pocket size. Thus decrease in free volume pocket size and fractional free volume certainly contributes to the significant drop in diffusion coefficient in thinner PMMA films. And this behavior is likely to be one of the general underlying causes for such thickness dependent diffusion behavior observed in a variety of other ultra-thin polymer films as well. With the decrease in fractional free volume in thin films, solubility was also affected to some extent. The percentage decreases in solubility was relatively less when compared to percentage change in fractional free volume and this is believed to be due to the loss of

some of the inaccessible free volume (relative to the size of the diffusing penetrant), whose loss does not affect solubility anyways. To extend the observation of drop in diffusion coefficient with film thickness to similar observations made in membrane separations and permeability, aging behavior of diffusion and solubility was studied. Diffusion coefficient was observed to not change with time, while solubility decreased with aging. Correlations of the results obtained to sPALS measurements reported by Rowe et al., [45] reveals that constant fractional free volume could be the possible reason for unchanged diffusion coefficient, while increase in number of in accessible free volumes could lead to decreased solubility in aged films. These hypotheses can be tested by measuring activation energy for diffusion in thin films due to aging, which should remain a constant confirming constant diffusion coefficient. sPALS study of free volume pocket size distribution as a function of aging could help understand the range of free volume pocket radius available in aged films and the percentage of inaccessible free volume (relative to penetrant size) that is comparable to observed change in solubility. Summary of the observations and hypothesized schematic representation of free volume pockets is shown in Table below.

Table 2.2 Summary of the observations and hypothesized schematic representation of free volume pockets

Thickness	Time
Diffusion coefficient decreases with decrease in film thickness. Because, **fractional free volume decreases** with in film thickness.Decrease in free volume pocket size and decrease in the number density of free volume pockets, leads to an increase in diffusion coefficient	**Diffusion coefficient is constant** with time. Because, **fractional free volume is constant** with time.Decrease in free volume pocket size could be compensated by an increase in number density of free volume pockets, such that diffusion coefficient remains unaffected. This can be tested by measuring activation energy as a function of time.
Solubility decreases with decrease in film thickness. Because, **fractional free volume decreases** with film thickness, but the percentage change in solubility is less than the percentage change in fractional free volume, because the free volume pockets in thick films were much larger than the penetrant diameter such that the decreased free volume pockets in thin films is still larger than the penetrant diameter. This excess volume loss is accounted in fractional free volume while solubility remains unaffected.	**Solubility decreases** with time. Because, **fractional free volume decreases** with time. The larger free volume pockets during aging reduce to more number of smaller free volume pockets such that fractional free volume remains a constant. The large number of smaller free volume pockets thus formed in aged films could lead to an increase in number of inaccessible free volume pockets for mass uptake and hence solubility decreases.
Thick film 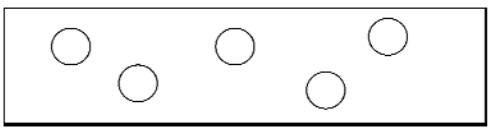 Thin Film 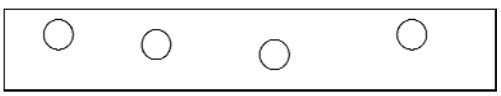	0^{th} day  120^{th} Day 

2.12 References

1. Perry, M.L., Fuller, T. F., *A Historical Perspective of Fuel Cell Technology in the 20th Century.* Journal of The Electrochemical Society, 2002. **149**(7): p. S59-S67.
2. Thompson L.F., et al., Willson C.J., *Introduction to Microlithography.* ACS: Washington, D.C., 1994.
3. Koros W.J., et al., ed. *Comprehensive Desk Reference of Polymer Characterization* ed. R.F. Brady. 2003. 680.
4. Chrisey D.B., et al., Chemical Reviews, 2003. **103**(2): p. 553.
5. Hines A.L., et al., ed. *Mass Transfer: Fundamentals and Applications*. 1985, Prentice-Hall: Englewood Cliffs.
6. Kittel, C., ed. *Introduction to Solid State Physics*. 7th ed.
7. Ito, H., *Chemical amplification resists: History and development within IBM.* IBM Journal of Research and Development, 1997. **41**(1.2): p. 119-130.
8. Fryer, D.S., Peters, R.D., Kim, E.J., Tomaszewski, J. E., de Pablo, J.J., Nealey, P.F., White, C.C., Wu, W-L., *Dependence of the Glass Transition Temperature of Polymer Films on Interfacial Energy and Thickness.* Macromolecules, 2001. **34**(16): p. 5627-5634.
9. Campoy-Quiles, M., Sims, M., Etchegoin, P. G., Bradley, et al., *Thickness-Dependent Thermal Transition Temperatures in Thin Conjugated Polymer Films†.* Macromolecules, 2006. **39**(22): p. 7673-7680.
10. Tate, R.S., Fryer, D. S., Pasqualini, S., Montague, M. F., de Pablo, J. J., Nealey, P. F., *Extraordinary elevation of the glass transition temperature of thin polymer*

films grafted to silicon oxide substrates. Journal of Chemical Physics, 2001. **115**(21): p. 9982-9990.

11. Soles, C.L., Lin, E.K., Lenhart, J.L., Jones, R.L., Wu, W-L., Goldfarb, D.L., Angelopoulos, M. *Thin film confinement effects on the thermal properties of model photoresist polymers*. 2001: AVS.
12. A. Huwe, F.Kremer, M. Arndt, P. Behrens, W. Schwieger, G. Ihlein, Ö. Akdogan, F. Schüth, *Glass Transition in Sub-Nanometer Confinement.* Materials Research Society Symposium Proceedings 1999. **543**.
13. D. J. Pochan, E.K.L., S. Satija, S. Z. D. Cheng, W-L. Wu, *Thermal Expansion and Glass Transition Behavior of Thin Polymer Films With and Without a Free Surface Via Neutron Reflectometry.* Materials Research Society Symposium Proceedings, 1998. **543**.
14. Wu, C.C., *Studies of the Polymer Thin Film Glass Transition Temperature Monitored With the Complex Viscoelastic Coefficients.* Materials Research Society Symposium Proceedings, 1998. **543**.
15. DeMaggio, G.B., Frieze, W. E., Gidley, D. W., Zhu, M., Hristov, H. A., Yee, A. F., *Interface and Surface Effects on the Glass Transition in Thin Polystyrene Films.* Physical Review Letters, 1997. **78**(8): p. 1524.
16. Singh L., Ludovice, P.J., Henderson, C.L., Thin Solid Films, 2004. **449**(1-2): p. 231.
17. Beaucage, G., Composto, R., Stein, R. S., *Ellipsometric study of the glass transition and thermal expansion coefficients of thin polymer films.* Journal of Polymer Science Part B: Polymer Physics, 1993. **31**(3): p. 319-326.

18. Kahle, O., Wielsch, U., Metzner, H., Bauer, J., Uhlig, C., Zawatzki, C., *Glass transition temperature and thermal expansion behaviour of polymer films investigated by variable temperature spectroscopic ellipsometry.* Thin Solid Films, 1998. **313-314**: p. 803-807.

19. Soles, C.L., Jones, R.L., et al., Proceedings of SPIE, 2003. **5039**: p. 366.

20. Soles, C.L., Douglas, J.F., Wu, W.L., et al., Macromolecules, 2003. **36**(2): p. 373.

21. Soles, C.L., Douglas, J.F., et al., Journal of Polymer Science Part B-Polymer Physics 2004. **42**(17): p. 3218.

22. Singh, L., Ludovice, P.J., Henderson, C.L., Thin Solid Films, 2004. **449**(1-2): p. 231.

23. Vogt, B.D., Soles, C.L., Langmuir 2004. **20**(4): p. 1453.

24. Vogt, B.D., Soles, C.L., Lee, H-J., Lin, E.K., Wu, W-L., *Moisture absorption into ultrathin hydrophilic polymer films on different substrate surfaces.* Polymer, 2005. **46**(5): p. 1635-1642.

25. Soles C.L., et al., Proceedings of SPIE, 2003. **5039**: p. 366.

26. Torres, J.M., Stafford, C.M., Vogt, B.D., *Elastic Modulus of Amorphous Polymer Thin Films: Relationship to the Glass Transition Temperature.* ACS Nano, 2009. **3**(9): p. 2677-2685.

27. Miyake, K., Satomi,N., Sasaki, S., *Elastic modulus of polystyrene film from near surface to bulk measured by nanoindentation using atomic force microscopy.* Applied Physics Letters, 2006. **89**(3): p. 031925.

28. Tweedie, C.A., Constantinides, G., Lehman, K.E., Brill, D.J, Blackman, G.S, Van Vliet, K.J., *Enhanced Stiffness of Amorphous Polymer Surfaces under*

Confinement of Localized Contact Loads. Advanced Materials, 2007. **19**(18): p. 2540-2546.

29. Vogt, B.D., Soles, C.L., et al., Polymer, 2005. **46**(5): p. 1635.
30. Vogt B.D., Soles, C.L., et al., Polymer, 2005. **46**(5): p. 1635.
31. Kent M.S., et al., Baker S.M., et al.,, Journal of Material Science, 1996. **31**: p. 927.
32. Kent M.S., et al., Journal of Adhesion 1999. **69**: p. 121.
33. Wu W.L., Orts, W., et al., Polymer Engineering Science, 1995. **35**(12): p. 1000.
34. Chen H., Jean, Y.C., et al., Macromolecules, 2007. **40**(21): p. 7542.
35. Lu C., et al., ed. *Applications of Piezoelectric Quartz Crystal Microbalances*. 1984, Elsevier: NewYork.
36. Crank J., ed. *The Mathematics of Diffusion*. second ed. 1975, Oxford University Press: New York.
37. Long F.A., Richman, D.J., Journal of the American Chemical Society, 1960. **82**: p. 513.
38. Satterfield, M.B., Benziger, J.B., *Non-Fickian water vapor sorption dynamics by Nafion membranes.* Journal of Physical Chemistry B, 2008. **112**: p. 3693.
39. Kabanova, O.P., Timofeev, D. N., *The determination of the diffusion coefficient of water vapor in granulated zeolites by adsorption from a carrier-gas current.* Chemistry and Materials Science, Russian Chemical Bulletin. **12**(1): p. 157.
40. Soles C.L., Douglas, J.F., et al., Journal of Polymer Science Part B-Polymer Physics 2004. **42**(17): p. 3218.
41. Vogt B.D., Soles, C.L., Langmuir 2004. **20**(4): p. 1453.

42. Jean, Y.C., ed. *Principles and Applications of Positron and Positronium Chemistry*. 2003, World Scientific Publishing Co: NewJersey.

43. Rowe, B.W., Pas, S.J., Hill, A.J., Suzuki, R., Freeman, B.D., Paul, D.R., *A variable energy positron annihilation lifetime spectroscopy study of physical aging in thin glassy polymer films.* Polymer, 2009. **50**: p. 6149.

44. Huang, Y., Wang, X., Paul, D.R., *Physical aging of thin glassy polymer films: Free Volume Interpretation.* Journal of Membrane Science, 2006. **277**: p. 219.

45. Rowe, B.W., Freeman, B.D., Paul, D.R., *Physical aging of ultrathin glassy polymer films tracked by gas permeability.* Polymer, 2009. **50**(23): p. 5565-5575.

46. van der Lee, A., et al., *Density Profiles in Thin PMMA Supported Films Investigated by X-ray Reflectometry.* Langmuir, 2001. **17**(24): p. 7664-7669.

47. DeMaggio, G.B., et al., *Interface and Surface Effects on the Glass Transition in Thin Polystyrene Films.* Physical Review Letters, 1997. **78**(8): p. 1524.

48. Sinha, A.K., *Design and Characterization of Materials and Processes for Area Selective Atomic Layer Deposition* in *Chemical & Biomolecular Engineering*. 2006, Georgia Institute of Technology.

49. Vrentas J.S., Duda, J.L., Journal of Polymer Science, 1977. **15**: p. 403.

50. Soles C.L., Douglas, J.F., Wu W.L., et al., Macromolecules, 2003. **36**(2): p. 373.

51. Wu W-L., Zanten J.V., et al., *Glass transition temperature of ultrathin polymer films on silicon.* Materials Research Society Symposium Proceedings, 1995. **381**: p. 147.

52. Marshall, A.S., Petrie, S.E.B., *Rate-determining factors for enthalpy relaxation of glassy polymers. Molecular weight.* Journal of Applied Physics, 1975. **46**(10): p. 4223-4230.

53. Huang, Y., Paul, D.R., *Physical aging of thin glassy polymer films monitored by gas permeability.* Polymer, 2004. **45**: p. 8377.

54. Huang, Y., Paul, D.R., *Physical aging of thin glassy polymer films monitored by optical properties.* Macromolecules, 2006. **39**: p. 1554.

55. Huang, Y., Paul, D.R., *Effect of temperature on physical aging of thin glassy polymer films.* Macromolecules, 2005. **38**: p. 10148.

56. Huang, Y., Paul, D.R., *Effect of film thickness on the gas permeation characteristics of glassy polymer membranes.* Industrial Engineering and Chemistry Research (ACS), 2007. **46**: p. 23426.

57. Turnbull, D., Cohen, M.H., *Effect of film thickness on the gas permeation characteristics of glassy polymer membranes.* Jouornal of Chemical Physics, 1961. **34**: p. 120.

CHAPTER 3

DIFFUSION IN PHOTORESISTS

3.1 Introduction

Acid catalyzed deprotection reaction of chemically amplified resists is an important step in photolithography technique followed in semiconductor industry. Resolution of the features formed during lithography process is greatly affected by diffusion of photoacids generated in these resists. Thus, the coupled effects of chemical kinetics of the reaction and diffusion on the nanoscale features printed using lithography techniques are being extensively studied using experimental and simulation methods [1-3]. In this study, the effect of film thickness on diffusion behavior of photoacids in chemically amplified photoresists is investigated. This study is focused on studying the diffusion behavior in thin chemically amplified photoresist (CAR) films, based on the observation of deviation in diffusion of ultra-thin polymer films from bulk and its dependence on film thickness reported in Chapter 2.

The phenomenal progress of semiconductor industry that focuses on doubling the number of transistors in an Integrated Circuit (IC), according to Moore's law, has been made possible by the development in photolithography technique, used to transfer circuit patterns. Photolithography using CAR involves spin coating a layer of solution mixture of a polymer resin and a photoacid generator (PAG) onto a silicon substrate. CAR or photoresist, on exposure to radiation, generates acid due to decomposition of photoacid generator or PAG. Commonly used PAGs in photolithography consist of ionic and \non-

ionic PAGs that are iodonium and sulfonium salts. These onium salts generate strong triflic acids on decomposition when exposed to radiation.

$$PAG \xleftrightarrow{h\gamma} PAG^{*} \rightarrow Acid$$

The acid thus generated by decomposition of PAG molecule diffuses under the influence of baking temperature. The diffusion of photoacid enables decomposition of resist polymer (deprotection of protecting group on a polymer resin) to generate base soluble functional groups. The deprotected polymer resin is then dissolved using a base called a developer. The processing steps involved in photolithography using chemically amplified photoresists, is shown in Figure 3.1. From the figure it can be seen that understanding effects of sample dimensions on acid transport within photoresist is very critical to control diffusion length of acids and enhance imaging performance of photoresist materials.

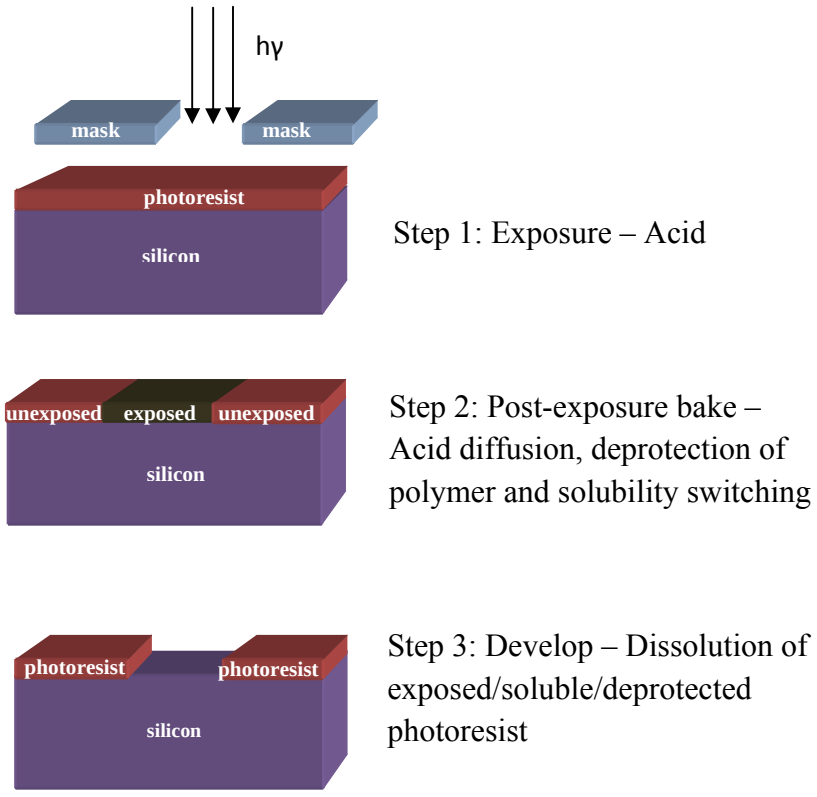

Figure 3.1 Processing steps involved in photolithography using chemically amplified photoresists

3.2 Experiment Details

Polyhydroxystyrene fully protected with t-butoxycarbonyl (PTBOCST), synthesized using a procedure described elsewhere [4], is the polymer resin chosen. Briefly, 2.1 g of Polyhydroxystyrene purchased from Sigma Aldrich Inc., was dissolved in acetonitrile and 0.254 g of Dimethylaminopyradine (DMAP) was added to this solution in a flask. To this solution mixture, 5.45 g of ditertbutyl carbonate was added. The reactants reacted and carbon-di-oxide evolved as a by-product. This was observed and confirmed by the swelling of a balloon attached to the opening of the flask. After the completion of reaction in 72 hours, the resulting solution mixture was precipitated in

water. The solid mixture from precipitation was purified and dried in vacuum oven. Characterization of the product was performed using H-NMR and thermo-gravimetric analyzer with a mass spectrometer.

Stock solutions of PTBOCST were prepared by dissolving it in propylene glycol monomethyl ether (PGMEA) purchased from Sigma Aldrich Inc., Triphenylsulfonium trifluoromethane sulfonate (TPS.TFMS) and Triphenylsulfonium perfluorobutane sulfonate (TPS.PFBS) also purchased from Sigma Aldrich Inc., were the photoacid generators (PAG) used in the formulation of model photoresists. Solutions of different concentrations (1 wt% to 7 wt%) were prepared to obtain different film thicknesses (~45 to 250 nm). The acid loading in these solutions were 0.5 wt% of the total polymer. PAG loading was chosen to be low to ensure sparse distribution of acid in the polymer matrix [3].

Table 3.1 Materials used in the preparation of model photoresists

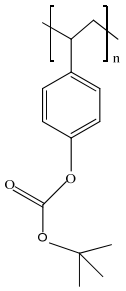	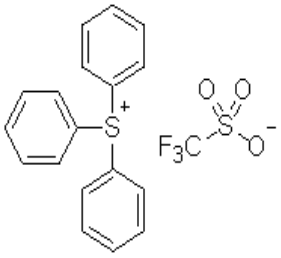	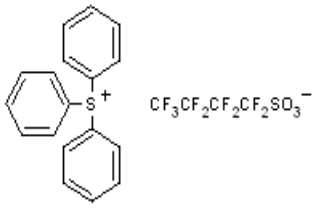
Polyhydroxystyrene fully protected with t-butoxycarbonyl (PTBOCST)	Triphenylsulfonium trifluoromethane sulfonate (TPS.TFMS)	Triphenylsulfonium perfluorobutane sulfonate (TPS.PFBS)

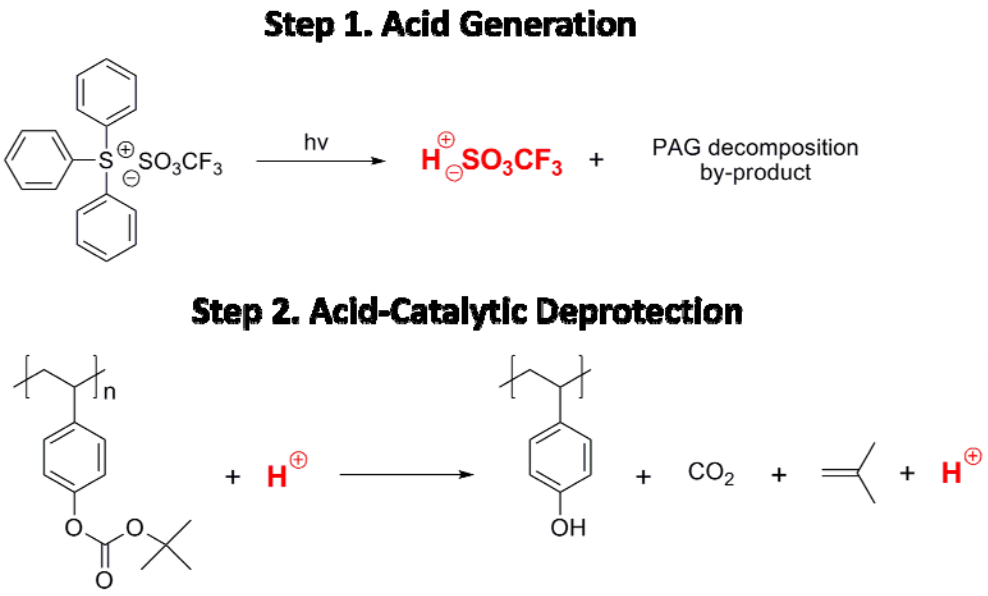

Figure 3.2 Reaction steps involved in photolithography using chemically amplified photoresists

Model photoresist solutions thus prepared were dispersed and spin coated using a spin coater (CEE Model 100 CB spin coat and bake system) at different spin speeds (1000 rpm to 4000 rpm), thus giving films of different thicknesses. Silicon wafers with 200 nm of gold deposited by e-beam evaporation (CVC SC 5000 E-beam Evaporator, CVC Inc.) were used as the substrate. About 20 nm of titanium was used as the adhesion layer for gold on silicon. This reflective substrate was needed for use of Grazing Angle Infra Red Spectroscopy in reflection mode, described in detail below. Spin coated films of photoresists were soft baked at 100^0C for 2 minutes on a custom-built contact hot plate to remove residual casting solvent. The film thickness was measured using an M-2000 ellipsometer (J.A. Woollam Inc.,) using a stack of polymer on gold, Cauchy model. The films were then flood exposed using an exposure source (model no. 87530-1000, Hg-Xe arc lamp) at a dose of 250 mJ/cm^2, using a 248 nm bandpass filter (bandwidth 11 nm,

FWHM). The exposure dose was chosen to ensure complete decomposition of all loaded PAG in the system. The exposed films were immediately post-expose baked (PEB) at different temperatures (70 - 110^0C) for about 2 minutes. Post exposure bake was performed on a temperature controlled hot-stage (model TS1400 XY Stage) from Linkam Inc., mounted on the platform of Hyperion Microscope of Bruker Vertex 80 V FTIR (Bruker Inc.,). The hot-stage is controlled by temperature controller (model TP94) also from Linkam Inc., with a precision of 0.1^0C. The temperature controller is used to ramp up the temperature of hot-stage from room temperature to desired temperature (at a ramp rate of 90^0C/min) and maintain it at that temperature. Grazing angle reflectance (GIR) mode was used on the Hyperion Microscope to monitor the change in chemical composition of the sample (in other words, the progress of deprotection), as the sample is being post-expose baked. Background spectrum was scanned on a blank gold coated silicon wafer on hot plate. To avoid any loss of deprotection information during focusing, the hot-stage mounted on the microscope was held in focus and each time the samples were inserted through a side door on the hot-stage. Rapid Scan Time Resolved (RSTR) measurement mode on the OPUS software (Bruker Inc.,) was used to enable repeated collection of spectra as a function of time. To collect data at higher frequency, averaging of 8 scans of interferrogram was used for each spectrum. The intensity of carbonyl stretch of PTBOCST (1764 cm^{-1}) was monitored for deprotection and 100% protected PTBOCST polymer was used as reference. Integration of area under carbonyl peak of background- corrected spectra was used to estimate the extent of deprotection based on the reference peak, measured for the 100% protected PTBOCST, in the beginning of the experiment. A sample spectrum is shown in Figure 3.3. The integration was also

performed using the OPUS software using the integration function. The raw data thus obtained based on the integrated area of the peak (1764 cm^{-1}) after the IR scans at regular time intervals while baking on the hot-stage is shown in Figure 3.5.

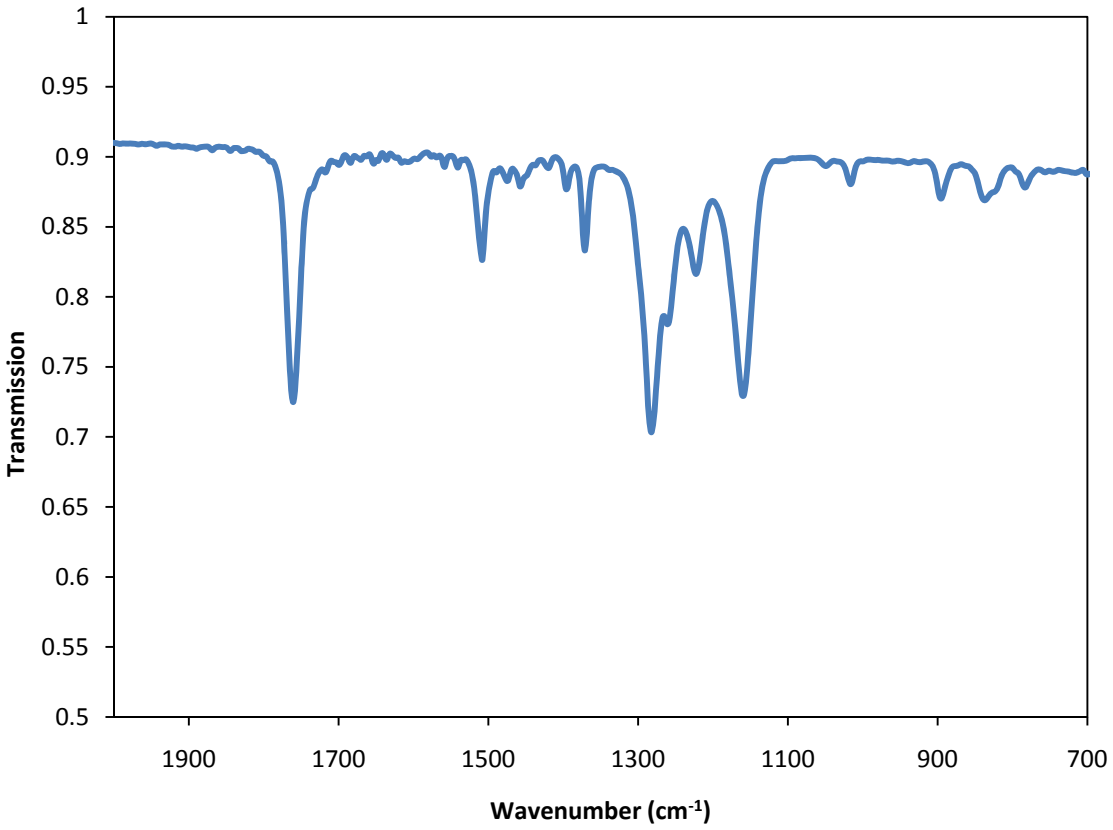

Figure 3.3 Sample plot of IR transmission spectrum of 100% protected PTBOCST on gold coated silicon substrate for a film thickness of about 238 nm. Area integrated under 1764 cm^{-1} peak – carbonyl stretch peak associated with t-BOC group, was used to monitor deprotection extent with time

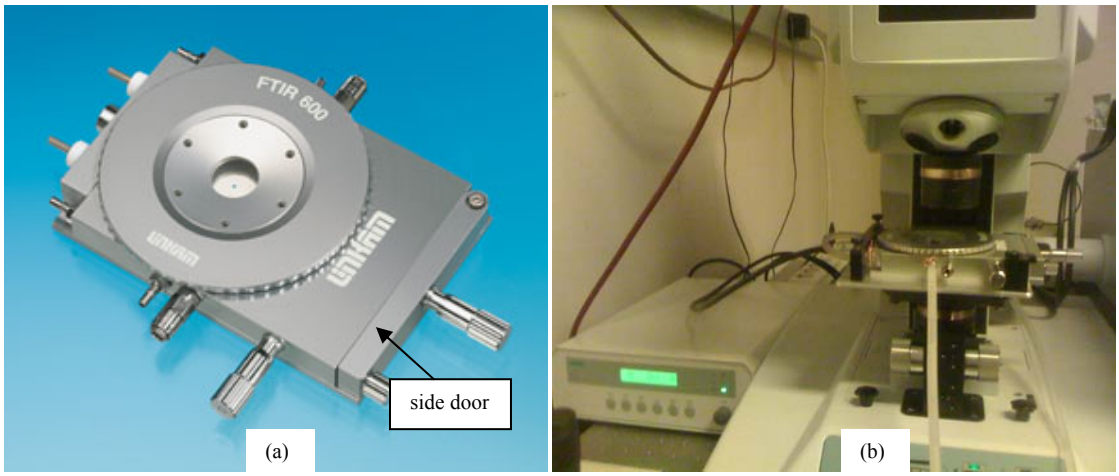

Figure 3.4: (a) Linkam hot-stage used for post-exposure bake. It enables sample replacement through side door, without the need to focus for every sample and any loss of information during focusing. (b) Experimental setup of Linkam hot-stage mounted on Hyperion microscope of Vertex 80 V FTIR to dynamically capture deprotection progress with time.

3.3 Results and Discussion

The extent of deprotection was calculated from the integrated area of the carbonyl peak with 100% protected peak area as reference. The experimental results for TPS.PFBS and TPS.TFMS at a constant PEB temperature of 90^0C are shown below. From Figure 3.5(a), careful observation of the raw data shows that for TPS.PFBS system, qualitatively the extent of deprotection is at its maximum for film thickness of about 238 nm. A maximum deprotection of about 60% is achieved (40% protected polymer remaining) for this thick film. In other words, extent of deprotection decreases with decrease in film thickness, with minimum deprotection observed for a film thickness about 45 nm. A similar trend for the extent of deprotection is observed with TPS.TFMS system as well. Maximum deprotection is observed for the thickest film about 242 nm with 85% deprotection (15%

protected polymer remaining) and minimum deprotection is observed for the thinnest film about 44 nm. So in both the systems, extent of deprotection is observed to decrease with decrease in film thickness. Now, a comparison of the maximum deprotection achieved in the two systems for thick films (238 nm and 242 nm) of comparable thicknesses are, 60% and 85% for TPS.PFBS and TPS.TFMS PAGs respectively. This difference in extent of deprotection for the two acids for almost comparable film thicknesses, suggests that there is a difference in diffusion coefficients of acids generated by the two PAGs. Molecular dimension comparison of the two PAGs from their molecular structures shown in Figure 3.2, suggests that TPS.PFBS is larger than TPS.TFMS. This difference in molecular dimensions of the PAGs could be directly associated with this observed phenomenon. As PFBS is larger than TFMS, diffusion coefficient of PFBS would be lesser than the diffusion of TFMS and hence the extent of deprotection achieved with TPS.PFBS is lesser than that achieved with TPS.TFMS. This observation is in agreement with similar results reported in literature, from a study of comparison of molecular sizes of PAGs [5]. These, however are only qualitative conclusions from the raw data based on the trends observed.

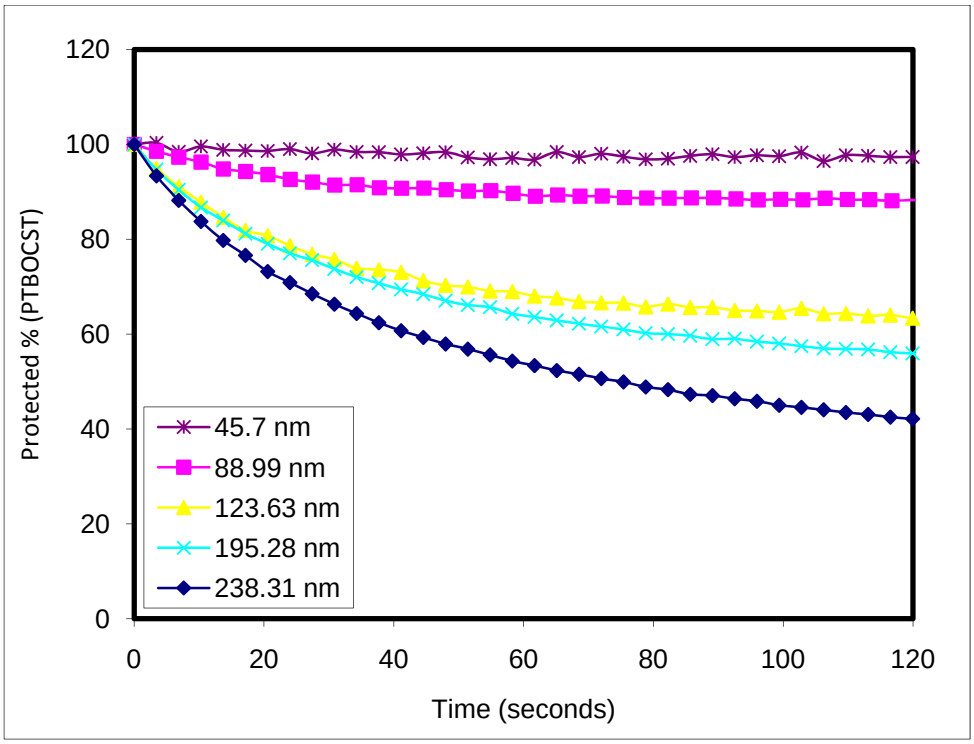

Figure 3.5(a) Experimental data showing the extent of deprotection observed in model photoresists as a function of film thickness in PTBOCST + PFBS

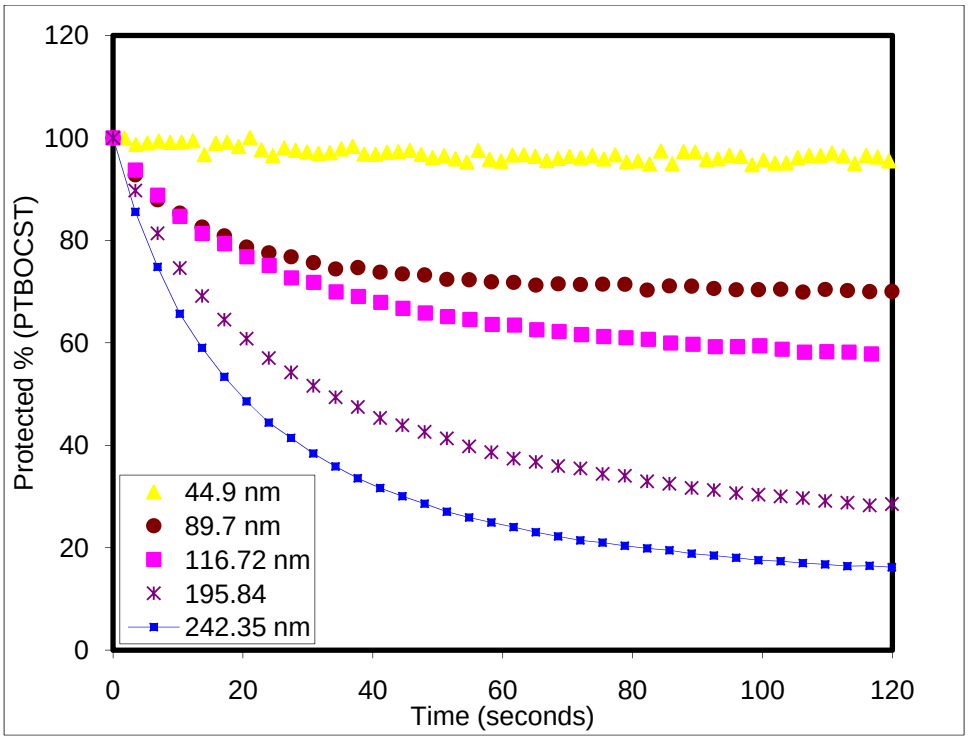

Figure 3.5(b) Experimental data showing the extent of deprotection observed in model photoresists as a function of film thickness in PTBOCST + TFMS

3.3.1 Theory

The deprotection reaction in a chemically amplified photoresist (CAR) is generally described as:

$$\frac{dC_p}{dt} = -k_{acid}C_pC_{acid} - k_{auto}C_pC_d - k_{thermo}C_p \qquad (1)$$

Where, C_p and C_d are concentrations of t-BOC protected and deprotected polyhydroxystyrene, respectively. The rate constants of acid-catalyzed, auto-catalyzed and thermolytic reactions are given by k_{acid}, k_{auto} and k_{thermo}. Thermolytic reactions are possible when the elevated temperature of post-exposure bake facilitates thermal

decomposition of the protecting group on polyhydroxystyrene. Auto-catalytic reactions are possible when the acidity of a deprotected polymer unit favors deprotection of a protected polymer unit. Auto-catalytic and thermal decomposition reactions of high activation energy protecting groups like t-BOC have been shown to occur at temperatures higher than 120^0C [6]. Since all the experiments presented here are at post-exposure bake temperatures lower than 120^0C, it is obvious that all the deprotection observed and reported are completely due to acid-catalyzed reactions only. Hence the deprotection rate equation reduces to,

$$\frac{dC_p}{dt} = -k_{acid} C_p C_{acid} \tag{2}$$

Thus, the rate of deprotection in a chemically amplified photoresist is largely dependent on the concentration of acid and the number of protected units of polymer to be deprotected. Further, in general, acid-catalyzed deprotection reaction in the presence of super-acids (like acid molecules used in this study) is fast compared to acid diffusion in the polymer matrix. The time scale for reaction and diffusion is compared in similar studies by Houle et al., [1] and diffusion is found to be the rate-limiting step. Thus the extent of deprotection observed in the study was attributed to the diffusion of acid, assuming an instantaneous deprotection reaction, when an acid reaches a protected site.

3.3.2 Simulation Details

In order to quantitatively extract the diffusion coefficients and understand the impact of thin film confinement effects on acid transport, a reaction-diffusion model was used. Stochastic reaction-diffusion model used here was adopted from stochastic

simulation algorithm proposed by Gillespie [7] and implementation of the algorithm has been reported earlier by Cheng-Tsung Lee from our research group [8]. The description of the reaction-diffusion model, its derivation and step-by-step algorithm are explained in detail in Chapter 5 of Cheng-Tsung Lee's dissertation. Briefly, the model consists of a three dimensional lattice structure with cells randomly assigned a PTBOCST group or an acid molecule, based on the chemical composition of the experimental system. The cells are assigned a volume equivalent to the volume of a PTBOCST group or an acid molecule. The cell dimensions were obtained using the molar density of the resist films, measured using a Quartz Crystal Microbalance (QCM) (setup description in Chapter 2). For this, mass of spin coated photoresists films on gold coated quartz crystal was calculated using the difference in the oscillating frequency of blank (f_{blank}) and film coated crystals (f_{film}). The frequency change was related to the mass of film using the Sauerbrey [9] equation

$$m_{resist} = \frac{f_{blank} - f_{film}}{C_f} \tag{3}$$

Where C_f is characteristic constant of the crystal related to its resonant frequency ($f_q \sim 5$ MHz), density of the crystal ($\rho_q = 2.649$ g/cm^3), and shear velocity of AT cut crystal ($v_q \sim$ 332,200 cm/s) through the equation,

$$C_f = \frac{2 f_q^2}{\rho_q v_q} \tag{4}$$

Mass of the film is then converted into molar density using measured film thickness and hence volume of the film. Cell dimensions of protected polymer matrix used in simulation is calculated using this molar density.

In order to characterize diffusivity in photoresists, the photoresists were flood exposed such that all the PAGs in the photoresist were decomposed. Macroscopically, there is a homogeneous distribution of acid molecules in the resist matrix such that there is no acid gradient in the resist and hence no diffusion of acid initiated due to concentration gradient. However, microscopically diffusion exists due to concentration gradient in a microscopic scale, which can be characterized using Fick's second law of diffusion. Initially the polymer is 100% protected and is represented by cells in the 3D lattice, which are randomly assigned either a protected polymer unit or an acid molecule, based on the composition of the resist i.e., ratio of PAG to polymer. During PEB, acid molecule is moved randomly to any of its six neighboring cells in the 3D lattice. Diffusion coefficient of the acid is dependent on the position of the acid in the 3D matrix. In other words, diffusion coefficient of the acid is different in a protected (PTBOCST) and deprotected (PHOST) polymer sites. Thus diffusion length for acid molecule is calculated based on the sum of half the length of its origin and destination cells.

The fit of experimental data to simulated model for the extent of deprotection as a function of time is shown below. The filled symbols represent experimental data and open symbols represent simulated model for each film thickness and in each PAG system. In the case of TFMS, experimental data could not be fit reasonably by simulation for the 44.9 nm film. This could be because of phase separation of photoacid generator and volatility of the acid, both of which are significantly pronounced at such low film

thicknesses for TPS.TFMS photoresist system as reported by Sundaramoorthi et al., [10]. Phase separation of TPS.TFMS PAG dispersed in polymer matrix was reported in films of thicknesses about 40 nm and lower using Time of Flight Secondary Ion Mass Spectroscopy (TOF-SIMS). In the same work, homogenous distribution of PFBS PAG was also reported for thicknesses up to 20 nm. The simulation model fits shown in the figures below, are better understood by the physical changes induced in the system due to reaction and diffusion that has been accounted for in the simulation model.

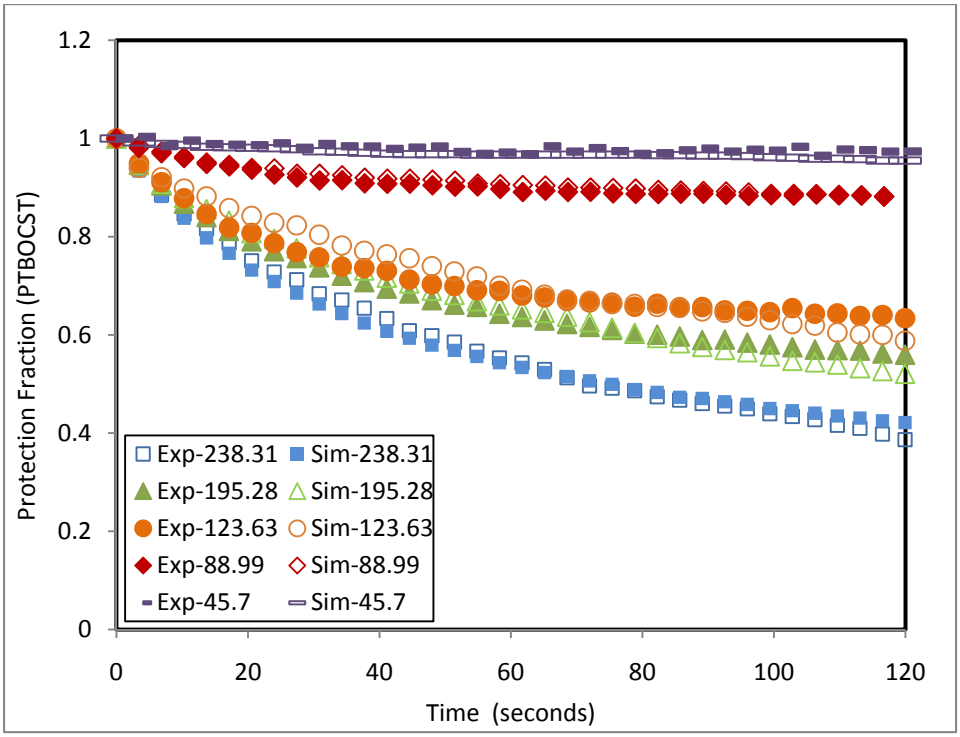

Figure 3.6(a) Simulated model fit to experimental data. Filled symbols represent deprotection extent from experiment data and open symbols represent deprotection extent from simulation in PTBOCST + PFBS

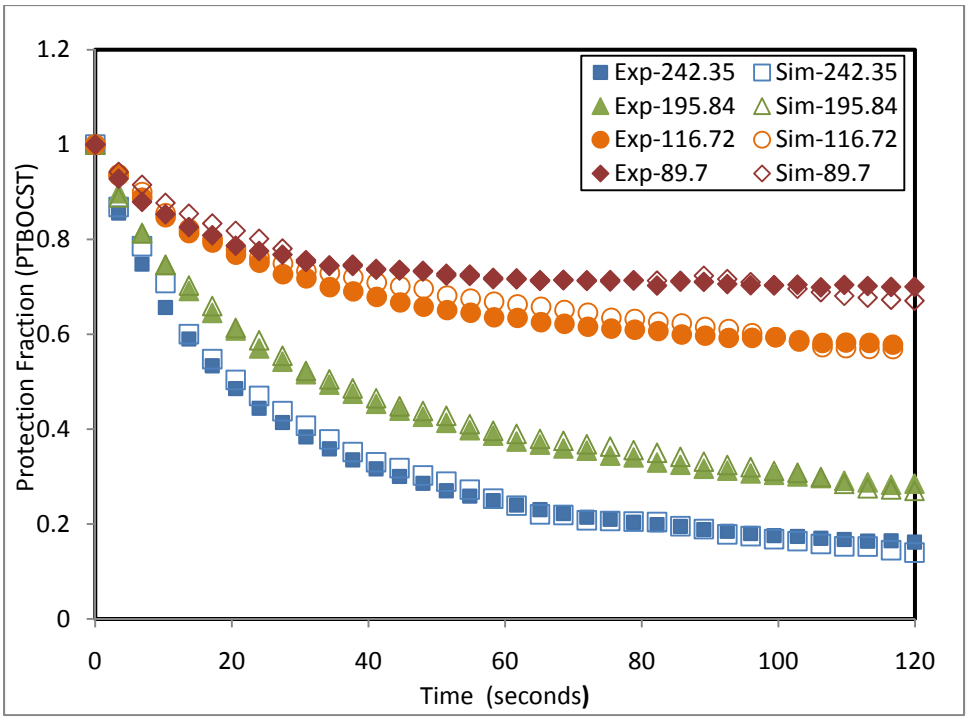

Figure 3.6(b) Simulated model fit to experimental data. Filled symbols represent deprotection extent from experiment data and open symbols represent deprotection extent from simulation in PTBOCST + TFMS

The simulation method used here takes local environment on the diffusing acid, size of the acid molecule and PEB time into account. These factors greatly impact acid diffusivity in a given resist film. Some of the assumptions used in the simulation and their validation are discussed: (i) deprotection reaction happens in any given cell instantaneously after the occurrence of diffusion of acid into the cell. Thus, the reaction is assumed to happen at a timescale much faster than that of diffusion, such that diffusion is the rate limiting step. This assumption is validated based on the reaction rate constants calculated by Houle et al., [1] for a 1200 nm film. The authors further mention that the rate constant was observed to be thickness dependent and that it was about 20% faster in

200 nm films relative to 1200 nm films. The film thickness used in the present study is less than 250 nm and the assumption of instantaneous reaction in each cell following diffusion, is thus reasonable for the entire thickness range reported here. (ii) Acid diffusivity studies in photoresist polymers performed using reaction-front model [11, 12] and surface exposure model [13] have identified two different diffusion coefficients for the protected and deprotected polymers. Also, increase in local acid mobility in protected regions where reaction is in progress relative to deprotected regions was pointed out explicitly in the reaction-front model [12]. Acids were observed to be relatively immobile and were reported to be trapped in deprotected regions and hence lost for any further deprotection of the system in reaction-front model studies [12]. In this model, acid loss due to trapping as mentioned in the reaction-front model is not explicitly accounted for. However, since two diffusion paths, one in protected cell and the other in deprotected cell, have been considered, and as the diffusion through deprotected cell is observed to be far lower than that in protected cell, acid trapping is indirectly taken into account as: when an acid molecule is surrounded by deprotected cells, the time taken by it to reach a protected cell through these deprotected cells is far too long, that it no more contributes for deprotection progress in the lattice. (iii) Free volume formulations due to volatile products have not been accounted for in the model. Shrinking lattice model is far more complicated. Further, under the assumptions, the stochastic model yielded reliable results, that addition of such details may impact all thicknesses equally thus causing little or no impact on the trend reported here. The diffusion coefficients thus extracted from simulation are tabulated below.

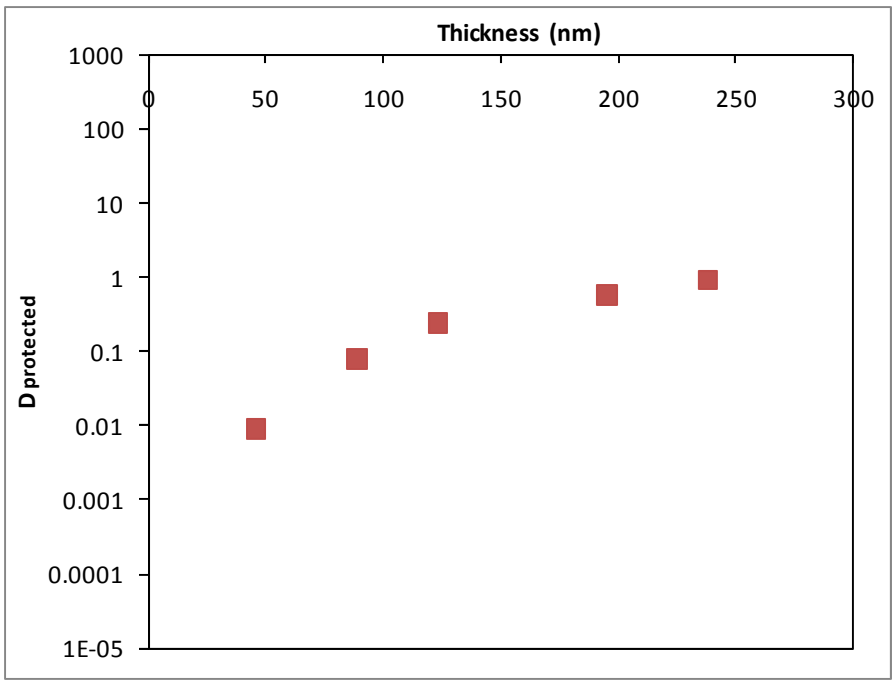

(a)

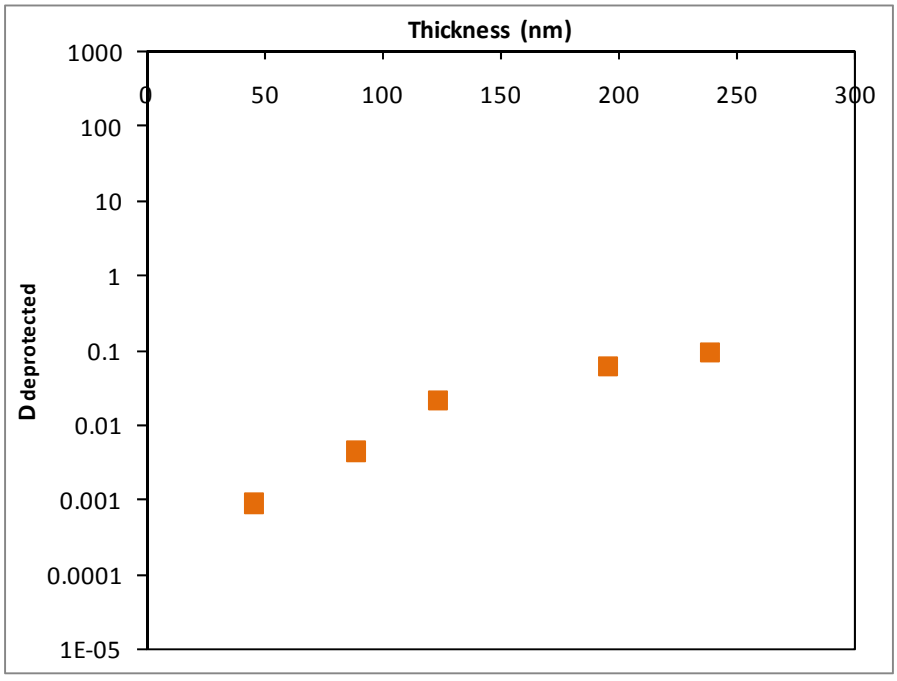

(b)

Figure 3.7 Diffusion coefficients in (a) protected (PTBOCST) and (b) deprotected polymer (PHOST) in case of PTBOCST + PFBS

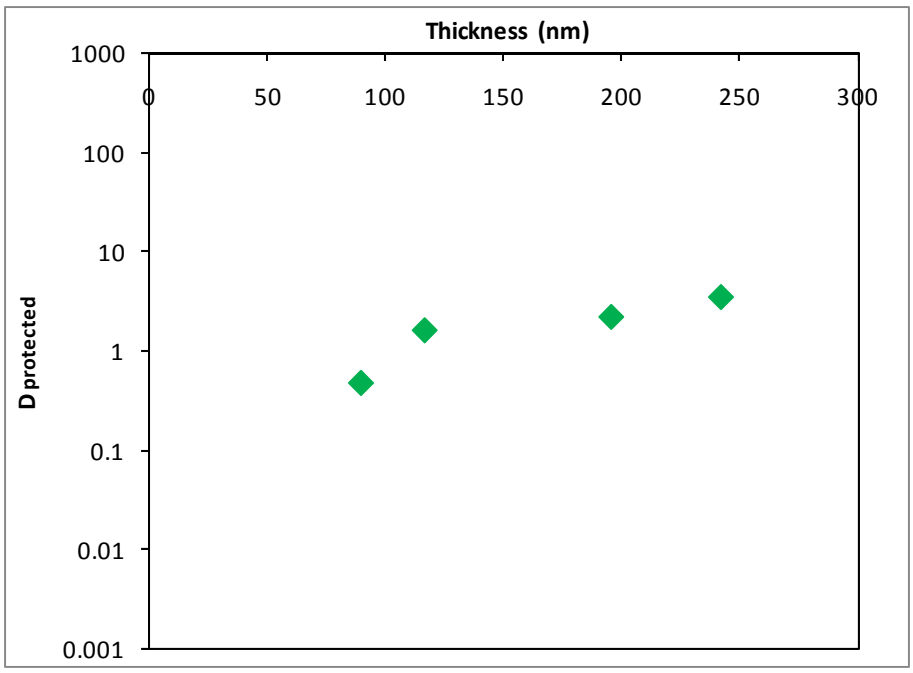

(a)

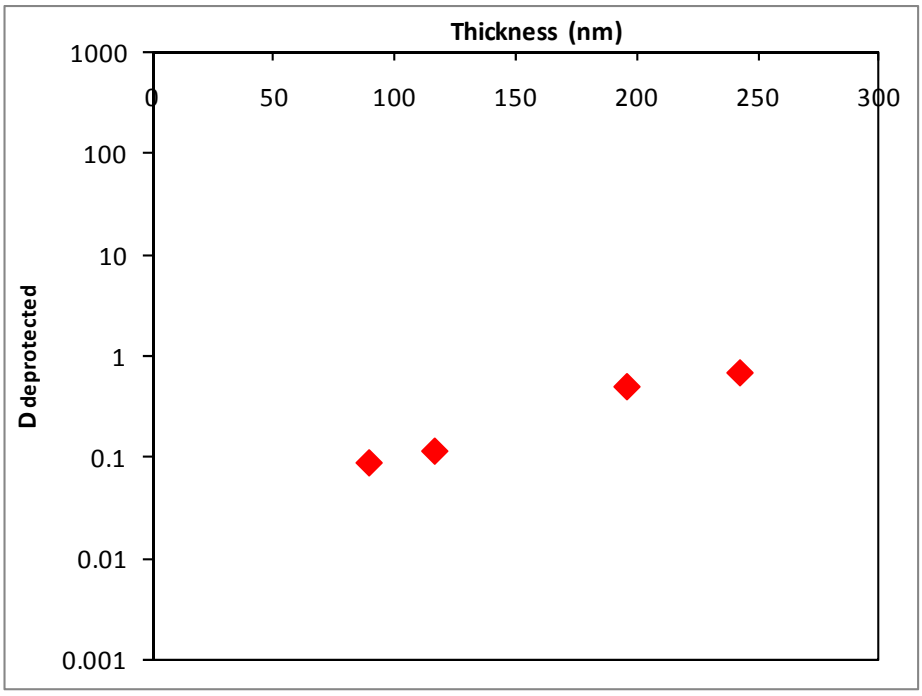

(b)

Figure 3.8 Diffusion coefficients in (a) protected (PTBOCST) and (b) deprotected (PHOST) polymer matrices in case of PTBOCST + TFMS

From Figures 3.7 and 3.8, it is seen that the diffusion coefficients of acid in protected polymer matrix, in the case of both PFBS and TFMS are greater than their corresponding diffusion coefficients in deprotected matrix by at least an order of magnitude. Further, the smaller molecular dimension of TFMS favors high mobility and hence higher diffusion coefficient than the larger PFBS is observed, for almost same film thickness. Also, the diffusion coefficient thus obtained from simulation was observed to change with change in film thickness in each of these systems. This trend is similar to that observed in pure polymer films of polymethylmethacrylate, as discussed in Chapter 2 [14]. About two orders of magnitude change in diffusion coefficient for a film thickness range of about 240 nm to 45 nm is observed in case of both pure PMMA films and in case of PTBOCST, PHOST films. Significant differences in the diffusivity of TFMS and PFBS in both protected and deprotected polymer matrices is directly attributable to the sizes of anions. Although the acid diffusion for deprotection is essentially only proton, in order to maintain local charge neutrality, the protons move as conjugate pair (proton and anion) within the polymer matrix. Thus the difference in the diffusivity of the acid associated with TFMS and PFBS is because of the anions providing stearic hindrance for mobility of its conjugate proton through the polymer matrix. In other words, the larger the acid, the higher is the transition energy required for crossing the energy barrier required for diffusion. This will be discussed in detail in the activation energy, Section 3.3.3.

Scaling of diffusion coefficient of acid with film thickness, in case of PTBOCST and PHOST polymer matrices was investigated. Such a scaling analysis would enable compare the thickness dependence of diffusion in photoresists to diffusion in pure

polymers seen in Chapter 2. While investigating the diffusion of acid at different temperatures to enable estimation of activation energy needed for diffusion, it was found that volatility of the TPS.TFMS acid affected the trend in deprotection (Figure 3.11). This will be explained in detail in section 3.3.3. From the trend in Figure 3.11, the choice of post exposure bake temperature of 90^0C used to investigate the diffusion of acid in TPS.TFMS system seemed to be affected by volatility of the acid. Hence the deprotection extent obtained at this temperature should include volatility of the acid through the film. Thus any scaling analysis for thickness dependence of diffusion of TFMS acid would be meaningless. Scaling of thickness dependence of TPS.PFBS acid in PTBOCST and PHOST are reported. As it can be seen in Figure 3.9 (a) and (b), the diffusion of acid shows approximately thickness squared dependence. The larger thickness dependence (from the power) observed in case of diffusion in this system relative to pure PMMA films reported in Chapter 2 could be because of thickness change in these films during the process of deprotection. Larger thickness dependence could be partly because of overestimation due to this average thickness used in scaling and may also be because of relatively larger activation energy for diffusion of acid in PTBOCST and PHOST relative to PMMA as will be seen in Section 3.3.3 and has been reported as chain stiffness difference between PTBOCST and PMMA in neutron scattering studies [15].

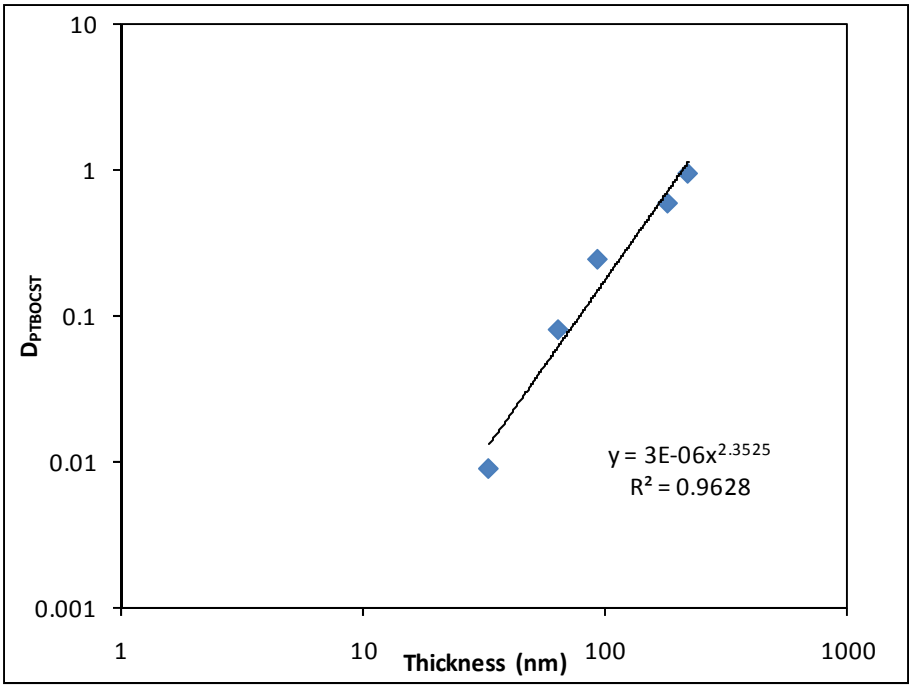

(a)

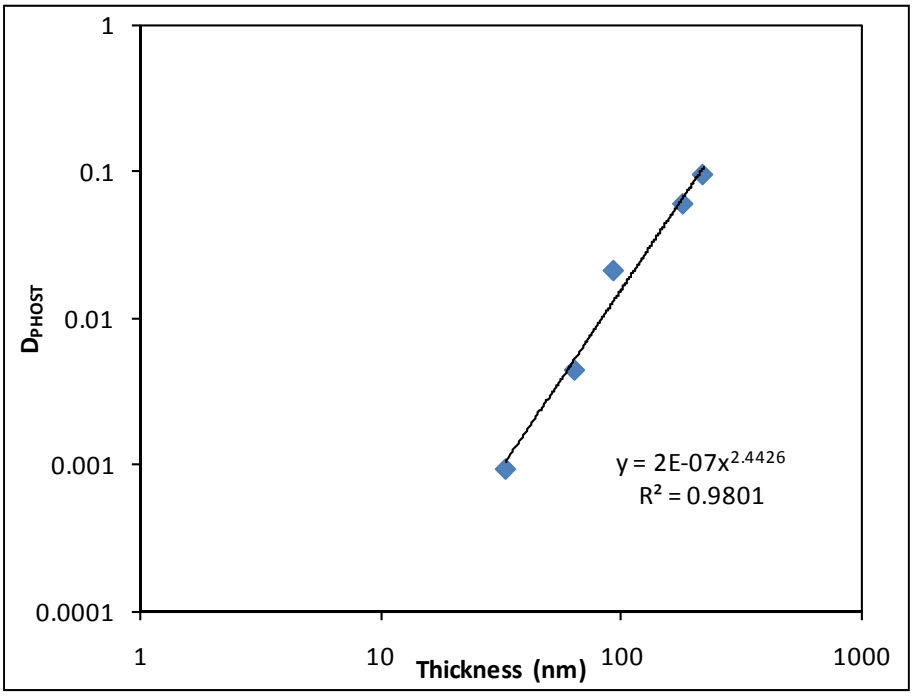

(b)

Figure 3.9 Thickness dependence of diffusion of TPS.PFBS acid in (a) protected PTBOCST matrix and (b) deprotected PHOST matrix

3.3.3 Activation Energy for Diffusion

Investigating diffusion of different acids in polymer matrix enabled investigation of influence of acid size in addition to film thickness influence, in the previous section. Dependence of diffusion on PEB temperature was investigated by baking the exposed PTBOCST + PFBS and PTBOCST + TFMS resists at different temperatures. Experimental data collected for PTBOCST + PFBS system, in a way similar to that explained in section 3.2 is shown below:

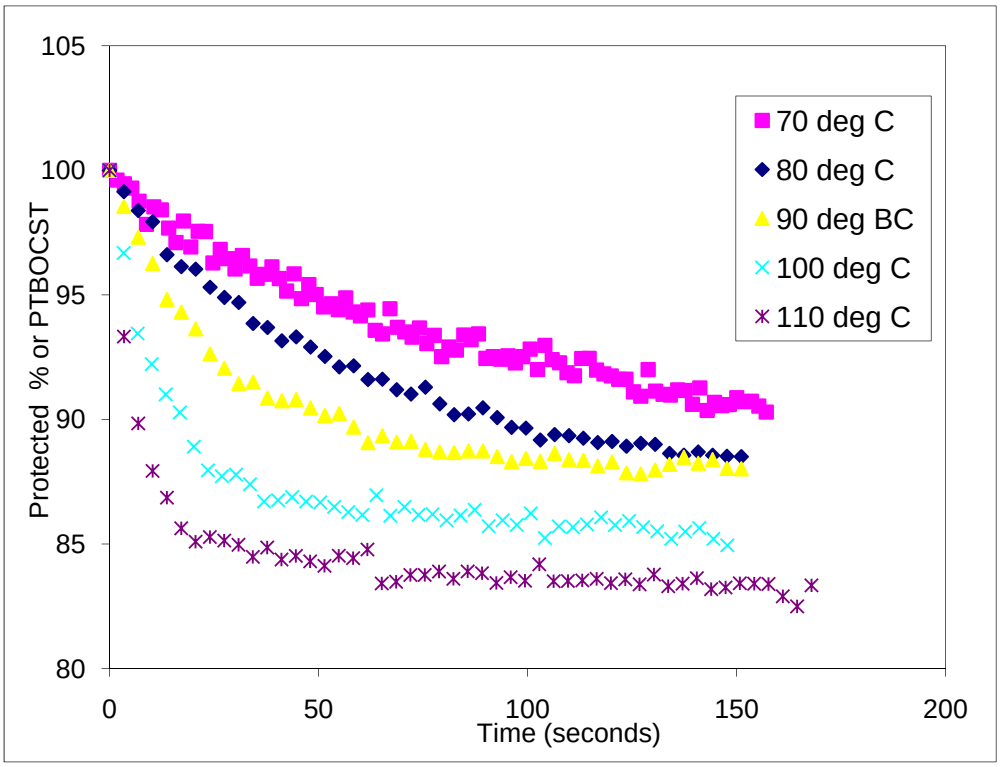

Figure 3.10 Protected percentage of PTBOCST matrix in 88.99 nm thick film from post-exposure bake at different temperatures, when acid generated from PFBS caused different deprotection extent based on diffusion length of acid at that temperature

From Figure 3.10, it can be seen that the extent of deprotection is more at higher temperatures than at lower temperatures. The observed decrease in deprotection rate at lower temperatures could be due to decrease in diffusion coefficient. This shows the dependence of diffusion on temperature. Unlike the PTBOCST + PFBS system, the extent of deprotection in PTBOCST + TFMS system (Figure 3.11) increases with increase in temperature from 70^0C to 90^0C and above 100^0C this trend is lost. The extent of deprotection is higher at 90^0C than at 100^0C or 110^0C. This is because of the high volatility of trifluoromethane sulfonic acid in PTBOCST + TFMS system. The high volatility of the acid [10] resulted in the trend in deprotection observed below:

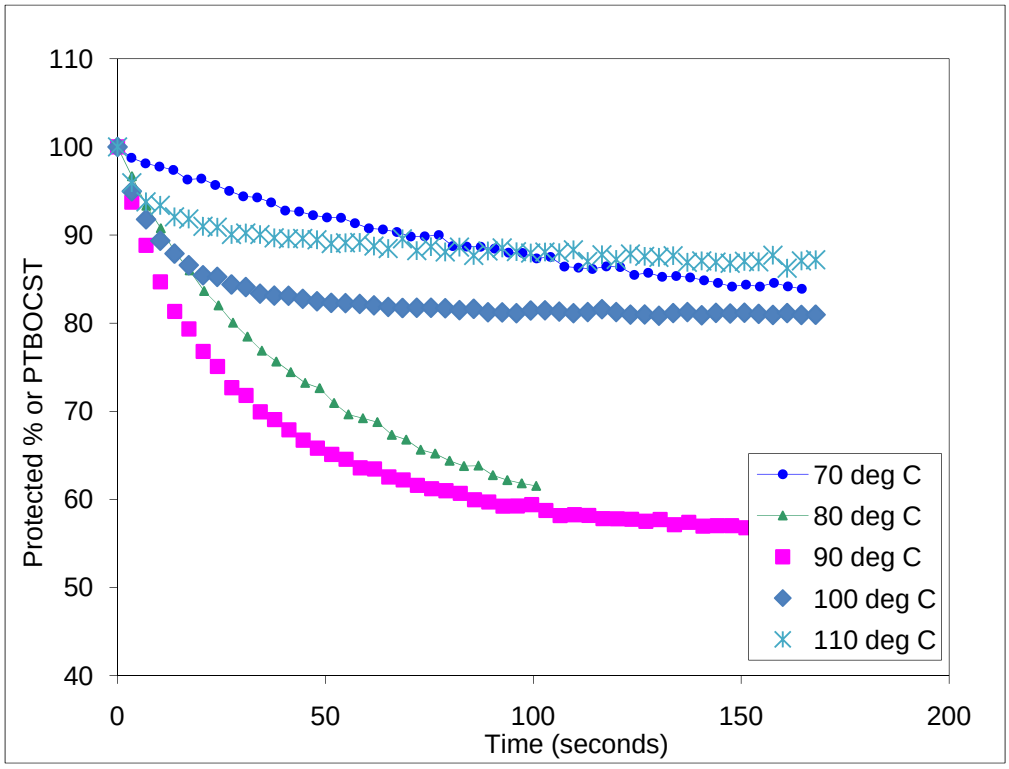

Figure 3.11 Protected percentage of PTBOCST matrix during post-exposure bake enables diffusion of acid generated from TPS.TFMS for a film thickness of 89.7 nm. High volatility of the acid at high temperatures results in an improper trend in deprotection of the matrix

Like the analysis of diffusion in PMMA, using the diffusion coefficients for photoresist films of different thicknesses, the diffusion observed at different temperatures enabled the estimation of activation energy for diffusion in the photoresist using Arrhenius relationship as:

$$D = D_0 e^{-\frac{E_a}{RT}} \tag{5}$$

$$\ln D = \ln D_0 - \frac{E_a}{RT} \tag{6}$$

An Arrhenius plot of natural logarithm of diffusion coefficient versus temperature inverse yields a negative slope from which activation energy for diffusion can be calculated.

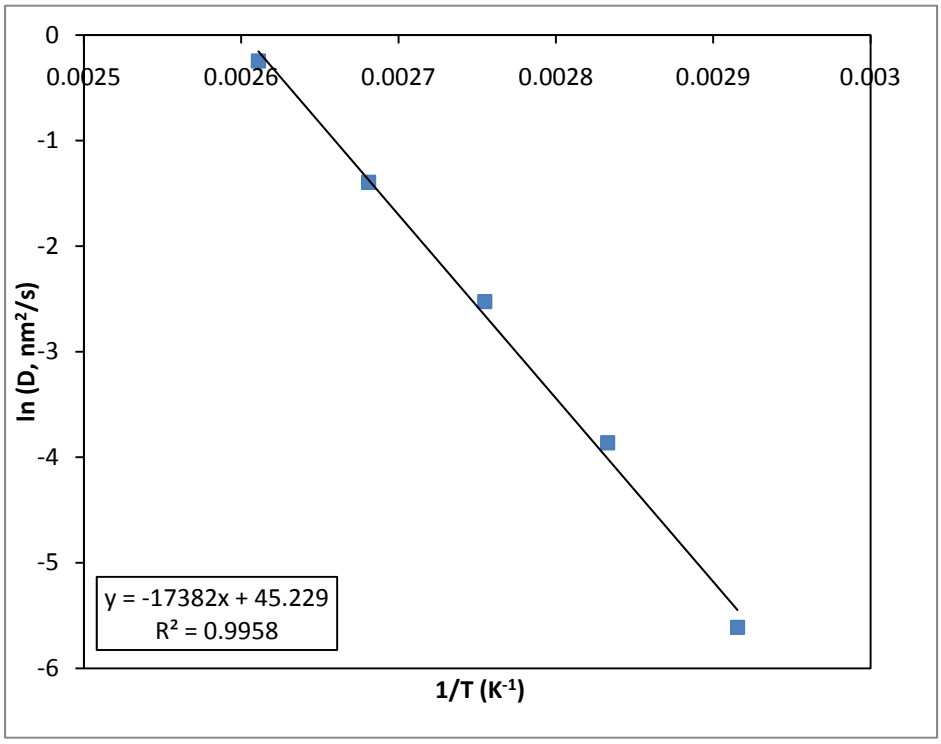

Figure 3.12 Arrhenius parameters for diffusion of perfluorobutane sulfonic acid in protected PTBOCST matrix for a film thickness of 88.99 nm

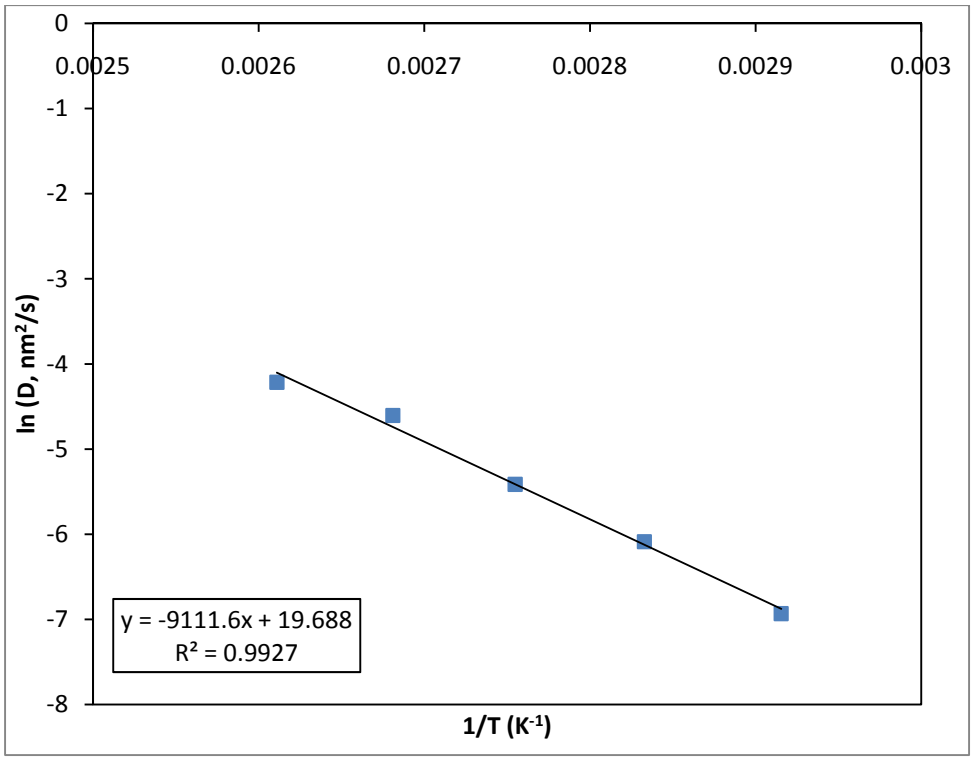

Figure 3.13 Arrhenius parameters for the diffusion of perfluorobutane sulfonic acid in deprotected PHOST matrix for a film thickness of 88.99 nm

Sample plots of diffusion of PFBS acid in 88.99 nm at different temperatures is shown in protected and deprotected polymer matrices in Figures 3.12 and 3.13. Activation energy and pre-exponential factor calculated for diffusion of PFBS in PTBOCST and in PHOST matrices for a film thickness of 88.99 nm are summarized below.

Table 3.2 Diffusion coefficients of acid in protected and deprotected polymer matrices for a film thickness of 88.99 nm

PEB Temp ^{0}C	$D_{PTBOCST}$ nm^2/s	D_{PHOST} nm^2/s
70	0.0037	0.000975
80	0.0210	0.002271
90	0.0800	0.004453
100	0.2478	0.010006
110	0.7825	0.014771

Table 3.3 Activation energy and pre-exponential factors for diffusion of acid in protected and deprotected polymer matrices for a film thickness of 88.99 nm

Arrhenius parameters	PTBOCST	PHOST
Ea (kcal/mol)	34.520652	18.0956376
D_0 (nm^2/s)	1.69434E+45	4.87528E+19

From Table 3.3, it is observed that the activation energy for diffusion of acid in PTBOCST is higher than that in PHOST matrix. This is interesting, because the diffusion coefficient in protected PTBOCST polymer matrix was observed to be higher than that in deprotected PHOST polymer matrix, from (Figures 3.7 and 3.8) for both TPS.PFBS and TPS.TFMS systems. Further, the values of Arrhenius parameters obtained here is comparable to that obtained for PFBS acid diffusion, by Houle et al., [1] and Lee et al., [8] which confirms the validity of the method used and reliability of the results. The difference in trends of Arrhenius parameters compared to diffusion coefficient trends

between protected and deprotected polymer matrix is primarily due to the interaction of acid with polymer matrix. Houle et al., [13] reported that the trends of Arrhenius parameters could be due to ionic nature of the diffusing acid which strongly interacts with polymer matrix compared to non-ionic penetrants. In other words, diffusion of ionic acids could be influenced by polarity of the polymer matrix, which in turn, could result in such trends.

Analysis of mobility of acid through the polymer matrix shows that the polar hydroxyl group available in the case of PHOST matrix energetically favors mobility of protonic acid relative to that of PTBOCST matrix and hence lower activation energy is required for diffusion through a deprotected PHOST polymer matrix. On the other hand, high diffusion coefficient in protected PTBOCST polymer sites relative to deprotected PHOST polymer sites is attributed to high pre-exponential factor in Arrhenius equation for protected PTBOCST polymer sites. As pointed out earlier in section 3.3.1, mobility of proton through the polymer matrix is largely influenced by the size of anion, as the conjugate pair of proton should be in proximity during its migration through the polymer film to maintain local charge neutrality. The pre-exponential factor, also known as the frequency factor or the stearic factor, though not significantly impacted by temperature, is a direct measure of the orientation of this diffusing acid conjugate pair for proton exchange with the polymer matrix. Hence, the significantly higher pre-exponential factor for less polar PTBOCST, of the order of approximately 25 above that of polar PHOST matrix, favors high diffusivity in a protected PTBOCST polymer matrix. This suggests that the strong interaction of the diffusing acid with the polar group of PHOST requires exact orientation between the acid and the hydroxyl group, to facilitate the mobility of

proton in the polar matrix through the energetically favorable path. This results in lower stearic factor and hence lower diffusion coefficient in PHOST matrix. A similar observation of stearic hindrance and orientation factor (or pre-exponential factor) dominating the diffusion of penetrating acid through interacting polymer is reported in a study of different PAGs in protected PTBOCST and deprotected PHOST matrices [6].

The activation energy for diffusion of acid impacted by temperature, in PTBOCST + PFBS films of different thicknesses was calculated in a similar way to see the impact of film thickness and is tabulated below.

Table 3.4 Activation energies for diffusion coefficients of TPS.PFBS acid in protected (PTBOCST) and deprotected (PHOST) polymer matrices as a function of film thickness

PTBOCST		PHOST	
Thickness (nm)	Ea (kcal/mol)	Thickness (nm)	Ea (kcal/mol)
45. 7	35.884	45.7	19.667
88.99	34.52	88.99	18.095
121.39	33.433	121.39	16.929
225.61	32.901	225.61	16.565

The pre-exponential factors in all these films remained fairly constant around 1 x 10^{35}nm^2/sec for PTBOCST and 4 x 10^{19} for PHOST. Increase in activation energy with

decrease in film thickness is in agreement with similar observation for diffusion in pure polymer films reported in Chapter 2.

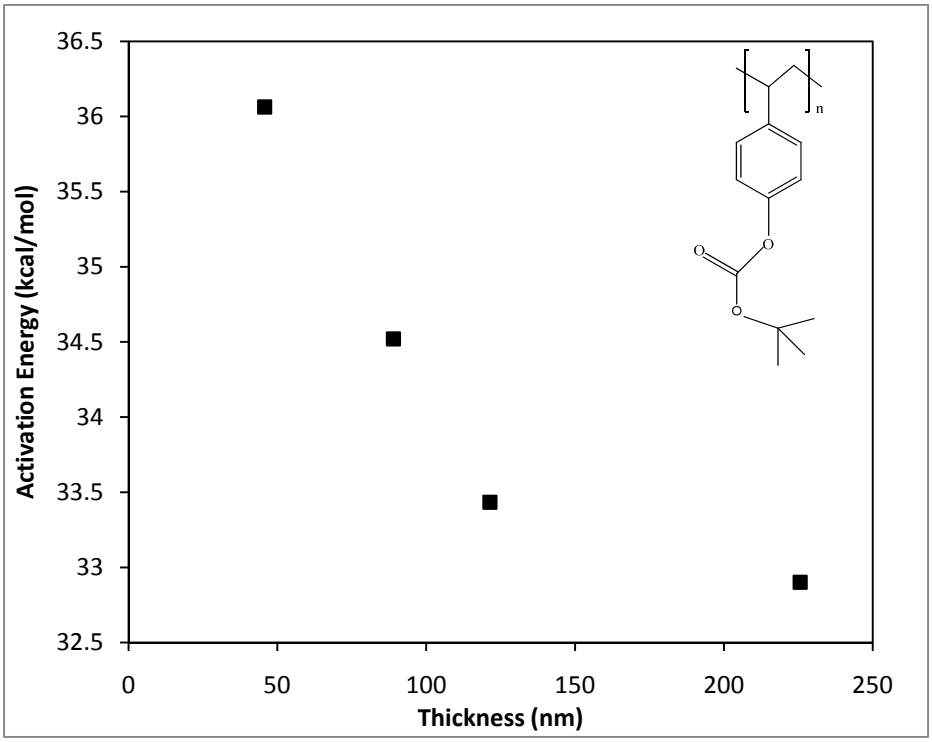

Figure 3.14 Activation energies for diffusion coefficients of TPS.PFBS acid in protected polymer (PTBOCST) as a function of film thickness

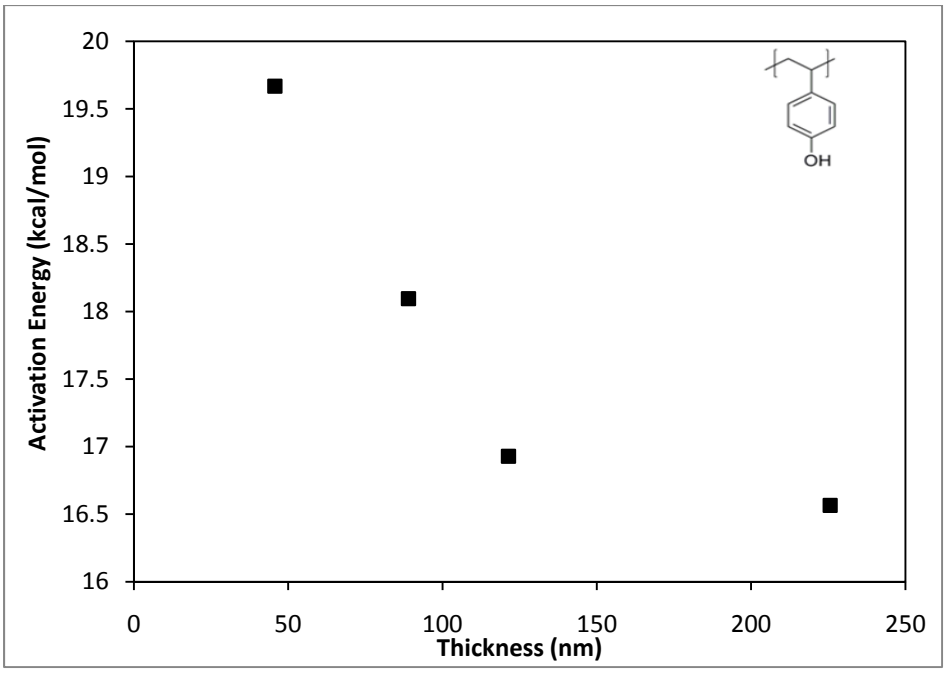

Figure 3.15 Activation energies for diffusion coefficients of TPS.PFBS acid in deprotected polymer (PHOST) as a function of film thickness

The magnitude of change in activation energy is higher than the change in case of pure polymer films. This is because the chain stiffness of PTBOCST polymer matrix is 70% higher than PMMA, as has been reported in neutron scattering studies [15]. Also the deviation in diffusion coefficient is in agreement with the change in diffusion coefficient observed with the change in film thickness, for water absorption in PTBOCST and PHOST reported earlier [16]. The experimentally obtained activation energies reported here compares satisfactorily to activation energies from similar experiments reported in literature by Houle et al., [13], further reinstating reliability of the results.

3.4 Conclusions

Investigation of diffusion characteristics of acid generated in chemically amplified photoresists showed thickness dependent behavior similar to that observed in pure polymer films [14]. The chemically amplified photoresists, while undergoing deprotection, have two distinct regimes for diffusion of acid: the protected polymer sites and the deprotected polymer sites. Diffusion behavior is distinct in these two regimes and both the diffusion coefficients show film thickness dependence and hence the influence of sample dimensions. This observation for pure polymer films and polymer composites like the photoresists described in this chapter prove that this thickness dependence of diffusion is an intrinsic property of ultra-thin polymer films. The activation energy for diffusion of acid in protected and deprotected polymer sites is affected by the size of diffusing acid, as higher transition energy is required to overcome the diffusion energy barrier for a relatively larger acid molecule. The increase in activation energy for diffusion of acid in protected and deprotected polymer matrices with decrease in film thickness clearly reveals an increase in energy barrier for diffusion of acid in ultra-thin films. This has been confirmed by the determination of activation energy for diffusion of acid, from the extent of deprotection observed in these films as a function of post-exposure bake temperature. These results are in agreement with the observation made in pure polymer films discussed in Chapter 2. Difference in diffusion coefficient of acid in thin and ultra-thin films from the bulk films and its decrease with decrease in film thickness, is an important factor to be considered in the process of photolithography used in semiconductor industry, where the film thickness is well within this range and

diffusion of acid is an important criterion that determines performance of photoresist materials.

3.5 References

1. Houle, F.A., et al., *Determination of coupled acid catalysis-diffusion processes in a positive-tone chemically amplified photoresist.* Journal of Vacuum Science & Technology B, 2000. 18(4): p. 1874-1885.

2. Gillespie, D.T., *Exact stochastic simulation of coupled chemical-reactions*. Journal of Physical Chemistry, 1977. 81(25): p. 2340-2361.

3. Lee, C.T., et al., *A simple method for measurement of photoacid generator photoreaction kinetics in formulated, chemically amplified photoresist films.* Electrochemical and Solid State Letters, 2007. 10(9): p. H273-H277.

4. Comeau, B.M., in *Chemical and Biomolecular Engineering*. 2007, Georgia Institute Of Technology: Atlanta.

5. Vogt, B.D., et al., *Measurements of the reaction-diffusion front of model chemically amplified photoresists with varying photoacid size.* Macromolecules, 2006. 39(24): p. 8311-8317.

6. Lee, C.-T., *Development and advanced characterization of novel chemically amplified resists for next generation lithography*, in *Chemical and Biomolecular Engineering*. 2008, Georgia Institute of Technology: Atlanta.

7. Gillespie, D.T., *General method for numerically simulating stochastic time evolution of coupled chemical-reactions.* Journal of Computational Physics, 1976. 22(4): p. 403-434.

8. Lee, C.-T., *In situ technique for determining acid diffusion behavior in chemically amplified resist films via mesoscale stochastic acid reaction-diffusion modeling of bulk resist deprotection chemistry.* J. Vac. Sci. Technol. B, 2008.

9. Erdem, U., Lu, C., Czanderna, A.W., *Applications of poezoelectric quartz crystal microbalances*. Journal of Physics E-Scientific Instruments, 1984. 17(12): p. 1100-1101.

10. Sundaramoorthi, A., Henderson, C.L., Younkin, T.R., *Elucidating the physiochemical and lithographic behavior of photoresist ultra-thin films.* Proceedings of SPIE, 2008. 7273-37.

11. Lin, E.K., Soles, C.L., Jones, R.L., Lenhart, J.L., Wu, W.L., Willson, G.L., *Direct Measurement of the Reaction Front in Chemically Amplified Photoresists* Science, 2002. 297(5580): p. 372-375.

12. Stewart, M.D., Somervell, M.H., Tran, H.V., Postnikov, S.V., Willson, C.G., *Study of acid transport using IR spectroscopy and SEM.* Proceedings of SPIE, 2000. 3999.

13. Wallraff, G.M., Hinsberg, W.D., Houle, F.A., Morrison, M., Larson, C.A., Sanchez, M., Hoffnagle, J., Brock, P.J., Breyta, G., *Experimental method for quantifying acid diffusion in chemicall amplified resists.* Proceedings of SPIE, 1999. 3678.

14. Sundaramoorthi, A., Lawson, R., Ludovice, P.J., Henderson, C.L., *Diffusion in Thin and Ultra-thin Polymer films.* Polymer, 2010. Submitted.

15. Soles, C.L., Douglas, J.F., Wu, W.L., et al., Macromolecules, 2003. 36(2): p. 373.

16. Vogt B.D., Soles, C.L., Langmuir 2004. 20(4): p. 1453.

CHAPTER 4

CHARACTERIZATION OF NAFION

4.1 Introduction

While transport of small water molecules through pure polymer films and transport of acid molecules through composite polymer matrices exhibit significant deviation from bulk behavior, it would be interesting to look at a useful application of such deviation. One important application would be mass transport through polymer electrolyte membranes used in fuel cells. A fuel cell is an electrochemical device that converts chemical energy of a fuel source into electrical energy, which can be used in different applications like powering electronic devices, automobiles, and appliances. With the growing demand for conservation of energy in the world, fuel cells show promise as a very good alternative for fossil fuels. There are different types of fuel cells using different chemistry, like hydrogen fuel cell, polymer exchange membrane fuel cell, solid oxide fuel cell, alkaline fuel cell, molten-carbonate fuel cell, phosphoric acid fuel cell, and direct-methanol fuel cell. Of these, Polymer Exchange Membrane Fuel Cell (PEMFC) appears to be the most suitable option for automobile applications. PEMFC was invented by Leonard Niedrach and Willard Thomas Grubb of General Electric in 1955 [1]. The low operating temperature and high power density are two great advantages of PEMFC over other choices of fuel cells. The main disadvantage however is the use of expensive catalysts. Like any typical fuel cell arrangement, a PEMFC also has an anode, a cathode, a polymer (a proton exchange membrane) that acts as the electrolyte

and also as a separator of cathode and anode, and a platinum surface that acts as a catalyst. A schematic representation of a PEM fuel cell is given in Figure 4.1.

Hydrogen gas entering the anode side of the fuel cell reaches the platinum surface and splits into H^+ ions and electrons. The electrons flow through anode to external circuit and return to cathode, thus conducting electricity. During this process, oxygen supplied on the cathode side reaches the catalyst surface and splits into oxygen atoms. The protons (H^+ ions) on the anode side diffuse through the solid polymer electrolyte membrane to the cathode. The combination of hydrogen ions with oxygen atoms and electrons from external circuit results in the formation of water molecules. Since the by-product of such a chemical reaction is water, it makes fuel cell environment-friendly over other energy conservation devices.

$$Anode: 2H_2 \rightarrow 4H^+ + 4e^-$$
$$Cathode: O_2 + 4H^+ + 4e^- \rightarrow 2H_2O$$
$$Overall: 2H_2 + O_2 \rightarrow 2H_2O$$

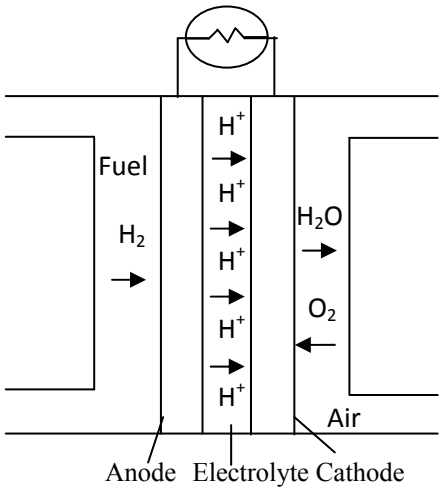

Figure 4.1 Schematic representation of a PEM fuel cell

Direct methanol fuel cell (DMFC) is another fuel cell that is comparable to PEMFC in terms of operating temperature. Typically, methanol is used as a fuel source for hydrogen in DMFC. Given below are the chemical reactions happening in DMFC.

$$Anode: CH_3OH + H_2O \rightarrow CO_2 + 6H^+ + 6e^-$$
$$Cathode: \frac{3}{2}O_2 + 6H^+ + 6e^- \rightarrow 3H_2O$$
$$Overall: CH_3OH + \frac{3}{2}O_2 \rightarrow CO_2 + 2H_2O$$

Advantage of DMFC over PEMFC is the use of liquid methanol, which can be transported, stored, and distributed more easily and using the existing systems for gasoline, unlike gaseous hydrogen. Besides other disadvantages of DMFC like the requirement for larger quantities of catalysts needed for reforming methanol to form hydrogen within the fuel cell stack, permeation of methanol through polymer electrolyte membrane and hence loss of fuel source is a big disadvantage that is economically undesirable. Hence, it is important to understand diffusion of molecules through these polymer membranes to enable control of permeation of fuel source, while keeping proton transfer through these membranes unchanged [2]. Many researchers focus on the study of proton transfer through these proton exchange membranes to help enhance the conductivity of proton exchange membrane and hence efficiency of the fuel cell [3-6]. Extensive research also focuses on decreasing the cost of fuel cell, incurred by platinum catalyst by looking for alternative catalysts [7, 8]. In this study, the aim is to understand the impact of film thickness on diffusion of molecules through polymer membranes, as

this can help control the loss of methanol via permeation through the proton exchange membrane.

4.2 Nafion

A proton exchange membrane used in fuel cells is a semi-permeable membrane that separates the reactants and enables transport of protons. The proton exchange membranes used in PEMFC or DMFC is usually ionomers consisting of pure polymers or composite polymer membranes that are polyaromatic or fluorinated. Besides proton conductivity and methanol impermeability, thermal and mechanical stability under operating conditions, are also essential characteristics of a proton exchange membrane. The most commonly used solid polymer electrolyte is the commercially available Nafion® membrane (trademark of Dupont Inc.,). Nafion is a perfluorinated polymer synthesized by copolymerization of perfluorinated vinyl ether comonomer with tetrafluoroethylene (TFE) [9].

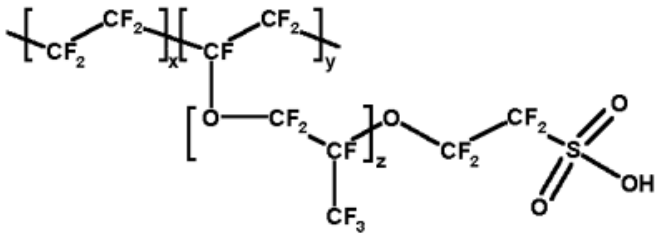

Figure 4.2 Structure of Nafion

The ability of Nafion to conduct under hydrated conditions has led to the focus of investigations of morphology of Nafion and the structure of water channels in them, to allow greater control of its properties [10-12]. Similarly, several researches are in

progress to reduce methanol permeability in DMFC by altering the morphology of Nafion. The morphological changes are effected by cross-linking of multilayer polymer electrolyte membranes [13], by impregnation of filler particles [14], surface modification of nafion membranes [15] etc., While each of these morphological alterations to polymer electrolyte membrane involves either complex chemistry or nanoscale modifications to the structure, exploitation of thin spin cast films of nafion could bring about enhancement of barrier properties with much simplicity. This is based on the observation of reduction in diffusion coefficient of small molecules through ultra-thin polymer membranes (in Chapter 2 and Chapter 3). In other words, several layers of thin nafion films with reduced diffusivity can be used to replace a single thick (in the order of microns) polymer electrolyte membrane, thereby enabling reduced permeability and hence enhanced barrier properties and efficiency of fuel cells. For this, whether diffusion coefficient of thin nafion films deviate from bulk (similar to other thin polymer films so far studied) needs to be investigated. This was done by the QCM experiments in a way similar to the studies reported in Chapter 2.

4.3 Diffusion of Water through Nafion Films

Nafion was purchased from Clean Fuel Cells, Inc., as a 5 wt% solution. Solution of Nafion was spin coated onto gold coated quartz crystals to be used in the Quartz Crystal Microbalance (QCM) setup. The spun coated films were then dried over-night in a vacuum oven at room temperature. Diffusion of water through Nafion was monitored using a QCM in a manner similar to that described in Chapter 2 (Section 2.2). The results showed a decrease in diffusion coefficient with decrease in film thickness. The drop was

significant and was similar to the trend observed in the case of diffusion of water in other pure polymer films of PMMA. Two orders of magnitude drop for a film thickness change from 1200 nm to about 120 nm. Dilution of commercially purchased stock solution (5 wt%) lead to film defects and dewetting while spin coating, and hence much thinner films could not be investigated. But the orders of magnitude drop in diffusion coefficient for change in film thickness is similar to that observed in case of pure PMMA films, Figure 2.5 in Chapter 2. Further, the log-log plot of diffusion coefficient and film thickness (Figure 4.4) shows a thickness squared dependence of diffusion coefficient on film thickness. The observed thickness squared dependence of diffusion coefficient appears to be a common phenomenon for ultra-thin polymer films, as proved in the case of polymethylmethacrylate and in composite polymer films like photoresists.

The diffusion coefficients reported in literature for commercially available Nafion membranes above 25 um, were reported to be different for absorption of water into and desorption from nafion membranes [16-18]. This is because, interfacial mass transfer limitation was observed in commercial nafion membranes. The experimentally determined diffusion coefficients of thin spin cast films of nafion during both sorption and desorption cycles are shown in the plot below (Figure 4.3). From the figure it can be seen that the diffusion coefficients obtained from absorption and desorption cycles do not appear to be statistically, significantly different. Thus, in thin spin coated films of nafion used in this study, diffusion coefficients calculated from absorption and desorption cycles were within the same orders of magnitude.

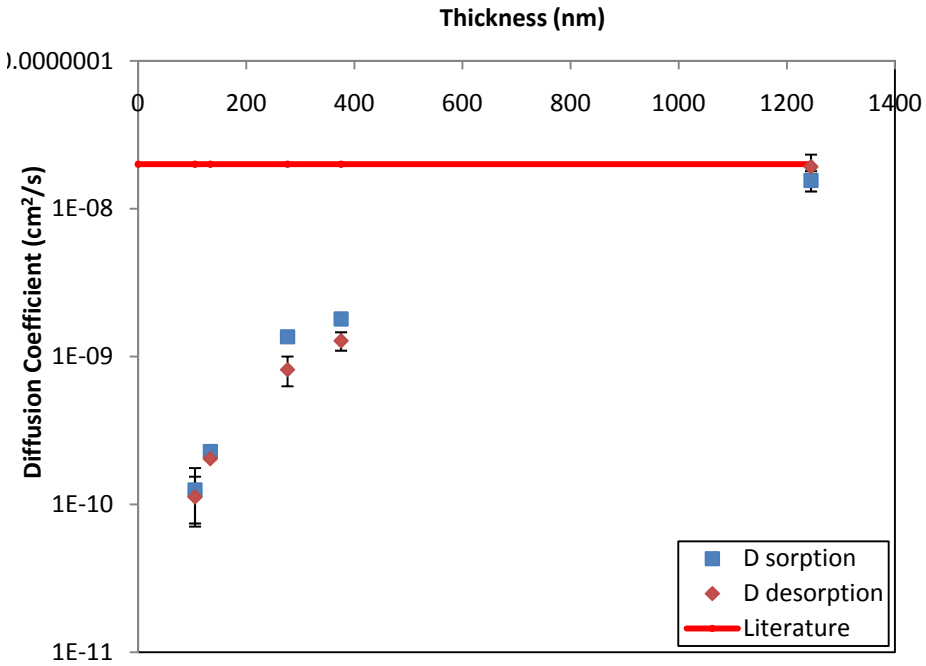

Figure 4.3 Diffusion coefficient of water through spun-coated Nafion films as a function of film thickness. Red line represents the literature reported bulk diffusion coefficient of nafion membranes

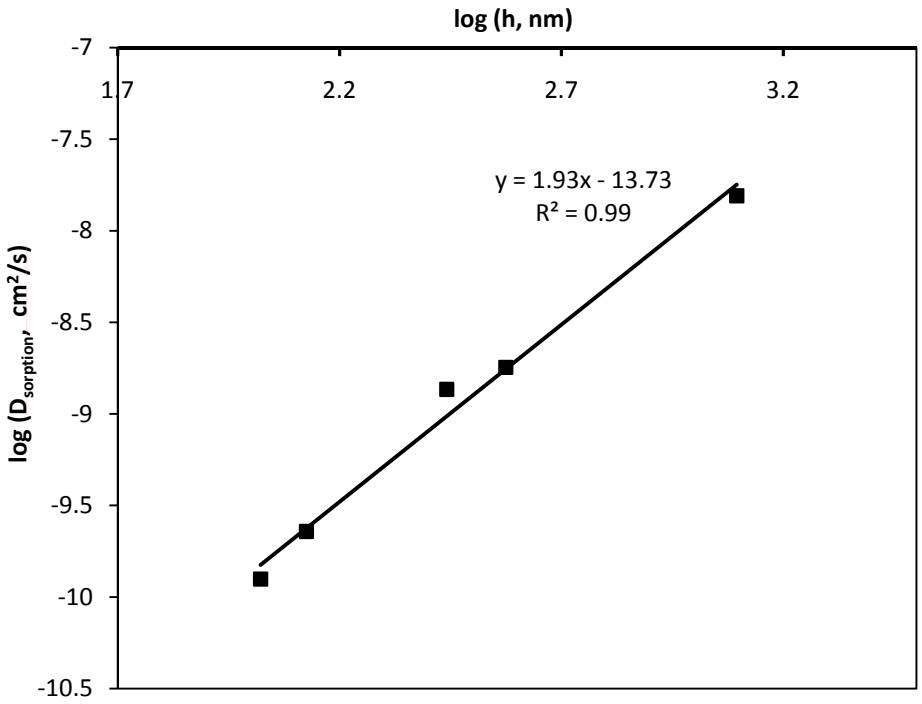

Figure 4.4 Log-log plot of diffusion coefficient of water through spun-coated Nafion film as a function of film thickness

4.4 Interfacial Mass Transfer in Nafion

For example, Majstrik et al., [19] have reported a difference in diffusion coefficient for absorption and desorption and the time scale for desorption is at least ten times faster than absorption for commercial Nafion membranes that are about 25 um and above in thickness. To understand this difference in rates, consideration of the processes involved in sorption and desorption reveal these steps: (i) interfacial mass transport of penetrant from the vapor phase to the membrane surface (ii) diffusion into (absorption) or out of membrane (desorption) and (iii) swelling (absorption) or shrinking (desorption) of the membrane. The differences in diffusion coefficient of absorption and desorption processes suggest that the rate limiting step for water transport is different because of which the time scales of measured diffusion coefficient are different. The normalized mass uptake in this case was better represented by the universal scaling of time normalized by thickness (t/l) instead of time normalized by thickness squared (t/l^2), as expected in case of a diffusion controlled transport [18]. This suggests that the transport across Nafion membrane film interface could be a rate-limiting step for mass transport in fuel cells. As a result, flux boundary condition is introduced at the membrane and gas interface for interfacial mass transfer control, instead of the assumption of a constant concentration at the boundary assumed for the diffusion controlled mass transport. This leads to fractional mass uptake equations given in Equation (3) [18]. Using these equations, the contribution of diffusion controlled and interfacial mass transport at the film interface in the case of the ultra-thin films is investigated here.

Diffusion controlled

$$\frac{M_t}{M_\infty} = \frac{2}{L}\left(\frac{Dt}{\pi}\right)^{\frac{1}{2}} \tag{1}$$

Interfacial mass transfer controlled

Flux at the film interface across the surface area A,

$$AL\frac{dC}{dt} = -Ak_{\text{int}}(C - C_\infty), C = 0\Big|_{t\to\infty} \tag{2}$$

Then, the loss of absorbed mass from the film is

$$\frac{M_0 - M_t}{M_0 - M_\infty} = 1 - \exp\left[-\frac{k_{\text{int}}t}{L}\right] \tag{3}$$

As it can be seen from the equations above, in case of diffusion controlled mass transport, the fractional mass uptake in the films scale as time per unit thickness squared (Equation (1)). In case of interface resistance controlled mass transport, the fractional mass uptake in the films scale as time per unit thickness. Further, natural logarithm of Equation (3) shows the relationship between fractional mass uptake and interfacial mass transfer coefficient (k_{int}). Shown in Figure 4.5 is a plot of natural logarithm of mass uptake (absorption) and mass lost (desorption) versus time per unit thickness. It can be seen from the plot that, the time scales for the absorption and desorption processes are almost identical. The small difference observed in the slope could be because of the time taken for the onset of polymer relaxation and swelling during absorption, which is relatively fast or insignificant for desorption. Thus, unlike commercially available Nafion membranes that are 25 um and thicker [18], interfacial mass transport was not the limiting step for ultra-thin spin cast Nafion films. Hence, from the results reported here,

the conclusion that water absorption is limited by interfacial mass transport in the case of Nafion membranes less than 500 um thick and below 90^0C reported by the authors in [19] is not applicable at least for spin-cast films of Nafion of thickness up to ~1200 nm at room temperature reported here.

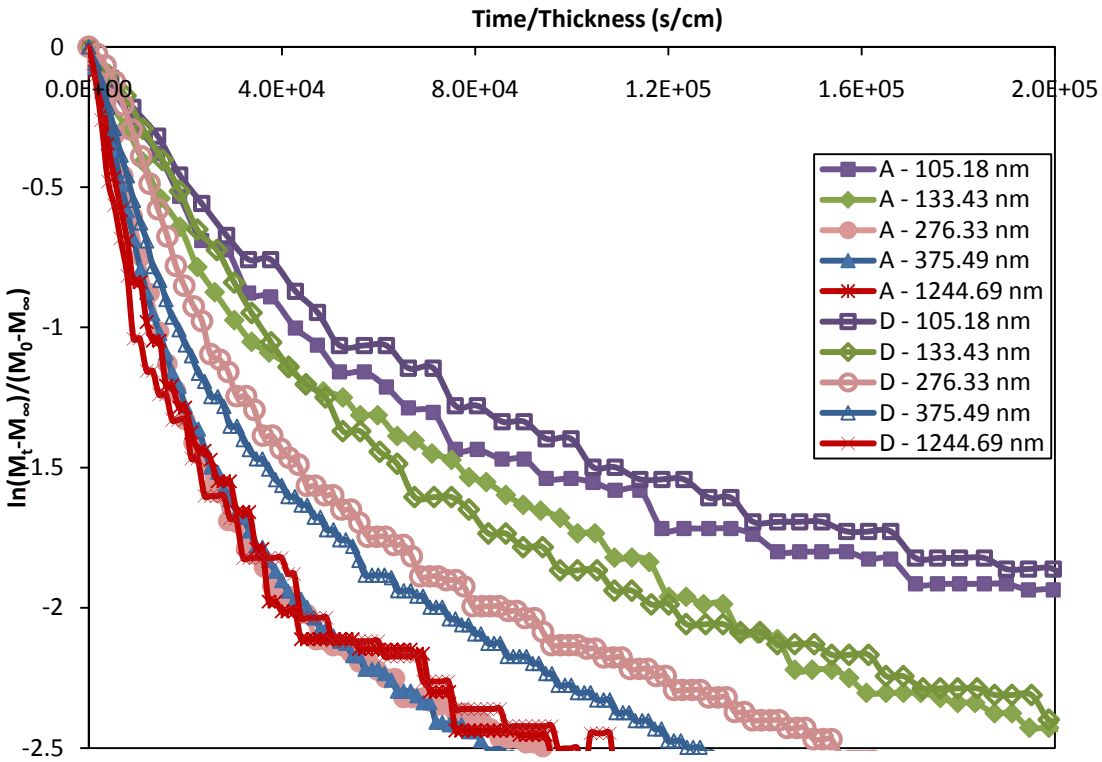

Figure 4.5 Rate of water transport through Nafion films during absorption and desorption

With respect to morphology of Nafion that has reverse miscellar structure, it has been reported that there is a preferential orientation of hydrophobic fluorine surface so as to minimize the energy of the system, on exposure to water. It has been reported that the existence of this teflonic layer limits transportation of water to Nafion membrane in case

of both absorption and desorption [19]. No such interfacial mass transfer resistance was observed for the ultra-thin Nafion films studied here.

4.5 Conductivity of Nafion

4.5.1 Experimental details

Nafion films spun from stock solution at different spin speeds were used to prepare films of different thicknesses (as described in detail in Section 4.2). The films were dried at room temperature in a vacuum oven overnight to remove residual casting solvent.

4.5.2 In-plane conductivity

Silicon wafer with 1 um thick silicon dioxide prepared by chemical vapor deposition was used as substrate. The thick layer of silicon dioxide acts as an insulator, such that only Nafion film contributes to the measured conductivity and any contribution from silicon wafer is avoided. Deionized (DI) water (Barnstead E-pure system) with 18 MΩ resistance was used for hydration of all Nafion films. To avoid any dissolution of ionic impurities from atmosphere in water during hydration of nafion films, nafion films were hydrated with DI water for about 15 minutes just before the impedance was measured. From diffusion experiments, this time is sufficient to hydrate Nafion films. To avoid any dehydration due to desorption, water sufficient to cover the film surface was retained on the wafer piece, even when the measurement was being made. Four point probe impedance measurement was made using Signatone Inc., four point probe station (model # S-302-4) shown in Figure 4.6. The impedance was measured using a Frequency

Response Analyzer (SI 1255 HF Frequency Response Analyzer from Solartron Analytical Inc.,) in conjunction with a potentiostat (SI 1286 Electrochemical Interface potentiostat from Solartron Analytical Inc.,) controlled Corrware software from Scribner Associates, installed in a PC. The software was also used for data acquisition.

Figure 4.6 Signatone four-point probe station used in the measurement of impedance of Nafion films reported here

4.5.3 Through-plane conductivity

Silicon wafers with 200 nm platinum dedposited via chemical vapor deposition was used as the substrate. After spin casting and drying nafion films of different thicknesses, platinum metal contacts were deposited on the film to enable through plane conductivity measurement, when resistance is measured between the contact platinum metal on top of the film and at the bottom of the film. To establish contact with bottom of the film, part of the nafion film was washed after spin coating such that the bottom metal electrode is exposed for contact. A schematic representation of Nafion film preparation for through plane conductivity measurement is shown below in Figure 4.7. A MilliOhmmeter with (4338B from Agilent Inc.,)

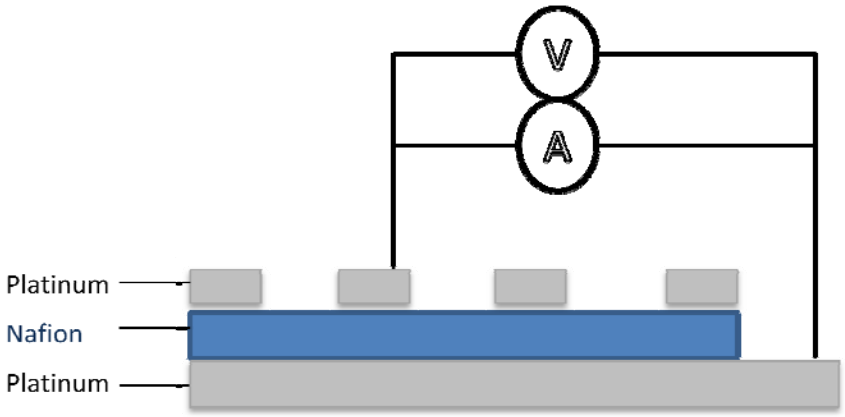

Figure 4.7 Schematic representation of Pt/Nafion film/Pt contacts for through plane conductivity measurements

4.6 Results and Discussion

4.6.1 In-plane conductivity

In case of a four-point probe, there are two outer current carrying probes and two inner voltage measuring probes, any contact and spreading resistance associated with voltage probe is minimal and hence more accurate results are obtained with the four-point probe measurement. Impedance spectroscopy was performed in the in-plane direction along the surface of the film using four-point probe shown in Figure 4.4 for measuring conductivity. Frequency limits of AC input was 1 MHz to 0.1 Hz, with an oscillation of 5 mV. Figure 4.8 shows a complex impedance plot (Nyquist plot or Cole-Cole plot) obtained for different film thicknesses from the measurement.

$$\text{Impedance, } Z = Z' + i\,Z''$$

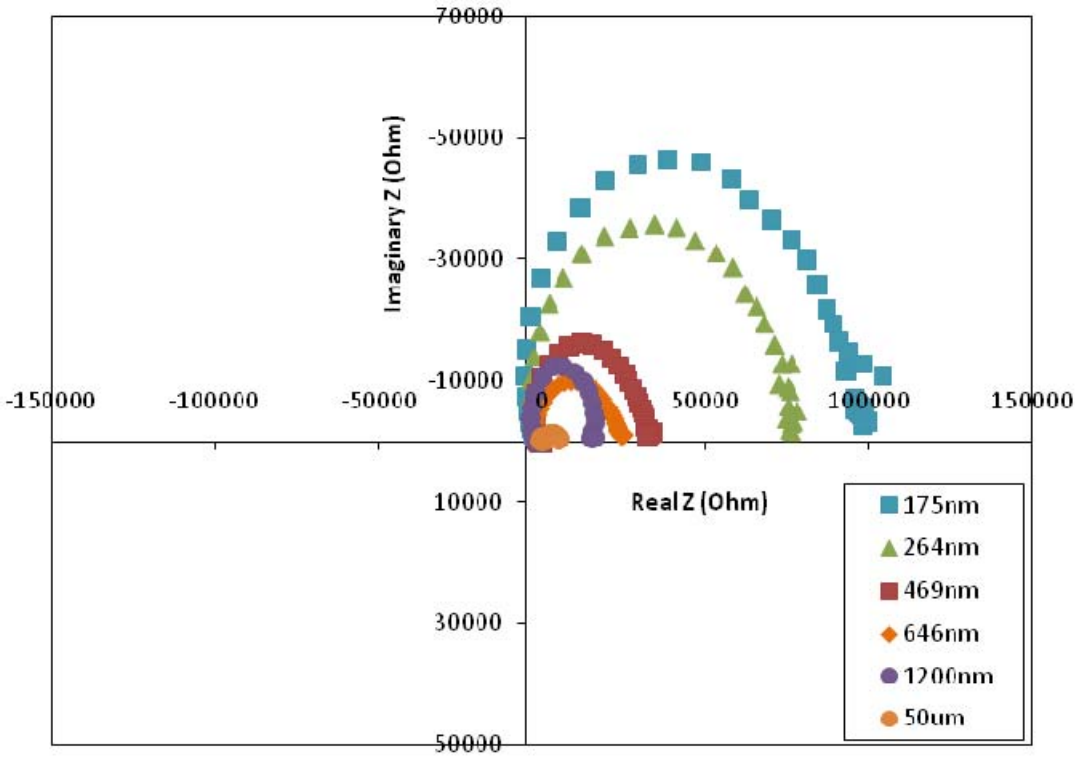

Figure 4.8 Nyquist response for different films obtained in a frequency range from 0.1 Hz to 1 MHz

Equivalent Cricuit Model (ECM) for the setup may include, charge-transfer resistance and double-layer capacitance R_{ct}/C_{dl} at film electrode interface in addition to interface contact resistance and interface capacitance R_{ic}/C_{ic}, bulk film resistance and capacitance R_f/C_f . As mentioned earlier, the four point probe arrangement with the potential measured with two inner electrodes minimizes any interface contact resistance such that R_{ic}/C_{ic} is negligible [20]. Further, in case of films with electrode interface polarization due to ion blocking at electrode film interface in case of spun castfilms measured with a four point probe, have shown a linear increase in imaginary part (Z") of

impedance at low frequencies, in the order of megaOhms. The number of RC parallel connections are known to show characteristic number of semicircles in Cole-Cole plot and same number of peaks in |Z|-log frequency plots [20]. Thus the semicircle spectra can be attributed to bulk film resistance [21]. Decrease in diameter of the semicircle spectra with increase in film thickness corresponds to a decrease in bulk film resistance [22]. Also, the bulk film capacitance is replaced by a Constant Phase Element (CPE) in the equivalent circuit model to account for any inhomogeneity on the film surface [23]. Because of the lack of frequency information on Nyquist plot, sample fit of the equivalent circuit is shown in the Bode plot (|Z|-log frequency and theta- log frequency plots), where the initial flat region of |Z| with frequency change upto ~10^4 Hz represents the resistive component with phase angle close to 0^0.

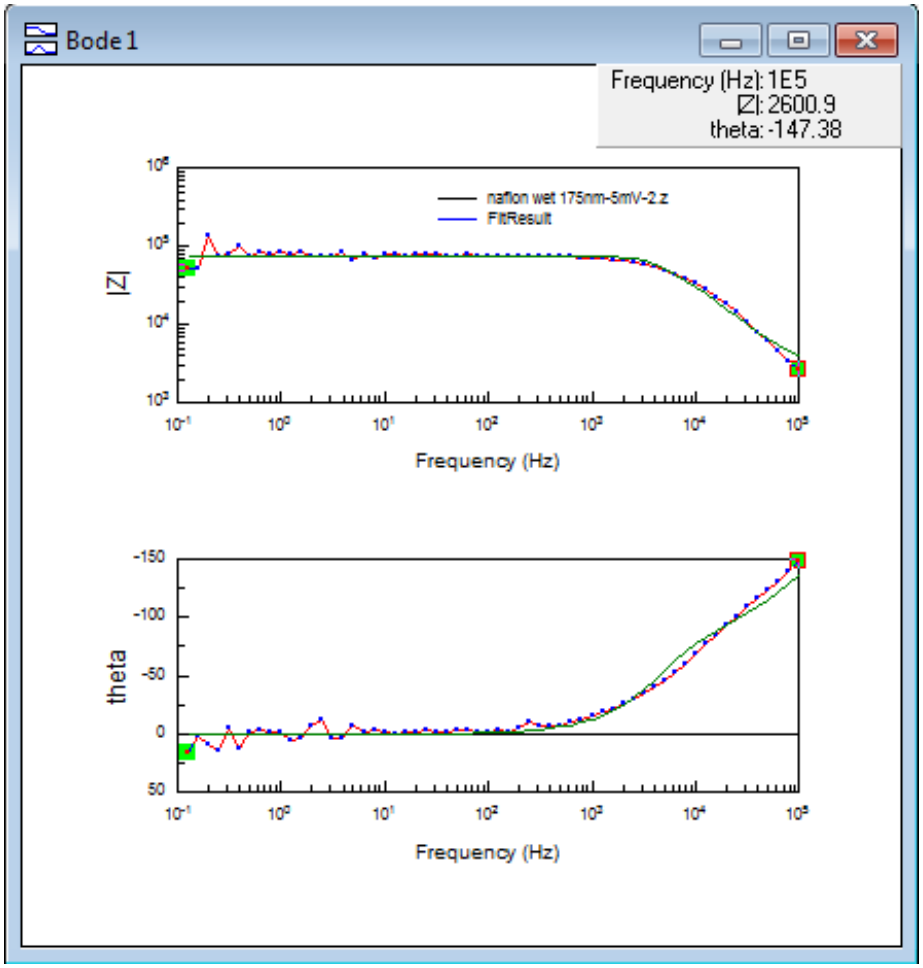

Figure 4.9 Sample of fit of experimental data using equivalent circuit model for a film thickness of about 175 nm represented in Bode plot for a frequency range from 0.1 Hz to 1 MHz

The fit of the data using equivalent circuit model shown in Figure 4.9 yielded bulk film resistance, Z in Ohm which was used to measure the conductivity of the film as:

$$\text{Conductivity} = \frac{1}{\rho}$$

Resistivity, $\rho = \rho_s$ x thickness

Where sheet resistivity, $\rho_s = \frac{\pi}{\ln 2}$ x Resistance (Ohms)

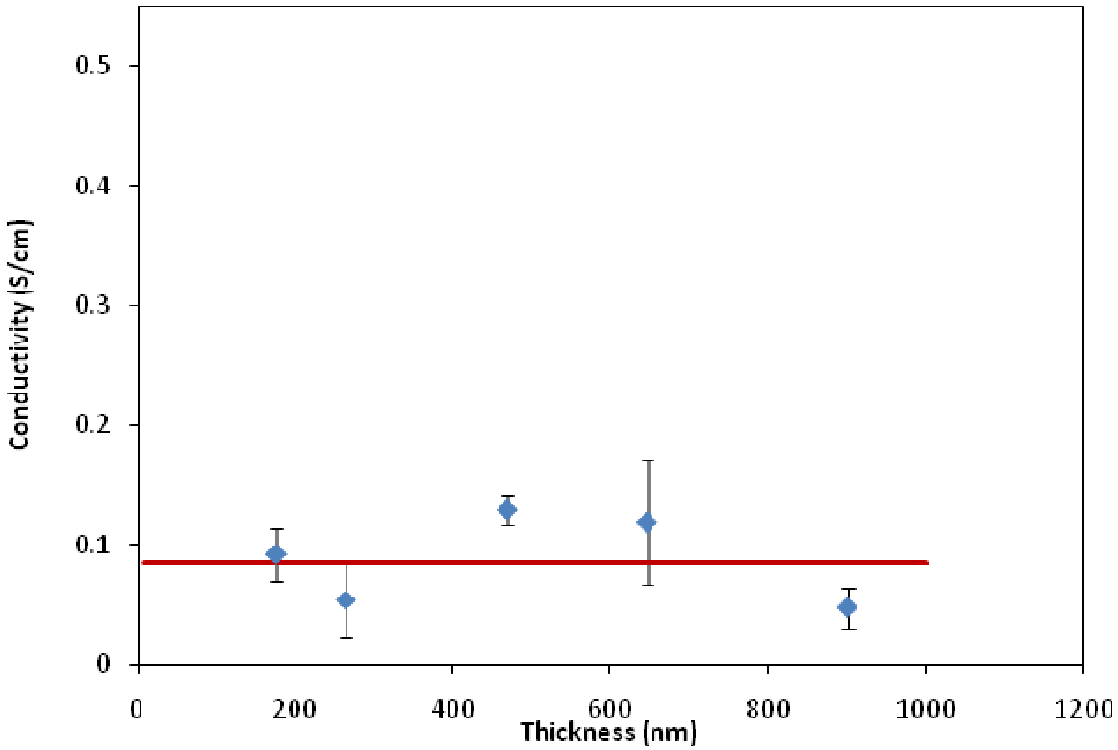

Figure 4.10 In-plane conductivity of thin spin cast films of Nafion measured using four-point probe. Red line represents the conductivity of a 50 um Nafion 112 membrane from Dupont

The conductivity thus obtained is plotted as a function of film thickness. No obvious trend is observed for change in conductivity with film thickness. The red line represents the conductivity measured in a 50 um commercial Nafion membrane (Nafion 112 from Dupont Inc.,). The conductivity corresponding to the red line is 84 mS/cm which compares well with the literature reported values for bulk conductivity of Nafion membranes. The scatter of measured conductivity of thin films about the bulk film conductivity suggests that the conductivity of these thin spin cast films of Nafion is not

widely different from bulk and there is no significant trend of conductivity with film thickness like that observed in case of diffusion. This makes sense as at such high activity of water vapor used in these experiments (100% Relative humidity), majority of proton conductivity in Nafion is due to contribution from bulk conductivity via Grotthuss mechanism, as reported by Choi et al., [24, 25].

4.6.2 Through-plane conductivity

The resistance measured using the four leads from milliohm meter enabled the measurement of resistance of film by applying AC current of 10 uA at a frequency of 1 KHz and measuring the potential across the film thickness. Measured resistance was converted into conductivity as follows:

$$\text{Conductivity, } \sigma = \frac{1}{\rho} = \frac{RA}{L}$$

Where ρ is the resistivity and (L/A) is the cell constant. A is cross sectional area and L is the length for the passage of current. Cross-sectional area was calculated based on the platinum contact diameter on the film surface and L is the film thickness.

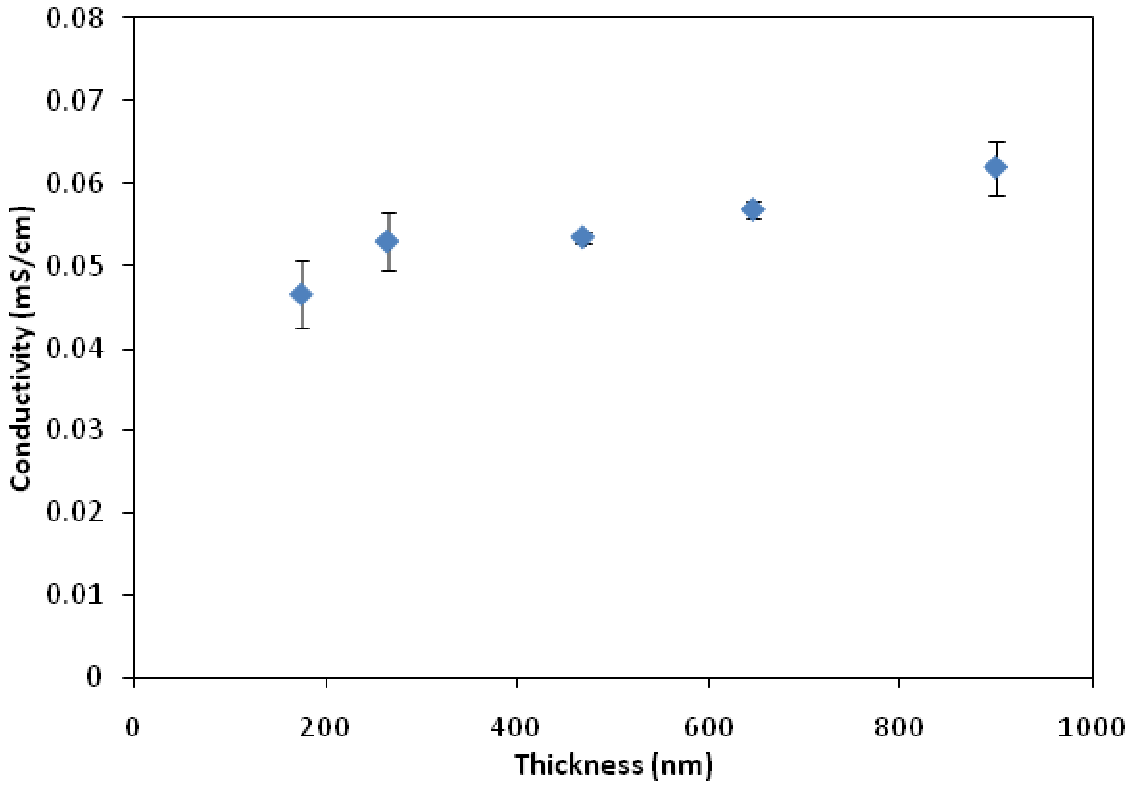

Figure 4.11 Through-plane conductivity of thin spin cast films of Nafion measured using four-point probe milliohm meter.

Shown in Figure 4.11 is the plot of through plane conductivity as a function of film thickness. In general conductivity is observed to decrease slightly with decrease in film thickness and the highest conductivity reported (65.9 mS/cm) is less than the bulk conductivity of Nafion films, 80 mS/cm. Unlike in-plane conductivity that did not change with film thickness, through plane conductivity decreases with decrease in film thickness. As a result in-plane conductivity is larger than through-plane conductivity. While diffusion coefficients measurements are also measured through the film thickness and are observed to decrease with decrease in film thickness, it is not possible to relate the observed decrease in through plane conductivity to decrease in diffusivity, as Grotthuss

mechanism of proton transport is the primary and major source of proton conduction in Nafion [24, 25]. A similar observation of anisotropic conductivity was reported in Nafion-117 membranes pretreated by hot pressing, by Soboleva et al., [21]. Also, in Nafion 117, through plane proton conductivity was reported to be 0.024 S/cm while the in-plane conductivity was 0.086 S/cm [26, 27] and this anisotropy was attributed to extrusion of Nafion membranes that resulted in an enhanced alignment of polymer chains. Since the results reported here also showed a lower through plane conductivity, anisotropy in spin cast films of Nafion was tested optically using IR-VASE ellipsometry in J.A. Woollam inc., Generalized anisotropy model was used to fit the film thickness and refractive indices of the film, in thickness (Nz) and in-plane directions (Nx). Lower electron density in through-plane direction was observed by a decrease in refractive index in through plane direction compared to in-plane. This could be a reason for lower conductivity in through plane direction. This needs to be studied in detail.

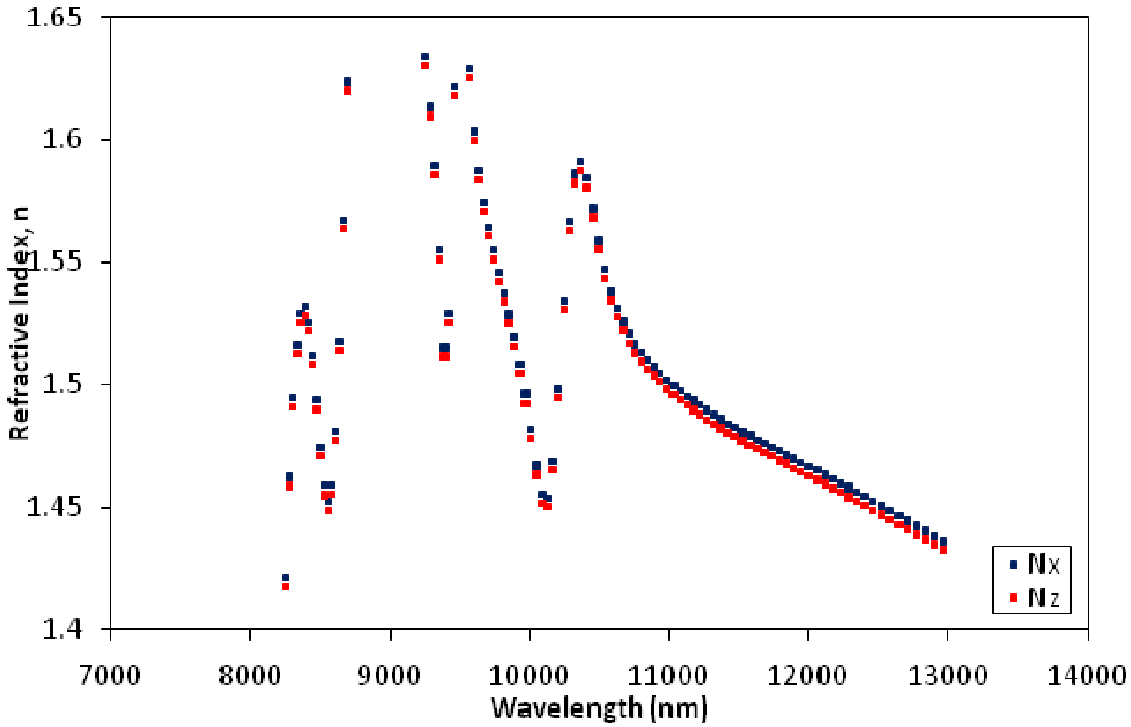

Figure 4.12 Difference in refractive index in in-plane (Nx) and through-plane directions (Nz)

4.7 Conclusions

It is hypothesized that layering of thin films of Nafion with the intrinsic property of ultra-thin polymer films with diffusion coefficients lower than that of bulk (by more than an order of magnitude), could decrease methanol cross over in fuel cells. Unlike the present alternatives for reducing methanol crossover like cross-linking and inorganic filler particles [28-30], reduced diffusivity in ultra-thin films is homogenous and could prove more effective in addressing the methanol crossover issues in proton exchange membrane used in fuel cells. Other alternatives to reduce methanol cross over like reduced hydration of Nafion membranes to enable reduction of solubility of methanol for cross over, with imidazole groups [31] would lead to heterogeneity in the film, with the

proton conducting contour largely different from the bulk polymer film. Use of ultra-thin films would bring the effect of reduced methanol cross-over, by their intrinsic property of reduced diffusivity brought about by the processing condition. Thus, multiple thin layers of spin cast Nafion films which add up to the thickness of the electrolyte layer in fuel cells could effectively reduce methanol transport. Multi-layers of ultra-thin films of nafion to build up to the thickness of a polymer electrolyte membrane can be made possible by using techniques like layer-by-layer assembly [32], polyelectrolyte multilayer technique[33] etc.,. The through plane conductivity of nafion used in proton exchange membranes used in fuel cell is found to decrease to a maximum of 30% from bulk, in the film thickness range investigated here. While the orders of magnitude drop in diffusion coefficient in nafion films could be used to avoid methanol cross over and loss, the decrease in conductivity in film thickness direction is a drawback. Thus, thin layers of spin cast Nafion films which add up to the thickness of the electrolyte layer in fuel cells, could effectively reduce methanol transport with relatively small loss in conductivity. The possibility of such multilayer electrolyte membrane and the study of the performance of ultra-thin films in terms of proton transport and their performance in a fuel cell setup are recommended in Chapter 7 under future work and recommendations, to enable efficient application of these thin films in fuel cell.

4.8 References

1. Perry, M.L. and T.F. Fuller, *A Historical Perspective of Fuel Cell Technology in the 20th Century.* Journal of the Electrochemical Society, 2002. **149**(7): p. S59-S67.
2. Rebai, M. and M. Prat, *Scale effect and two-phase flow in a thin hydrophobic porous layer. Application to water transport in gas diffusion layers of proton exchange membrane fuel cells.* Journal of Power Sources, 2009. **192**(2): p. 534-543.
3. Tian, A.H., et al., *Surface-modified Nafion membrane by trioctylphosphine-stabilized palladium nanoparticles for DMFC applications.* Journal of Physics and Chemistry of Solids, 2009. **70**(8): p. 1207-1212.
4. Tsai, J.-C., J.-F. Kuo, and C.-Y. Chen, *Nafion®/nitrated sulfonated poly(ether ether ketone) membranes for direct methanol fuel cells.* Journal of Power Sources, 2009. **194**(1): p. 226-233.
5. Su, Y.-H., et al., *Increases in the proton conductivity and selectivity of proton exchange membranes for direct methanol fuel cells by formation of nanocomposites having proton conducting channels.* Journal of Power Sources, 2009. **194**(1): p. 206-213.
6. Choe, Y.-K., et al., *Nature of proton dynamics in a polymer electrolyte membrane, nafion: a first-principles molecular dynamics study.* Physical Chemistry Chemical Physics, 2009. **11**(20): p. 3892-3899.

7. Antolini, E. and E.R. Gonzalez, *Tungsten-based materials for fuel cell applications.* Applied Catalysis B: Environmental, 2010. **96**(3-4): p. 245-266.

8. Lee, K.R.W., Seong Ihl, *Polyol synthesis of ruthenium selenide catalysts for oxygen reduction reaction.* Korean Chemical Society, 2010. **31**(11).

9. Mauritz, K.A. and R.B. Moore, *State of Understanding of Nafion.* Chemical Reviews, 2004. **104**(10): p. 4535-4586.

10. Affoune, A.M., A. Yamada, and M. Umeda, *Conductivity and surface morphology of Nafion membrane in water and alcohol environments.* Journal of Power Sources, 2005. **148**: p. 9-17.

11. *Perfluorinated Ionomer Membranes*. ACS Symposium Series. Vol. 180. 1982: AMERICAN CHEMICAL SOCIETY. 516.

12. Gierke T, D., E. Munn G, and C. Wilson F, *Morphology of Perfluorosulfonated Membrane Products*, in *Perfluorinated Ionomer Membranes*. 1982, AMERICAN CHEMICAL SOCIETY. p. 195-216.

13. Lin, H., et al., *Low water swelling and high methanol resistant proton exchange membrane fabricated by cross-linking of multilayered polyelectrolyte complexes.* Journal of Membrane Science, 2009. **345**(1-2): p. 242-248.

14. Casciola, M., et al., *Conductivity and Methanol Permeability of Nafion–Zirconium Phosphate Composite Membranes Containing High Aspect Ratio Filler Particles.* Fuel Cells, 2009. **9**(4): p. 394-400.

15. Wang, J., et al., *A facile surface modification of Nafion membrane by the formation of self-polymerized dopamine nano-layer to enhance the methanol barrier property.* Journal of Power Sources, 2009. **192**(2): p. 336-343.

16. Morris, D.R. and X.D. Sun, *Water-Sorption and Transport-Properties of Nafion-117-H.* Journal of Applied Polymer Science, 1993. **50**(8): p. 1445-1452.

17. Takamatsu, T., M. Hashiyama, and A. Eisenberg, *Sorption Phenomena in Nafion Membranes.* Journal of Applied Polymer Science, 1979. **24**(11): p. 2199-2220.

18. Satterfield, M.B., Benziger, J.B.,, *Non-Fickian Water Vapor Sorption Dynamics by Nafion Membranes.* Journal of Physical Chemistry B, 2008. **112**: p. 3693-3704.

19. Majsztrik, P.W.S., M. B. Bocarsly, A. B. Benziger, J. B., *Water sorption, desorption and transport in Nafion membranes.* Journal of Membrane Science, 2007. **301**(1-2): p. 93-106.

20. Ma, S., Z. Siroma, and H. Tanaka, *Anisotropic Conductivity Over In-Plane and Thickness Directions in Nafion-117.* Journal of The Electrochemical Society, 2006. **153**(12): p. A2274-A2281.

21. Soboleva, T., et al., *Investigation of the through-plane impedance technique for evaluation of anisotropy of proton conducting polymer membranes.* Journal of Electroanalytical Chemistry, 2008. **622**(2): p. 145-152.

22. Berger, C.M., *Measuring Acid Generation Kinetics in Photoresist Films via Capacitance Techniques* in *Chemical and Biomolecular Engineering*. 2004, Georgia Institute of Technology: Atlanta.

23. *Autolab application note*, in *Electrochemical Impedance Spectroscopy (EIS): 3. Data Analysis*, Metrohm Autolab B.V.: Netherlands.

24. Choi, P., N.H. Jalani, and R. Datta, *Thermodynamics and Proton Transport in Nafion.* Journal of The Electrochemical Society, 2005. **152**(3): p. E84-E89.

25. Choi, P., N.H. Jalani, and R. Datta, *Thermodynamics and Proton Transport in Nafion.* Journal of The Electrochemical Society, 2005. **152**(3): p. E123-E130.

26. C.L.Gardener and A.V.Anantaraman, Journal of Electroanalytical Chemistry, 1995. **395**.

27. C.L.Gardener and A.V.Anantaraman, Journal of Electroanalytical Chemistry, 1998. **449**: p. 209.

28. Kim, D.S., et al., *Proton conductivity and methanol transport behavior of cross-linked PVA/PAA/silica hybrid membranes.* Solid State Ionics, 2005. **176**(1-2): p. 117-126.

29. Kjaer, J., et al., *Solid-State Electrolyte Membranes for Direct Methanol Fuel-Cells.* Solid State Ionics, 1991. **46**(1-2): p. 169-173.

30. Poltarzewski, Z., et al., *Novel proton conducting composite electrolytes for application in methanol fuel cells.* Solid State Ionics, 1999. **119**(1-4): p. 301-304.

31. Hudiono, Y., et al., *Porous layered oxide/Nafion® nanocomposite membranes for direct methanol fuel cell applications.* Microporous and Mesoporous Materials, 2009. **118**(1-3): p. 427-434.

32. Daiko, Y., K. Katagiri, and A. Matsuda, *Proton Conduction in Thickness-Controlled Ultrathin Polycation/Nafion Multilayers Prepared via Layer-by-Layer Assembly.* Chemistry of Materials, 2008. **20**(20): p. 6405-6409.

33. Elbert, D.L., C.B. Herbert, and J.A. Hubbell, *Thin Polymer Layers Formed by Polyelectrolyte Multilayer Techniques on Biological Surfaces.* Langmuir, 1999. **15**(16): p. 5355-5362.

CHAPTER 5

INTRODUCTION TO PROTRACTED COLORED NOISE DYNAMICS (PCND)

5.1 Introduction

Protracted Colored Noise Dynamics (PCND) was developed and implemented by Jerry W. Jenkins [1] for an NVT ensemble, to enable relaxation of system to equilibrium structures in a computationally realizable time scale and to sample the phase space efficiently in condensed phase systems. This approach was mainly motivated by the limitation of Molecular Dynamics (MD) simulation to relax a system to a low energy equilibrium state within the timescales of typical simulation. PCND focused on the introduction of random forces characterized by a systematically chosen Monte-Carlo (MC) move for a period of time. This stochastic force correlated in time is called *Protracted Colored Noise.* Protracted Colored Noise, when applied to non-equilibrium systems, is proven to increase phase space sampling. And PCND approach has been proven to sample phase space more efficiently than white noise, which is a stochastic force uncorrelated in time, for a one-dimensional bistable potential energy function and highly viscous system such as Lennard-Jones glass. These random forces are comparable to vibrational and translational motion characteristics of molecular systems. However, in dense and viscous systems, introduction of such forces, often leads to a higher energy system and hence the resulting conformation of the system is accepted with little or no probability, towards minimum energy equilibrium states. Thus, the stochastic force

correlated in time was found to be efficient, only with finer details of modeling molecular system to be able to successfully sample phase space.

5.2 Origin of Stochastic Modeling

In 1827, Robert Brown, a Scottish botanist, examined pollen grains suspended in water under microscope and observed ceaseless movement. He explained that the random movement of pollen grains was due to the fact that the pollen grains were alive and that they moved at their will [2] .The observation was actually not due to a living being in motion but because of the molecular interactions. The diffusion coefficient can be computed by fitting the long time behavior of the mean squared displacement to time using Einstein's relationship for a three-dimensional system as:

$$\left\langle \left| r(t) - r(0) \right|^2 \right\rangle = 6Dt \tag{1}$$

In 1908, after the study of random diffusion processes by Einstein and Smoluchowski, Paul Langevin, a French physicist, stated that there should be two forces acting on a particle, (a) stochastic force that is fluctuating - representing the random impact of liquid molecules and time average of this force is zero, and (b) the force due to viscous drag of suspended medium, which is defined in hydrodynamics by Stokes law [3].

$$m\frac{d^2x(t)}{dt^2} = \eta(t) - m\varsigma\frac{dx(t)}{dt} \tag{2}$$

Where η (t) is the stochastic force and ζ is the friction coefficient from Stoke's law. This can be related to the mean squared displacement in Brownian motion as:

$$\left\langle \left| x(t) - x(0) \right|^2 \right\rangle = \left(\frac{2kT}{m\zeta} \right) t \tag{3}$$

Ryogo Kubo derived the generalized Langevin equation [4]. As per his derivation ζ (t), the time dependent frictional coefficient, is related to η (t) as:

$$\zeta(t) = \frac{\langle \eta(t)\eta(0) \rangle}{mkT} \tag{4}$$

where the variance of random forces is proportional to the frictional coefficient.

Here, the random force, η, is fluctuating. And the frictional coefficient is considered dissipative and is known as the 'second fluctuation-dissipation theorem'. From the equation, it is seen that the continued increase in the fluctuation would increase the friction coefficient. And hence, the damping term in the force equation above, would eventually dominate and fall in the over damped regime. However, a major limitation of the generalized Langevin equation comes from the fact that the friction coefficient and diffusion coefficient are related based on the derivations from Einstein and Langevin as follows:

$$\zeta = \frac{kT}{mD} \tag{5}$$

This equation states that as the frictional coefficient approaches zero, which is valid for dilute systems, the diffusion coefficient becomes infinite. However, for viscous

systems, decoupling variance of random forces and friction coefficient would help increase the fluctuations, and thereby sample the viscous systems and increase the sample space.

White noise is defined by the Gaussian distribution of random forces that are completely uncorrelated in time while colored noise is defined to be correlated in time. Ornstein and Uhlenbeck[20] defined the colored noise to be exponentially related and stated the relation as:

$$\dot{\varepsilon}(t) = \frac{\Omega^{1/2}\dot{\eta}(t) - \varepsilon(t)}{\tau} \tag{6}$$

where Ω is the magnitude of the random force, η is the white noise, and τ is the decay time of the random force, with the conditions that the average of forces with respect to time is zero, and the variance of this colored noise is given by exponential decay in time:

$$\left\{\left\langle \varepsilon(t)\varepsilon(s)\right\rangle\right\} = \left(\frac{\Omega}{\tau}\right) e^{\frac{|t-s|}{\tau}} \tag{7}$$

The average in this case is done for initial conditions to give good results, according to Fox et al., [5]. However, the energy imparted to the system due to random forces does work on the system, and so the temperature of the system should be controlled in order to conserve the energy of the system [6]. Thus, the energy balance for the system is given by:

$$m\frac{d^2x(t)}{dt^2} = -\nabla U(x) + \varepsilon(t) - \zeta(t)\frac{dx(t)}{dt} \tag{8}$$

$$\frac{d\zeta(t)}{dt} = \frac{1}{Q}\left[\frac{T_i(t)}{T_{bath}} - 1\right] \tag{9}$$

Where, Q is a parameter used to couple the space and momentum variables, T_i is the instantaneous temperature and T_{bath} is the constant set temperature of the system.

5.3 Lennard-Jones glass

Verlet and Levesque, in 1960, did some of the early work in molecular dynamics in detail in Lennard-Jones system [7-9], where they modeled particles interacting in Lennard-Jones fluid. Rahman et al., quenched a system of particles in liquid state and formed a glass with a reduced glass transition temperature of 0.8 [10]. The radial distribution function thus calculated had a split in its second peak, which indicated random dense packing of hard spheres and thus the formation of glass. Further, the split disappeared on heating and reappeared on cooling [10, 11]. In order to predict the glass transition temperature of materials that have not yet been observed in glassy state, Hudson and Andersen [12] calculated the effective hard sphere packing fraction in atomic liquids. There has been a lot of work done in this area and reported in literature, such as the work by Vollmayr [13], Goldstein [14], Wallace [15], and Thirumalai [16] to prove and show that the Lennard-Jones system forms glass.

Following the successful implementation and testing of PCND algorithm on a bistable potential function, the algorithm was planned to be tested on polymers. The motivation for the implementation of the algorithm to understand polymer chain

dynamics was based on the previous work on molecular simulations of atactic polypropylene films, which suggested that the fractional free volume distribution becomes more homogeneous as films become thinner [17]. In this study of atactic polypropylene films, Delaunay Tessellation tiles the inter-atomic space in the simulated class into a tetrahedron and is used to characterize the free volume distribution in the simulated polymer films. Thus, the diffusion coefficient can be compared to the free volume distribution, and hence the correlation existing between them under thin film conditions can be obtained. This can be used to understand the underlying phenomenon for the observed experimental results on diffusion through ultra-thin polymer films.

5.4 Simulation Details

Protracted Colored Noise Dynamics algorithm was developed with fine details of the model molecular system, and was tested on a one dimensional bistable potential function by Jerry W. Jenkins in his doctoral thesis [1]. Jerry had designed, developed, tested, and confirmed better phase space sampling of stochastic equation of motion. For this, the stochastic forces were correlated to be exponentially decaying in time and Nose´-Hoover temperature controller kept the dynamic system at a constant average kinetic energy. The bistable potential function used to test the stochastic algorithm had a depth of ΔE and minimum energy at σ, such that the potential energy U is given by,

$$U(x)=\left(\frac{\Delta E}{\sigma^4}\right)x^4-\left(\frac{2\Delta E}{\sigma^2}\right)x^2 \qquad (10)$$

The parameters for Lennard Jones glass were adopted from Rigby and Roe [18] for CH_2 groups of spherical molecules. The parameters used in the simulations were:

Depth of the energy well, $\varepsilon = 500$ J/mol

Minimum energy at a distance, $\sigma = 0.38$ nm

Reduced units technique suggested in [1, 19] was used for all the quantities used in the simulation. The simulation was carried out at a thermodynamic point in the system, below the glass transition temperature. The glassy state was then defined by volume, from the number of particles, and density. Thus, the simulation was carried using a NVT ensemble, where the number of particles, volume and the temperature of the system were maintained constant. The initial conformation of the system was then defined by placing a particle at random in the cube, and then placing the next particle in the system only if the distance between the two particles is greater than a minimum cut off distance. Initial Gaussian distributed random numbers were generated based on Box-Mueller Algorithm. Further integration of the equations of motion involves half-step integration using Verlet algorithm [7], and back calculation of first-step in velocity by leap-frog algorithm described by Allen and Tildesley in [19]. The reduced units and integration schemes are well explained in [1]. Described below is the flow of the PCND algorithm starting from the initial generation of their positions and velocities.

Step 1: Initial Conformation

a. A cubic box of volume, based on the number density and number of atoms, is created.

b. Atoms are assigned random positions based on Boltzmann Energy distribution and avoiding overlap
c. Steepest descent energy minimization of the generated positions minimizes the energy of the system
d. Initial velocity of each atom in the system is assigned based on the temperature of the system, and hence the kinetic energy

Step 2: Colored Noise Force

a. Based on the initial position of atoms, calculate the Lennard-Jones force and noise forces (based on the width of the Gaussian distribution and relaxation time constant) acting on the atoms, through each time step
b. Back integrate velocity for each atom, from the total force acting on the system, and in each direction could help begin the integration
c. For each of the atoms in the system, calculate the nth step velocity in each direction using half-step leap frog algorithm as described in [1]
d. Integrate (n+1/2)th step velocities in each direction for each atom
e. Integrate positions based on the velocity
f. Update half step velocities for each atom and loop them back to Step 2 – c for integration of every atom
g. Integrate frictional coefficient for each atom
h. Calculate instantaneous temperature of the system based on the sum of squares of velocities at this instant in time
i. Temperature controller tuned based on the energy of the system

j. Dimensionless long-range corrections (LRC) based on the cut-off radius (r_c), ensured to be less than or equal to half the simulating box length, is calculated according to [19] for an NVT ensemble as,

   i. $$E^*_{LRC} = \frac{8}{9}\pi N \rho^* r_c^{*-9} - \frac{8}{3}\pi N \rho^* r_c^{*-3}$$

   ii. $$P^*_{LRC} = \frac{32}{9}\pi \rho^{*2} r_c^{*-9} - \frac{16}{3}\pi \rho^{*2} r_c^{*-3}$$

   iii. These long-range energy corrections are applied to the results after simulation.

k. Apply calculated energy corrections to find instantaneous pressure, potential and kinetic energies of the system.

l. Repeat the integration through each time step by looping back to (Step 2 – i), where calculations are repeated for the velocities and positions from the last time step instead of initially generated conformations

m. Calculate thermodynamic averages and fluctuations in each variable based on the average over the entire length of simulation time.

The adjustable parameters in PCND are the mean squared size of the colored noise forces (Ω/τ). The results reported in the following chapter are the time taken for system equilibration as a function of the random force Ω, decay time constant τ, coupling constant Q (Nosé -Hoover Temperature Controller), and reference temperature of the system T_{ref}. With the preliminary work described here, optimization of the PCND parameters was targeted to define the favorable region and the range of parameters far from a molecular dynamics simulation condition of zero noise force.

5.5 References

1. Jenkins, J.W., *Novel Efficient Simulation Techniques In Molecular Modelling*, in *School of Chemical and Biomolecular Engineering*. 2000, Georgia Institute Of Technology: Atlanta.
2. Phil Stone, J.H., ed. *Nelson Science Chemistry*. 2nd ed.
3. Langevin, P., *Sur la theorie du movement brownien, C.R.Academic Sience (Paris) 146, 530-533 (1908) - "On the theory of Brownian Motion. American Journal Of Physics*, 1997. **65**(11): p. 1074.
4. Ryogo, K., ed. *Many Body Theory*. 1966, Benjamin Publishers: Newyork.
5. Fox, R.F.et al., Physical Review A, 1988. **38**: p. 1538.
6. Shtiichi, N., *A unified formulation of the constant temperature molecular dynamics methods.* Journal of Chemical Physics, 1985. **81**: p. 511.
7. Verlet, L., *Physical Review A*, 1967. **159**: p. 98.
8. Verlet, L., *Physical Review A*, 1968. **165**: p. 201.
9. Verlet, L., Levesque, D., *Physical Review A*, 1970. **2**: p. 2514.
10. Finney, J.L., *Random Packings and the Structure of Simple Liquids. II. The Molecular Geometry of Simple Liquids.* Proceedings of the Royal Society of London Series A., 1970. **319**: p. 495.
11. Finney, J.L., *Random Packings and the Structure of Simple Liquids. I. The Geometry of Random Close Packing.* Proceedings of the Royal Society of London Series A., 1970. **319**: p. 479.
12. Hudson, S., Andersen, H.C., Journal of Chemical Physics, 1978. **69**: p. 2322.

13. Vollmayr, K., Kob, W., Binder, K, *How do the properties of a glass depend on the cooling rate? A computer simulation study of a Lennard-Jones system.* Journal of Chemical Physics, 1996. **105**: p. 4714.

14. Goldstein, M., *Viscous Liquids and the Glass Transition: A Potential Energy Barrier Picture.* Journal of Chemical Physics, 1969. **51**(3728).

15. Wallace, D.C., *Statistical entropy and a qualitative gas-liquid phase diagram.* Physical Review A, 1988. **38**: p. 469.

16. Thirumalai, D., Mountain, R.D., *Activated dynamics, loss of ergodicity, and transport in supercooled liquids.* Physical Review E, 1993. **47**: p. 479.

17. Singh, L., Ludovice, P.J., Henderson, C.L, *Characterization of property variation in ultra-thin polymer films from molecular simulation. Proceedings of SPIE*, 2005. **5753**.

18. Rigby, D., Roe, R.,, *Polymer liquid and glass.* Journal of Chemical Physics, 1988. **89**(8): p. 15.

19. Allen, M.P., Tildesley, D.J.,, ed. *Computer Simulation of Liquids*. 1989, Oxford Science Publications: Suffolk.

CHAPTER 6

PROTRACTED COLORED NOISE DYNAMICS

6.1 Optimization of Noise Parameters

The relaxation of a system of particles under the influence of colored noise source was tested and proved to be faster than MD by Jerry Jenkins [1]. He had shown that the system relaxes faster in the presence of colored noise source with a decay time constant than the time taken for the relaxation of an NVT ensemble under the influence of MD. For a choice of noise parameters (Ω/τ) = 1.5 and for a decay time constant of τ = 5 and 0.5, the hypothesis that the exponentially correlated noise could span the phase space efficiently and equilibrate it faster within the simulation time was proven. In order to extend the application of PCND, it is essential to characterize the dynamics and optimize the noise parameters to be universally applicable for more complicated systems. In order to this, the algorithm was extended to be applicable in 3-dimensional system of Lennard-Jones system and the various parameters influencing the dynamics were investigated. The primary parameters of a colored noise force are: the amplitude of the force or the width of the Gaussian distribution given by Ω and the decay time constant, τ. The secondary parameters controlling the physical condition of the system are the temperature of the system, T and the coupling constant, Q of Nose´- Hoover temperature controller. Hence a number of simulation runs were repeated for different choice of noise parameters. It was observed that the convergence of PCND influenced Lennard-Jones system were higher than that for the same conditions of the density and number of atoms, under the influence of MD. The results are shown below for a system of 1080 atoms at a temperature, T* =

0.1 and density = 0.95. At this density a Lennard Jones system was observed to form a glass under quenching [2].

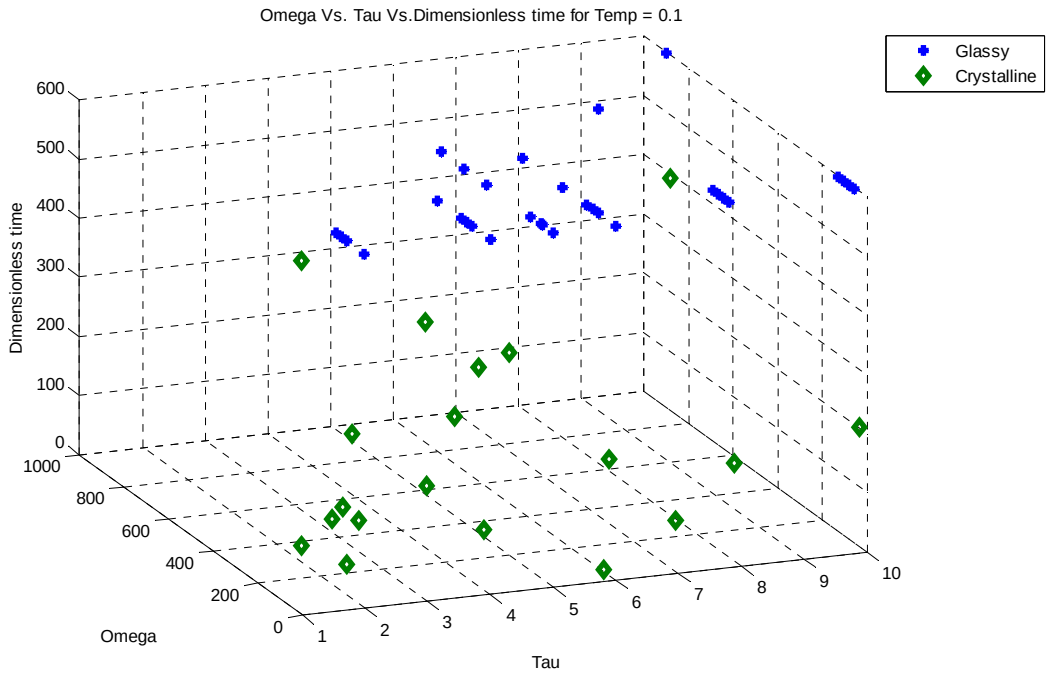

Figure 6.1 Convergence of Lennard-Jones spheres under the influence of PCND. For a dimensionless simulation time of 600, the probability of system reaching an equilibrium state was high under the influence of PCND forces

In this case the primary noise parameters of force and decay time constant are varied. The 3D representation with dimensionless time is mainly to indicate the relatively faster convergence of PCND within a maximum time. However, in terms of the optimum choice of noise parameters, it is observed that a larger force is compensated by a lower decay time constant. This can be better understood with a 2-dimensional representation of just the noise parameters as shown below.

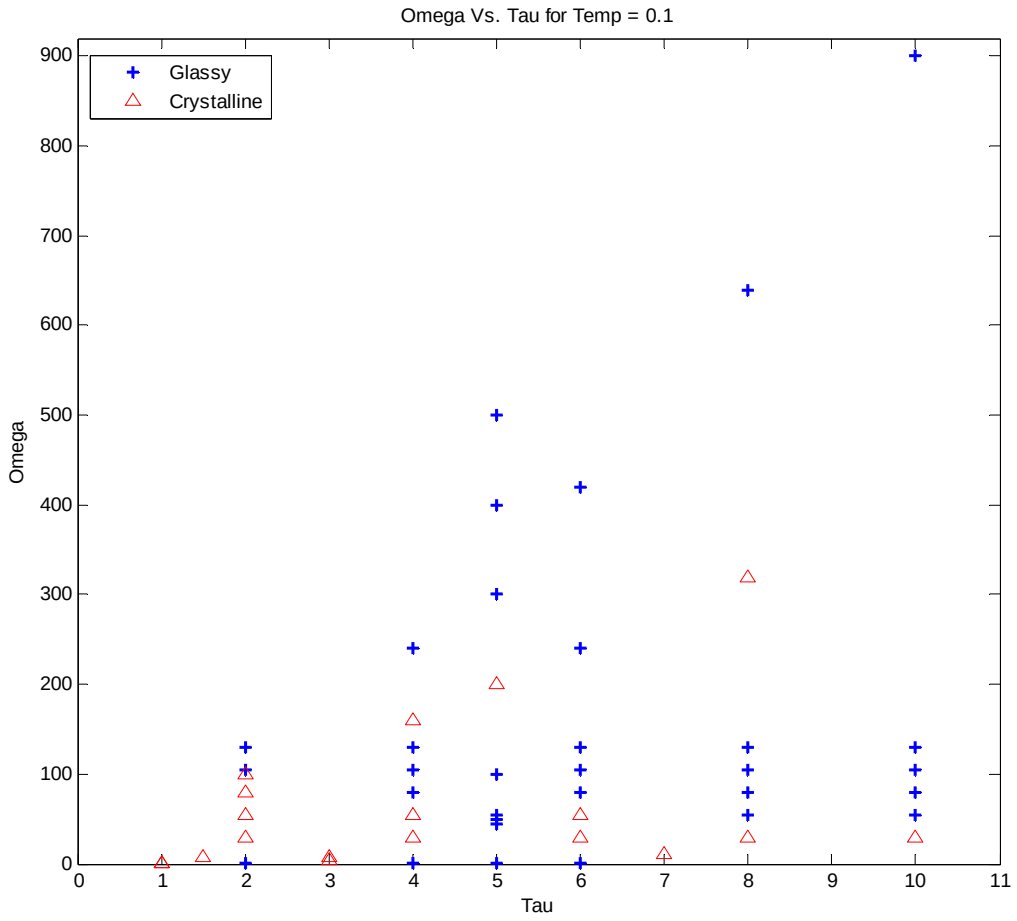

Figure 6.2 Plot of systems reaching equilibration (crystal) by the variation of PCND noise parameters, omega or amplitude of noise force and decay time constant, tau

From the results shown, it can be observed that no obvious pattern in the choice of noise parameters could be obtained, for strong recommendations with confidence for future simulation runs as optimum colored noise force for equilibration. This is in contradiction to what is expected, as colored noise forces are zero in case of an MD run and is non-zero in case of PCND, one would expect that noise parameters would work efficiently for convergence of non-equilibrium states for a distance from MD or $\Omega = 0$ and then there would be a limit to this applied force, beyond which protracted colored

noise would no more help the system to cross the energy barrier and there by setting an upper limit for the variation of noise parameters. Since the amount of force applied is correlated in time and from the above observation and Jerry's results [1], it can be seen that larger force with smaller correlation time could help the system to go to an energy state lower than that obtained with the larger correlation time, it would be worthwhile to look at the optimum of noise parameters (Ω/τ) and τ versus, Ω and τ. Shown below is a plot of the (Ω/τ) and τ.

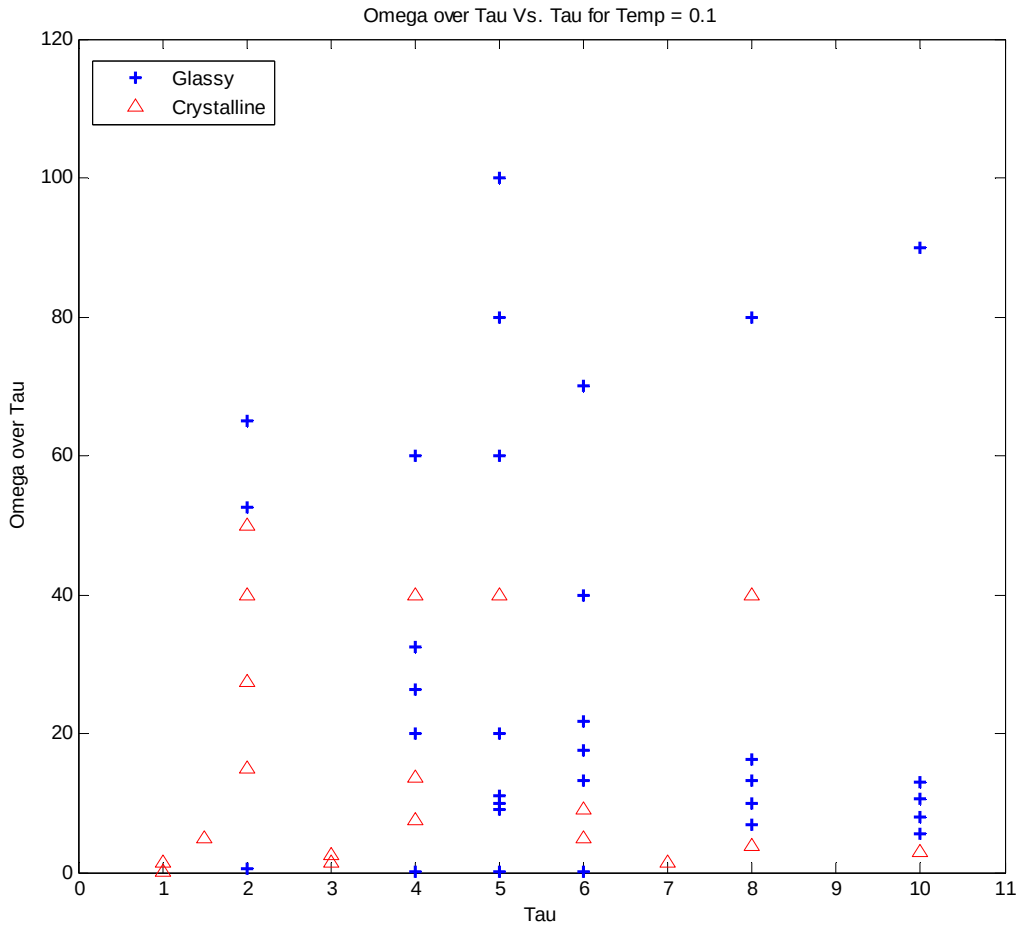

Figure 6.3 Plot of systems reaching equilibration (crystal) by the variation of PCND noise parameters, omega or amplitude of noise force and decay time constant, tau

This plot does not reveal a pattern either. Hence an overall comparison of the PCND parameters to results from MD would be more insightful to comment on noise parameters. Here is a 3D plot of noise parameters and their convergence and the convergence of MD under different system conditions.

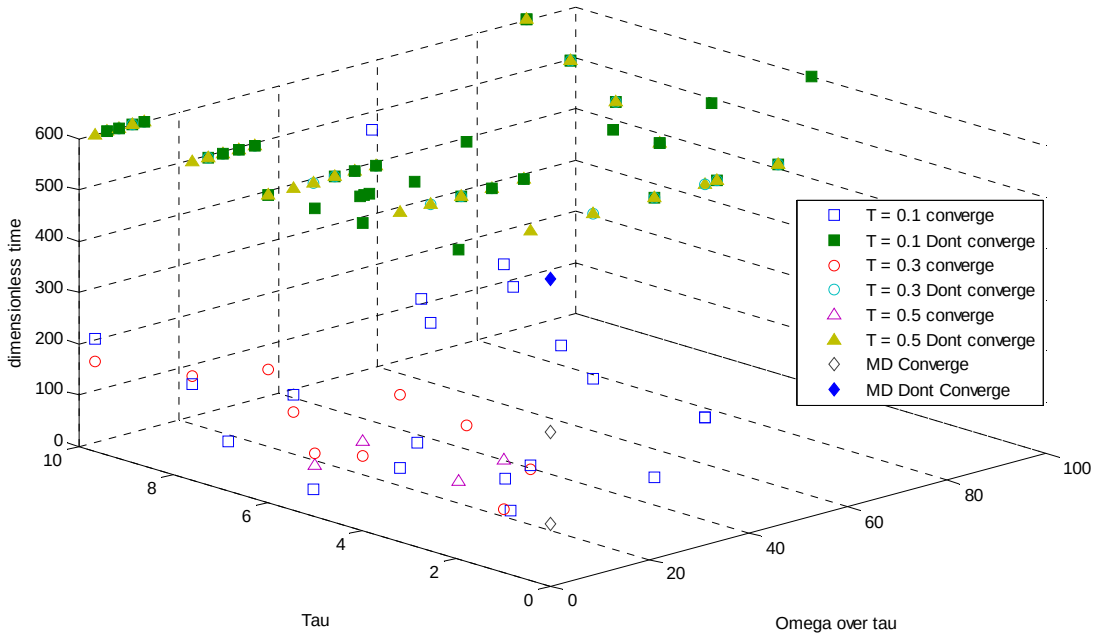

Figure 6.4 Crystalline structures resulting from PCND and MD runs for different states of the system, T = 0.1, 0.3, 0.5

It can be observed that the system under the influence of PCND parameters converge more often and within a short simulation time relative to MD. This is expected and is convincing that the system under the influence of colored noise performs faster than the same system under the influence of molecular dynamics. However, the optimization of noise parameters due to the absence of any obvious pattern in its implication, to enable their application extendable to more complex systems and

polymers, remains a concern. In an investigation of this concerning fact, the randomization involved in the process was analyzed. Since every simulation reported in literature for Molecular Dynamics (MD), Monte-Carlo (MC) simulation [3, 4] begins with a random initial conformation from one or more statistical energy distribution it is less likely however, would be useful to look into the initial states of these systems.

6.2 Initial Conformation

The algorithm for initial conformation involves random positioning of atoms and the probability of acceptance of the random positions, based on Boltzmann energy distribution. While the first atom is placed randomly in the simulation volume, subsequent placing of an atom is dependent on (i) a minimum distance from other atoms existing in the system to avoid overlap of atom positions and (ii) the energy of the system is minimum, which is estimated from the differential of Lennard-Jones potential calculated from the new position. The new random position is accepted only when the probability of the acceptance of the position is one, which is possible only for low energy systems. This way, the positioning of the last few atoms takes a little longer relative to the other atoms, because of very few positions possible while packing 1080 atoms at a density of $\rho^* = 0.95$. In this case, there is little or no possibility of applying the probability of acceptance based on Boltzmann energy distribution, since it is rather difficult to get the energy minimized further. Under such circumstances, an alternative probability based on a random number comes handy, where there is a probability of acceptance of one or more positions that have been tried in the last few trials and rejecting based on the energy change induced.

With the aforementioned details of the algorithm used for building the system of atoms, for a systematic choice of initial conformations, about 10,000 runs of initial conformations based on the Boltzmann energy distributed conformations were repeated to ensure the distribution of initial energy is Gaussian and for a statistical choice of initial conformation. Shown below is the histogram of the initial energy of the system after random positioning of atoms. It can be seen that, for a dimensionless potential energy bin width of 100, the mean is -6585. The scaling used for energy is the depth of potential energy level (500 J/mol). It can also be noticed that the width of the initial energy distribution of the system is no greater than 150. This suggests that a random choice of initial structure, in the absence of such a systematic approach of choosing from a Gaussian distribution of 10000 trials, would still yield systems with very little difference in energies.

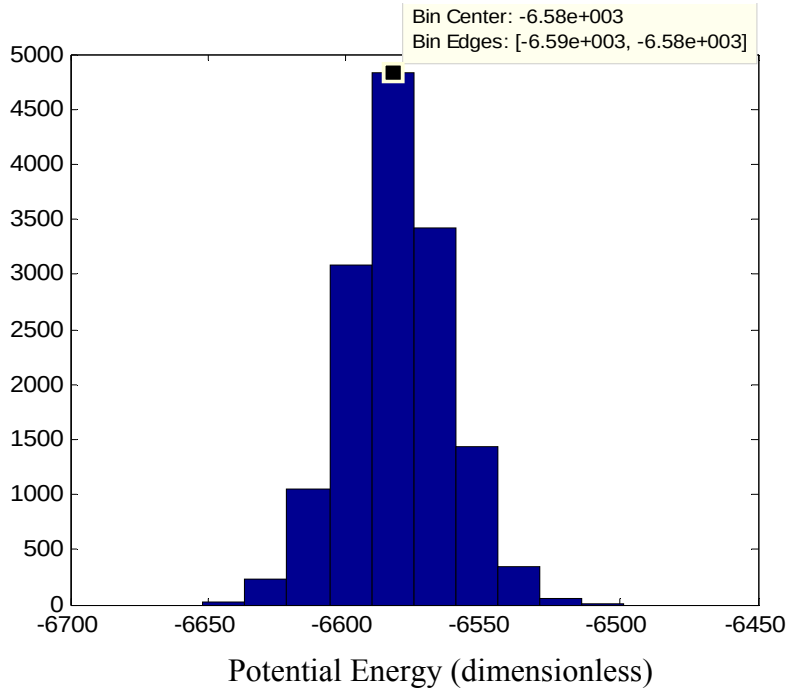

Figure 6.5 Gaussian distributed initial energy of Lennard-Jones glass

With such low differences in energy among the random orientation of atoms generated by initial conformation algorithm, it was interesting to look at the structure of these conformations. The pair distribution function (pdf) or radial distribution function (rdf) defined as the ratio of local density to overall density given by [5-7],

$$g(r) = \rho^{-2} \left\langle \sum_i \sum_{j \neq i} \delta(r_i) \delta(r_j - r) \right\rangle = \frac{V}{N^2} \left\langle \sum_i \sum_{j \neq i} \delta(r - r_{ij}) \right\rangle$$

It is useful to look at the pair distribution function of the system to know the physical state of the system. For all the above energy distributions, the pair distribution or radial distributed represented that of an amorphous state of the system. A representative initial amorphous state of the system represented by pair distribution function, g(r) is shown below.

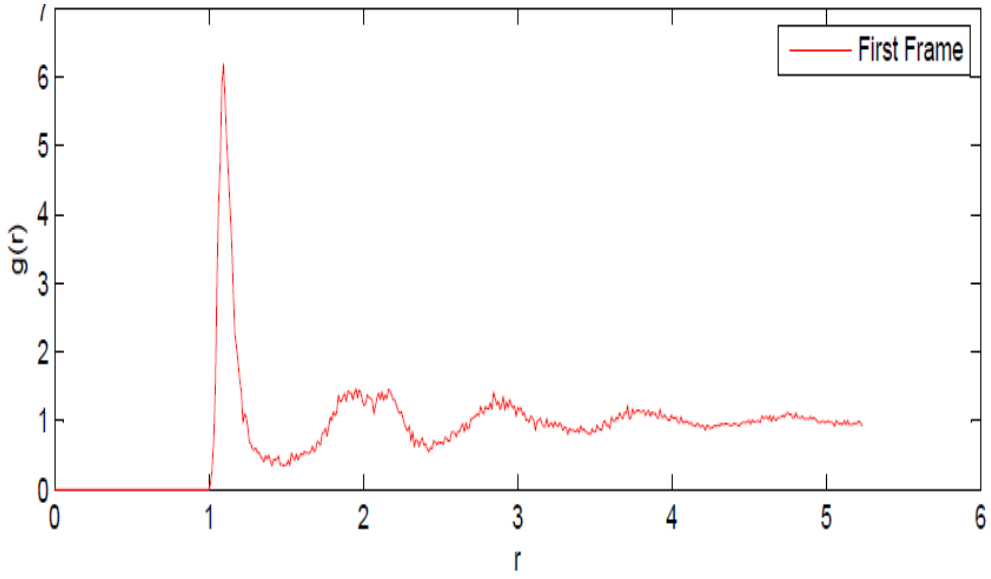

Figure 6.6 Radial distribution function (rdf) of initial conformations

Although the pair distribution function for all of these energies suggest an amorphous initial conformation, the distribution of atoms in a cubic cell would confirm this. The positions of 1080 atoms in their initial states oriented through the Boltzmann energy distribution, for a dimensionless density of 0.95 is shown below. It can be seen that, for almost identical initial potential energies, the departure of the initial state of the system from equilibrium state seems to vary widely. In other words, the alignment of atoms (denoted by blue asterisks) seems more oriented in the case of the dimensionless potential energy of -6600 than in other two cases of 6600 +/- 15. This is interesting and shows an existence of degree of departure of the system from equilibrium and that it varies widely for a negligible difference in total energy and no difference in physical state. This just suggests that a random choice of initial conformation can thus lead to different beginning levels of departure of the system from equilibrium state and hence work favorably in some cases to yield a faster convergence to an face centered cubic (fcc) crystal.

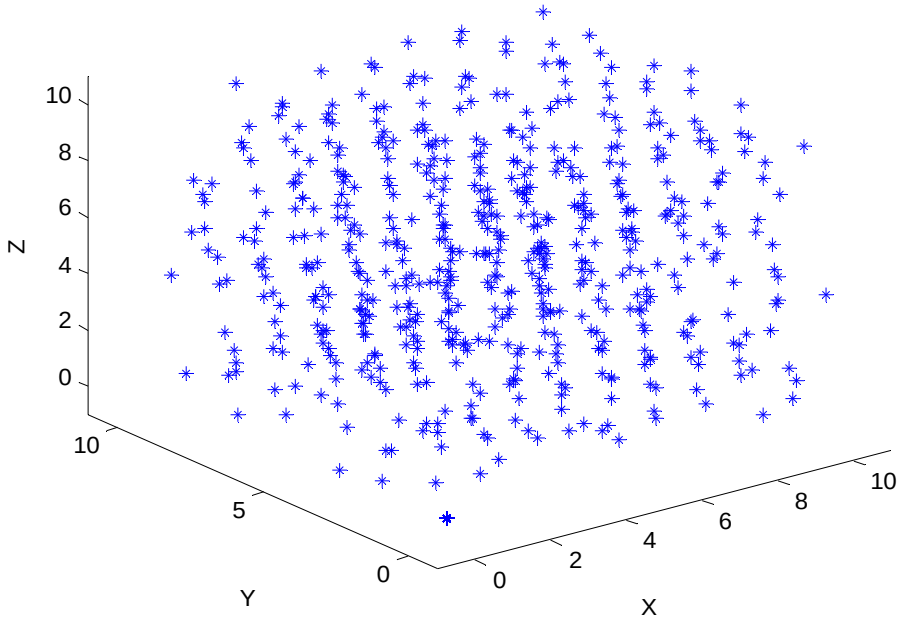

(a)

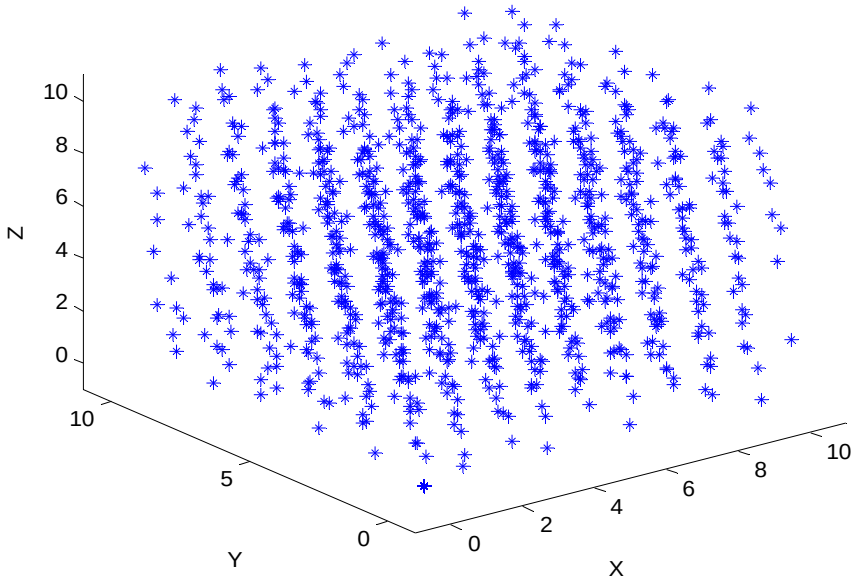

(b)

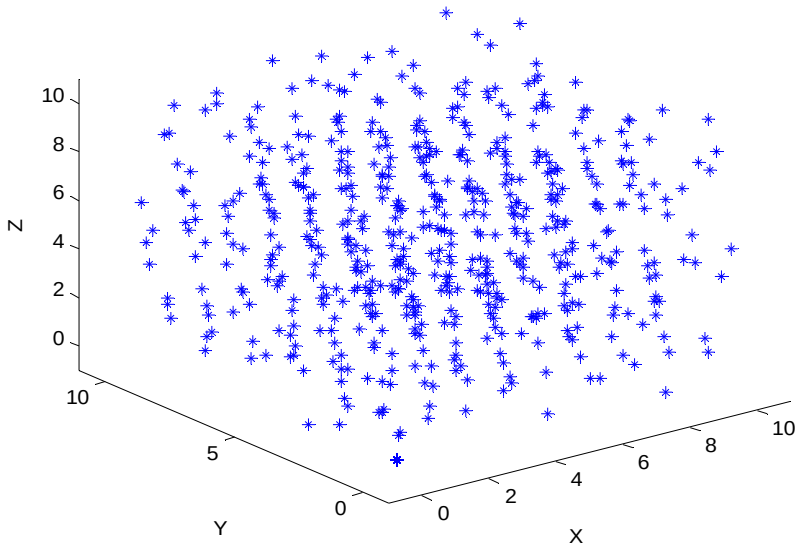

(c)

Figure 6.7 Orientation of atoms from initial conformation for a dimensionless Potential energy of (a) – 6585 (b) – 6600 (c) – 6570

This, in turn, can work in preference of PCND, letting it to converge much faster than MD, and hence the test of PCND algorithm to render faster convergence of non-equilibrium states within in real simulation times is in question.

The results for nine configurations around the mean of the initial energy Gaussian distribution is shown below.

Table 6.1 Relaxation of nine different configurations of amorphous material under the influence of PCND and MD

Configurations	Trial 1	Trial 2	Trial 3	Trial 4	Trial 5	MD
1	Crystal	Crystal	Crystal	Crystal	Crystal	Crystal
2	Glass	Becoming a Crystal	Becoming a Crystal	Glass	Glass	Becoming a Crystal
3	Glass	Glass	Glass	Glass	Glass	Becoming a Crystal
4	Crystal	Glass	Becoming a Crystal	Becoming a Crystal	Glass	Becoming a Crystal
5	Becoming a Crystal	Becoming a Crystal	Becoming a Crystal	Becoming a Crystal	Glass	Glass
6	Becoming a Crystal	Crystal	Glass	Becoming a Crystal	Glass	Glass
7	Glass	Glass	Glass	Glass	Glass	Glass
8	Glass	Glass	Glass	Glass	Glass	Glass
9	Glass	Becoming a Crystal	Becoming a Crystal	Becoming a Crystal	Glass	Becoming a Crystal

Out of the nine configurations simulated, as it can be seen, the probability of convergence of an amorphous system to a crystal is approximately 16% for a set of noise parameters of $\Omega = 0.1$ and $\tau = 0.6$, chosen from a 24 x 24 possible variations of noise parameters and found to have a higher probability of equilibrating the system. The pair

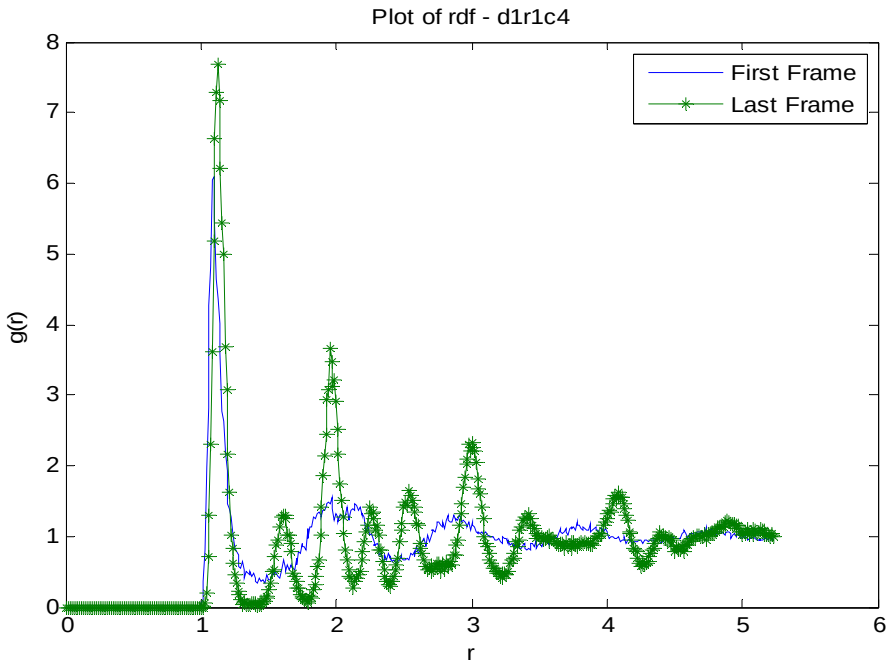

Figure 6.8 Crystal

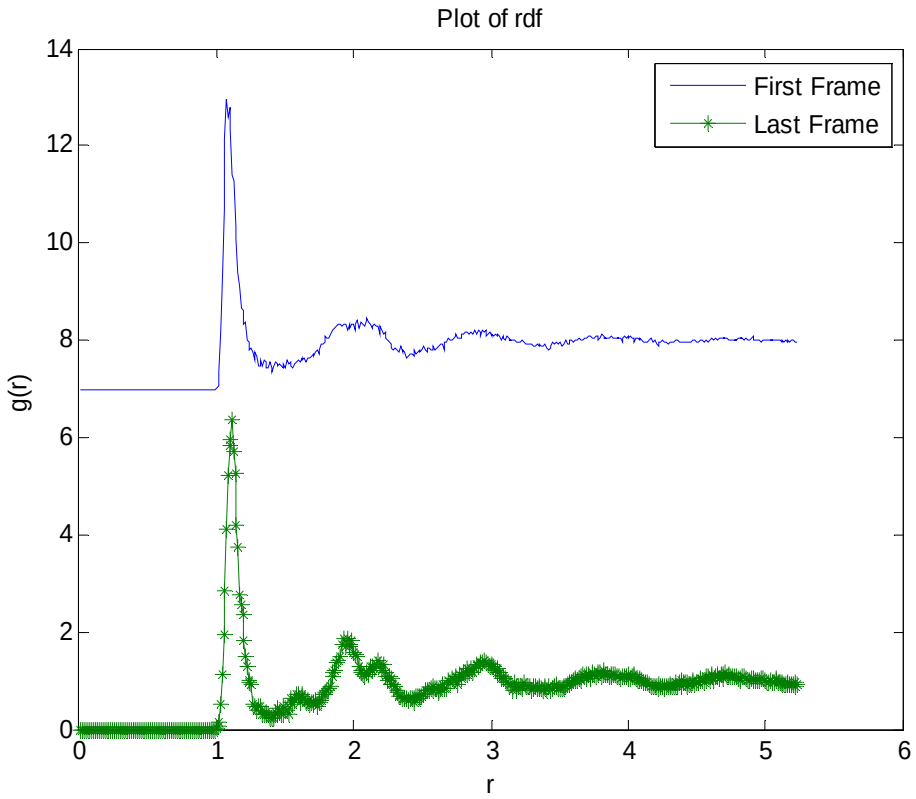

Figure 6.9 Becoming a Crystal

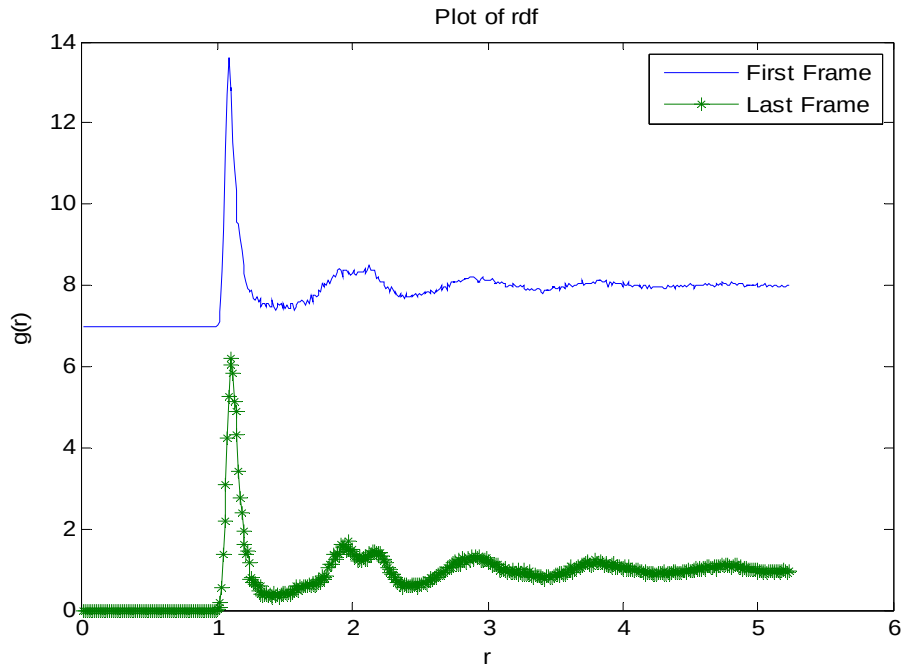

Figure 6.10 Glassy State

It can be seen that all the three cases begin with an amorphous radial distribution function (rdf) and end in crystalline, glassy states. The dip in the second peak of radial distribution functions is characterized as glass-transition state [8]. Besides the peaks at r = 1 and at r =2 in an amorphous or glassy systems, the beginning of the appearance of another peak in $1 < r < 2$ characteristic of crystalline states only (refer figure for crystal), can be evidenced in the figure for 'becoming a crystal' and these are marked distinctly instead of classifying under either category to show those simulation runs, which when run a little longer then would end in a crystalline state within next 100 dimensionless time units.

From the above table configurations 4 and 6 were chosen and were tested for different noise parameters and were observed to converge with the probability similar to that resulting from molecular dynamics simulation.

6.3 Bistable Potential

In order to test the dimensionality dependence of PCND, a simple system under the influence of bistable harmonic oscillator shown below was used to test the performance of PCND over MD. The efficiency of PCND to enable the molecules the cross the energy barrier was tested using this bistable potential function.

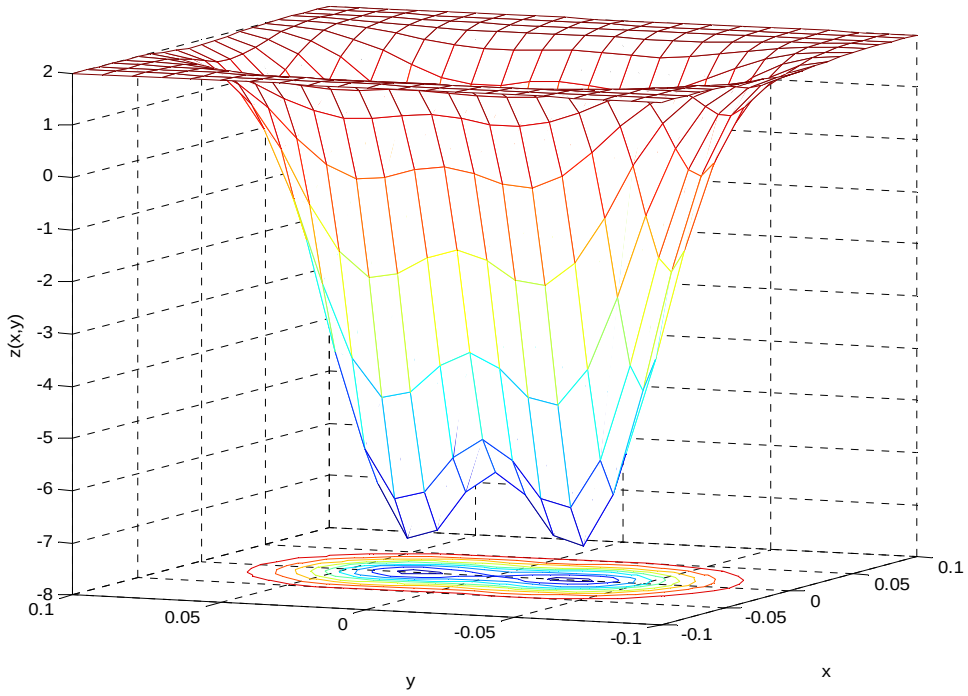

Figure 6.11 Bistable potential harmonic oscillator

The frequency of PCND enabled barrier cross-over of the molecules, were monitored. Shown below is the summary of result for the frequency at which the molecules crossed the potential energy barrier using PCND relative to MD.

The system was maintained at a dimensionless temperature of 0.3. Hence the kinetic energy of the system drives the energy barrier cross over in the case of Molecular Dynamics. In the case of PCND, in addition to the kinetic energy imparted by the temperature of the system, the introduction of random forces at relaxation time constants (PCND - 0.5 and PCND1 – 5.0), enables twice the frequency relative to MD.

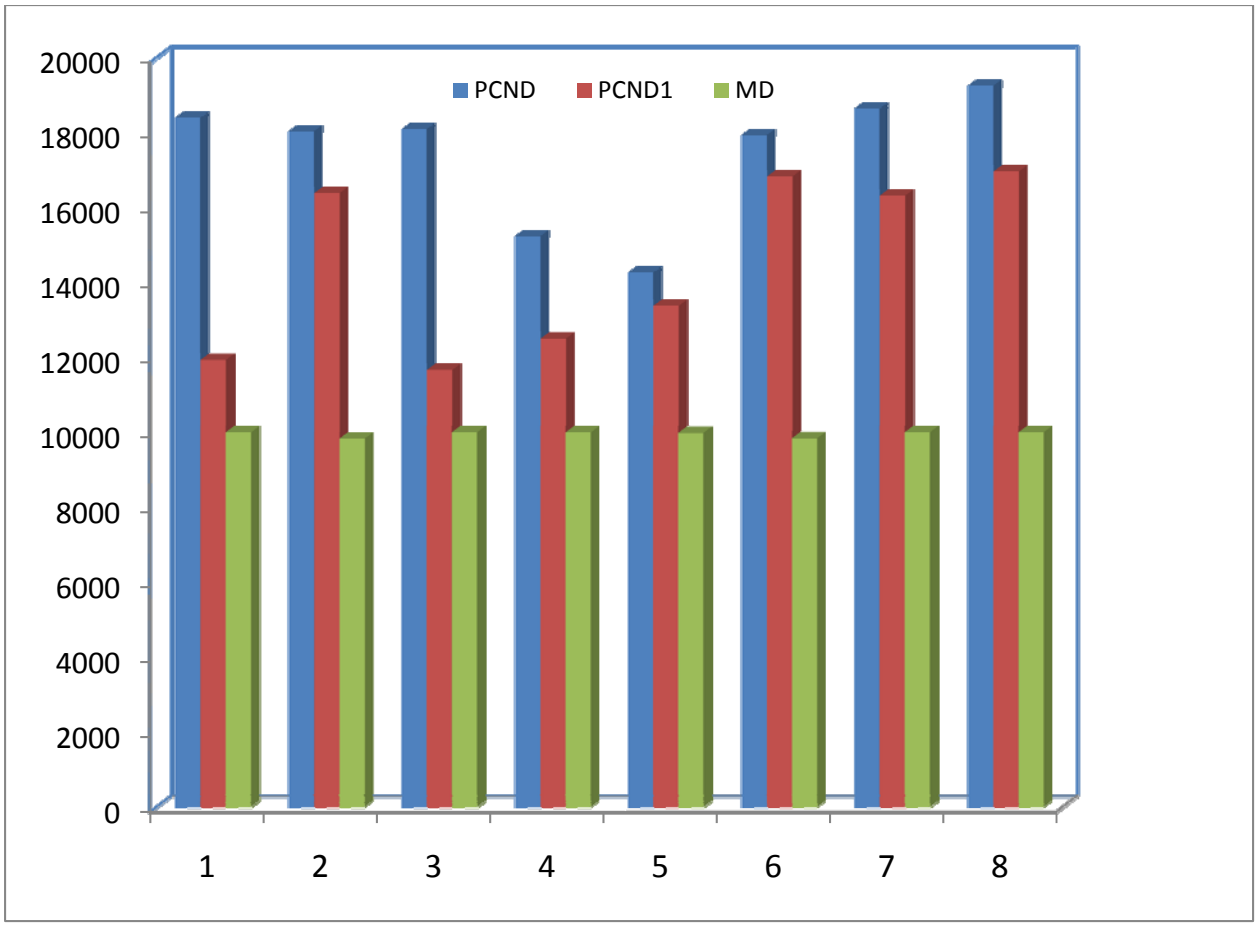

Figure 6.12 Bar chart showing performance of PCND over MD, for a system under bistable harmonic oscillator, shown in Figure 6.11. PCND: $\Omega/\tau = 1.5$ and $\tau = 0.5$ and PCND1: $\Omega/\tau = 1.5$ and $\tau = 5.0$

As can be seen from the result reported using the bar chart, the performance of PCND is almost always better than that of MD and the efficiency is better with shorter time constant for the force relative to longer ones, from the parameters chosen. In order to investigate to be able to better comment on the range of forces and/or time constant used in the stochastic random force, the bistable potential system was tested for various time constant and the magnitude of the root mean squared force, while holding the variance of the distribution of the stochastic force a constant. Shown below are the results

from such an analysis and as it can be seen here, there is no tremendous change in the performance for longer time constants. However, in all the cases, it has been observed to performance better than MD. The high confidence intervals highlight the stochastic nature of these noise forces.

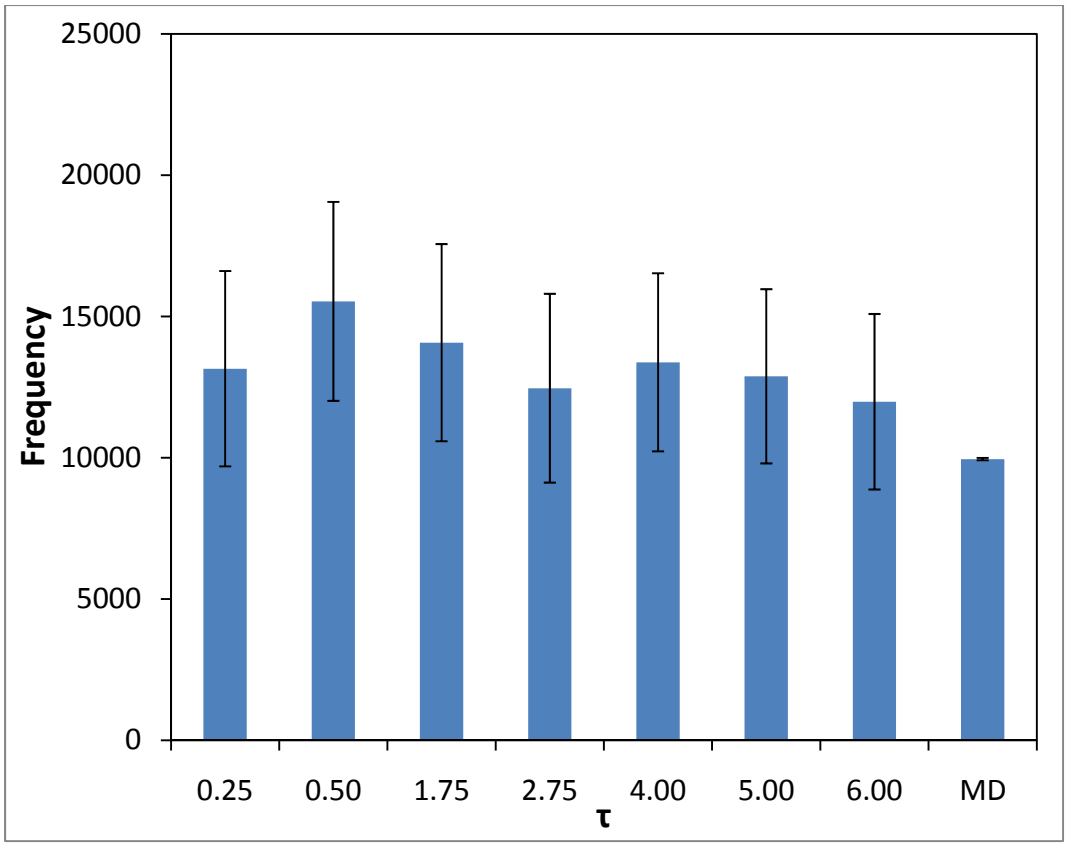

Figure 6.13 Performance of PCND for various time constants

6.4 Conclusions

Protracted Colored Noise Dynamics was developed to efficiently sample phase space in viscous systems that are not well simulated with the existing MD and MC simulation methods within realistic simulation times. The algorithm was observed to perform efficiently and equilibrate systems remarkably faster than an MD simulation in a wide range of noise force parameters. However, the optimizations of noise parameters were not possible, due to the absence of any statistically significant pattern in the choice of noise parameters. For this, investigation of random Boltzmann energy distributed initial state of the system, had largely influence the observed PCND results. Although all initial states of the systems were confirmed to be amorphous, the orientation of the individual spheres in the systems varied largely with respect to their departure from the equilibrium crystalline states. The probability of the convergence with the help of PCND increased with initial systems close to the equilibrium systems and the colored noise force enabled the system to overcome the configurational energy barrier. However, in systems in initial states that were very far from equilibrium, a random choice of colored noise force that exponentially decayed with a specific decay time constant worked. For systems in between the two states, the probability of convergence in the presence of colored noise forces were equally likely as would be in the case of an MD simulation. In the case of the use of bistable potential harmonic oscillator, the efficiency of PCND over MD was proved, or a wide range of PCND parameters.

6.5 References

1. Jenkins, J.W., *Novel Efficient Simulation Techniques In Molecular Modelling*, in *School of Chemical and Biomolecular Engineering*. 2000, Georgia Institute Of Technology: Atlanta.
2. Rahman, A., Mandell, M.J., McTague, J.P., *Molecular dynamics study of an amorphous Lennard-Jones system at low temperature.* Journal of Chemical Physics, 1976. **64**: p. 1564.
3. Broughton, J.Q., Gilmer, G.H., Weeks, J.D.,, *Constant-Pressure molecular dynamics simulations of the 2D r-12 system: comparison with isochores and isotherms.* Journal of Chemical Physics, 1981. **75**: p. 5128.
4. Metropolis, N., Rosenbluth, A.W., Rosenbluth, M.N., Teller, A.H., Teller, E.,, *Equation of state calculations by fast computing machines.* Journal of Chemical Physics, 1953. **21**: p. 1087.
5. Hansen, J.P.M., I.R., ed. *Theory of simple liquids*. 1986, Academic Press: Newyork.
6. McQuarrie, D.A., ed. *Statistical Mechanics*. 1976, Harper and Row: Newyork.
7. Allen, M.P., Tildesley, D.J.,, ed. *Computer Simulation of Liquids*. 1989, Oxford Science Publications: Suffolk.
8. Basak, S., Clarke, R., Nagel, S.R.,, *Pair distribution function and its relation to glass-transition in an amorphous alloy.* Physical Review B, 1979. **20**(8): p. 3388.

CHAPTER 7

SUMMARY AND RECOMMENDATIONS

7.1 Summary

Diffusion coefficient of water molecules in films of poly (methyl methacrylate) (PMMA) has been studied as a function of film thickness. Film thicknesses investigated range from 25 nm to 2000 nm. Over this thickness range, diffusion coefficient of water decreases by over four orders of magnitude as the films get thinner. Above 2000 nm thickness, diffusion coefficient approaches the reported bulk value of diffusion coefficient for water in PMMA (10^{-8} cm^2/s). The diffusion coefficient is observed to scale with film thickness squared below 1300 nm. This change in diffusion coefficient occurs over a much larger range of thicknesses than has been previously reported in polymer ultra-thin film confinement effect studies on properties such as glass-transition temperature, coefficient of thermal expansion [1] and penetrant diffusion behavior [2]. In the study of glass-transition temperature (T_g) and coefficient of thermal expansion (α') [1], the bulk value of Tg and α' are reached at a film thickness of about 200 nm. The deviation in the properties below 200 nm, have been explained to be due to film confinement on the substrate. However, the deviation observed here in diffusion coefficient extends up to 1300 nm and hence film confinement cannot be the explanation for deviations at such length scales. Thus, it is important that thickness be considered for all diffusion studies, even those that were previously thought to behave as bulk films. The thickness dependence does not appear to be due to residual casting solvent. Slow Positron Annihilation Lifetime Spectroscopy (sPALS) was used to probe the free volume pocket

size, its distribution within the film, and its total amount as a function of film thickness in PMMA. The results from sPALS showed that thicker films have more free volume pockets than thinner films and that the average free volume pore radius is smaller in thin films than in thick films. This change in free volume size was observed to correlate with the measured activation energy change with film thickness for the process of diffusion. The density measurements also agreed with change in free volume pocket size. Thus decrease in free volume pocket size and fractional free volume certainly contributes to the significant drop in diffusion coefficient in thinner PMMA films. And this behavior is likely to be one of the general underlying causes for such thickness dependent diffusion behavior observed in a variety of other ultra-thin polymer films as well. With the decrease in fractional free volume in thin films, solubility was also affected to some extent. The percentage decreases in solubility was relatively less when compared to percentage change in fractional free volume and this is believed to be due to the loss of some of the inaccessible free volume (relative to the size of the diffusing penetrant), whose loss does not affect solubility anyways. To extend the observation of drop in diffusion coefficient with film thickness to similar observations made in membrane separations and permeability, aging behavior of diffusion and solubility was studied. Diffusion coefficient was observed to not change with time, while solubility decreased with aging. Correlations of the results obtained to sPALS measurements reported by Rowe et al., [45] reveals that constant fractional free volume could be the possible reason for unchanged diffusion coefficient, while increase in number of in accessible free volumes could lead to decreased solubility in aged films. These hypotheses can be tested by measuring activation energy for diffusion in thin films due to aging, which should

remain a constant confirming constant diffusion coefficient. sPALS study of free volume pocket size distribution as a function of aging could help understand the range of free volume pocket radius available in aged films and the percentage of inaccessible free volume (relative to penetrant size) that is comparable to observed change in solubility.

The investigation of diffusion characteristics of acid generated in chemically amplified photoresists showed thickness dependent behavior similar to that observed in pure polymer film. The chemically amplified photoresists while undergoing deprotection has two distinct regimes for diffusion of acid: the protected polymer sites and the deprotected polymer sites. The diffusion behavior is distinct in these two regimes and the diffusion coefficient changes by 2 orders of magnitude for a film thickness change of about 240 nm to 45 nm. This change in magnitude is comparable to PMMA, implying thickness dependence of diffusion coefficient in photoresist films. This proves that this thickness dependence of diffusion is an intrinsic property of ultra-thin polymer films. The activation energy for the diffusion of acid in the protected and deprotected polymer sites are affected by the size of the diffusing acid, as higher transition energy is required to overcome the diffusion energy barrier for a relatively larger acid molecule. The stearic and orientation significance of the pre-exponential factor of Arrhenius equation is dominant and influences the mobility of acid through the polar hydroxyl group in a deprotected polymer, though not affected largely by temperature. The increase in activation energy for the diffusion of acid in the protected and deprotected polymer matrices with decrease in film thickness clearly reveals an increase in energy barrier for the diffusion of acid in ultra-thin films. This has been confirmed by the determination of activation energy for the diffusion of acid, from the deprotection observed in these films

as a function of the post-exposure bake temperature. This deviation in diffusion coefficient of acid in thin and ultra-thin films from the bulk films is an important factor to be considered in the photolithography industry in semiconductor industry, where the film thickness is well within this range and the diffusion of acid is an important criterion that determines performance like line edge roughness.

It is hypothesized that layering of thin films of Nafion with the intrinsic property of the ultra-thin polymer films with low diffusion coefficients could decrease the methanol cross over. Unlike the present alternatives for reducing methanol crossover like cross linking and inorganic filler particles [3-5], reduced diffusivity in ultra-thin films is homogenous and hence would prove more effective in addressing the methanol crossover issues in proton exchange membrane fuel cells. Other alternatives to reduce methanol cross over like, reduced hydration of Nafion membranes to enable reduction of the solubility of methanol for cross over, with imidazole groups would lead to heterogeneity in the film, with the proton conducting contour largely different from the bulk polymer film. Use of ultra-thin films would bring the effect of reduced methanol cross-over, by their intrinsic property of reduced diffusivity brought about by the processing condition. The through plane conductivity of nafion used in proton exchange membranes used in fuel cell is found to decrease to a maximum of 30% from bulk, in the film thickness range investigated here. While the orders of magnitude drop in diffusion coefficient in nafion films could be used to avoid methanol cross over and loss, the decrease in conductivity in film thickness direction is a drawback. Thus, thin layers of spin cast Nafion films which add up to the thickness of the electrolyte layer in fuel cells, could effectively reduce methanol transport with relatively small loss in conductivity.

Protracted Colored Noise Dynamics was developed to efficiently sample phase space in viscous systems that are not well simulated with the existing MD and MC simulation methods within realistic simulation times. The algorithm was observed to perform efficiently and equilibrate systems remarkably faster than an MD simulation in a wide range of noise force parameters. However, the optimizations of noise parameters were not possible, due to the absence of any statistically significant pattern in the choice of noise parameters. For this, investigation of random Boltzmann energy distributed initial state of the system, had largely influence the observed PCND results. Although all initial states of the systems were confirmed to be amorphous, the orientation of the individual spheres in the systems varied largely with respect to their departure from the equilibrium crystalline states. The probability of the convergence with the help of PCND increased with initial systems close to the equilibrium systems and the colored noise force enabled the system to overcome the configurational energy barrier. However, in systems in initial states that were very far from equilibrium, a random choice of colored noise force that exponentially decayed with a specific decay time constant worked. For systems in between the two states, the probability of convergence in the presence of colored noise forces were equally likely as would be in the case of an MD simulation.

7.2 Future Work and Recommendations

Significant deviation in diffusion behavior of ultra-thin films relative to bulk films with film thickness was well investigated and reported to be due to free volume and

activation energy needed to enable a diffusion jump. Based on the results observed for aging, the unchanged diffusion coefficient observed here could be tested by studying the behavior of activation energy for diffusion of water in thin PMMA films as a function of time. Unchanged activation energy would support the argument made here, that the increase in intensity compensates for decrease in free volume pocket size. The decrease in solubility in aged films due to the increase in number of inaccessible free volume pockets could be studied by investigating free volume distribution in films as a function of time. Also, different casting solvents used in the preparation of spin cast films could enable the study of the impact of initial fractional free volume (due to difference in boiling point of casting solvent that leads to different chain alignment during spin coating) on the observed trends in diffusivity and solubility. This study could also be extended to diffusion of different solvents in polymer films like organic solvents that are capable of swelling the polymer films. This would help compare the impact of mass uptake due to swelling and the influence of film thickness in solubility in such cases.

The study of diffusion and solubility in different polymers with structural significance like cross-linked, block copolymers and photoacid generator bound polymer films could enable the applicability of these deviation for enhancing the performance of polymer films used in various applications. Extension of this study to other polymer films could enable generalized understanding of the morphology of polymer films characteristics of ultra-thin spin coated films. Investigation of diffusion of acid on different substrates would be interesting to note any substrate influence in a reaction diffusion system. Different processing conditions for the preparation of ultra-thin polymer films could also be tested to understand if the above reported results are specific

and intrinsic properties of spin-coated films only. This would enable to take advantage of processing conditions to change and exploit properties of material for economical and application-oriented advantages

Proton conductivity of Nafion under hydrated conditions is due to the hoping of protons through the water swollen channels lined with sulfonic acid groups via a Grotthuss-like mechanism [6, 7]. The study of proton conductivity of these ultra-thin Nafion films can be used to understand if the proton transport via Grotthuss mechanism is affected or not affected, similar to diffusion coefficients of these thin films. This study of conductivity and any related observation on the impact of conductivity due to film thickness in this thickness regime would be a significant contribution for the suggested use of these thin films in fuel cells to reduce fuel cross-over. If the through plane conductivity of thin films is not affected, then it favors the use of multiple layers of thin films in a fuel cell set up, where the diffusion coefficient deviation will help reduce methanol cross over while proton conductivity is unaffected. This in turn means better fuel efficiency and unaffected performance of fuel cells. The processing involved in the preparation of multiple layers of thin films like layer-by-layer assembly [8], polyelectrolyte multilayer technique [9] needs to be investigated to enable its use in a fuel cell set up. Also, mechanical stability of multilayers of thin films should be tested under the operating conditions of a fuel cell. The observed trend in through plane conductivities should be tested in a fuel cell setup arrangement to enable its efficient application. The observed decrease in through plane conductivity from bulk may or may not be significant in a fuel cell setup and hence the diffusion observation could be exploited for better performance of polymer electrolyte membranes to avoid loss of methanol. However, if

the conductivity decrease is much higher than that observed here, then better fuel cell performance due to decreased loss of methanol and the extent of impairment of conductivity in thin films need to be compared to employ such multiple layers of thin films.

Based on the results reported here the algorithm for Protracted Colored Noise Dynamics is largely sensitive to initial state of the system unlike the conventional relaxation methods reported in literature earlier. This sensitivity limits the extensive applicability of the algorithm. This could be largely due the application of equal random force to all atoms involved in the system. Development of algorithm to apply weighted force to atoms, relative to their departure from equilibrium could enable to overcome this drawback. The efficiency of PCND algorithm to enable the relaxation of systems much faster than molecular dynamics could bring down the computational cost proportional to the order of magnitude difference in the length of simulation time. This in turn, would enable to span the space that are otherwise limited by simulation time and better study the real time relaxation of a number of system including condensed and viscous systems.

7.3 References

1. Singh L., Ludovice, P.J., Henderson, C.L., Thin Solid Films, 2004. **449**(1-2): p. 231.
2. Vogt B.D., Soles, C.L., Langmuir 2004. **20**(4): p. 1453.
3. Kim, D.S., et al., *Proton conductivity and methanol transport behavior of cross-linked PVA/PAA/silica hybrid membranes.* Solid State Ionics, 2005. **176**(1-2): p. 117-126.
4. Kjaer, J., et al., *Solid-State Electrolyte Membranes for Direct Methanol Fuel-Cells.* Solid State Ionics, 1991. **46**(1-2): p. 169-173.
5. Poltarzewski, Z., et al., *Novel proton conducting composite electrolytes for application in methanol fuel cells.* Solid State Ionics, 1999. **119**(1-4): p. 301-304.
6. Mauritz, K.A., Moore, R.B., *State of Understanding of Nafion.* Chemical Reviews, 2004. **104**(10): p. 4535-4586.
7. Agmon, N., *The Grotthuss Mechanism.* Chemical Physics Letters, 1995. **244**(5-6): p. 456-462.
8. Daiko, Y., Katagiri, K., Matsuda, A., *Proton Conduction in Thickness-Controlled Ultrathin Polycation/Nafion Multilayers Prepared via Layer-by-Layer Assembly.* Chemistry of Materials, 2008. **20**(20): p. 6405-6409.
9. Elbert, D.L., Herbert, C.B., Hubbell, J.A., *Thin Polymer Layers Formed by Polyelectrolyte Multilayer Techniques on Biological Surfaces.* Langmuir, 1999. **15**(16): p. 5355-5362.